2012-04-10

Gene Therapy for Very Long Chain Acyl-coA Dehydrogenase Deficiency Using Adeno-Associated Virus Vectors: A Dissertation

Allison M. Keeler
University of Massachusetts Medical School

GENE THERAPY FOR VERY LONG CHAIN ACYL-COA DEHYDROGENASE DEFICENCY USING ADENO-ASSOCIATED VIRUS VECTORS

A Dissertation Presented

By

ALLISON MAY KEELER

Submitted to the Faculty of the
University of Massachusetts Graduate School of Biomedical Sciences, Worcester
In partial fulfillment of the requirements for the degree of

DOCTOR OF PHILOSOPHY

APRIL, 10 2012

GENE THERAPY

GENE THERAPY FOR VERY LONG CHAIN ACYL-COA DEHYDROGENASE DEFICIENCY USING ADENO-ASSOCIATED VIRUS VECTORS

A Dissertation Presented By

Allison M. Keeler

The signatures of the Dissertation Defense Committee signifies completion and approval as to style and content of the Dissertation

Terence Flotte, M.D., Thesis Advisor

Daryl Bosco, Ph.D., Member of Committee

Xandra Breakefield, Ph.D., Member of Committee

Anthony Carruthers, Ph.D., Member of Committee

Miguel Esteves, Ph.D., Member of Committee

The signature of the Chair of the Committee signifies that the written dissertation meets the requirements of the Dissertation Committee

Guangping Gao, Ph.D., Chair of Committee

The signature of the Dean of the Graduate School of Biomedical Sciences signifies that the student has met all graduation requirements of the School

Anthony Carruthers, Ph.D.
Dean of the Graduate School of Biomedical Sciences

Interdisciplinary Graduate Program
April 10, 2012

DEDICATION

I would like to dedicate my thesis to my mother, Nancy McCullough Keeler Katzen. My mother has taught me through example how to be strong, independent and graceful under great adversity. As well as, taught me how to make the most of all situations and to always remember to laugh. She always encouraged my pursuit of education and refused to let me give up when times got more difficult. She was diagnosed with cancer in December 2008, in my second year of graduate school, and subsequently passed away in 2009. I know she would be proud of my accomplishments, and knowing that has been a driving factor.

ACKNOWLEDGMENTS

First and foremost, I would like to acknowledge my wonderful thesis advisor, Dr Terence R. Flotte. He has been incredibly encouraging and supportive of me throughout my graduate career both inside and outside of the laboratory. He has taught me to be an independent thinker, yet always supplied help when I needed it. He has taught me through example if you are unhappy with how things are, that you can and should make the changes necessary. I am truly lucky, to be given the project and opportunity to work in his lab, and forever grateful to him.

I would also like to acknowledge Dr. Miguel Esteves-Sena. Attending his lab meetings has been beneficial to my development as a scientist. Although he has many students in his lab, he always took time to meet with me and discuss my data, and I am especially thankful for all his help and guidance on the brain transduction study.

I would also like to acknowledge my collaborators at the University of Florida, primarily Thomas Conlon and Glenn Walter. Thomas greatly helped organize and move forward the experiments at Florida as well as perform pharm/tox. Glenn performed the MRS studies. Also at Florida, Ann Dongtao, has been very helpful as part of the pathology core.

Within the Flotte Lab, I would like to acknowledge Alisha Gruntmann for thesis edits as well as fellow graduate student companionship. Cynthia Greer for taking care of the mice and Qiushi Tang for teaching me tail vein injections. Chris and Sofia Mueller, Lina Song, and Dmitiry Ratner always make being in lab a little more interesting

I would also like to acknowledge my good friend and fellow graduate student Alison Bright, who has offered hundreds of hours of support as well as help with confocal microscopy.

Finally I would like to acknowledge my fiancé, John Klunk, for supporting me and for all his photoshop help.

ABSTRACT

Very long chain acyl-coA dehydrogenase (VLCAD) is the rate-limiting step in mitochondrial fatty acid oxidation. VLCAD deficient mice and patients' clinical symptoms stem from not only an energy deficiency but also long-chain metabolite accumulations. VLCAD deficient mice were treated systemically with $1x10^{12}$ vector genomes of rAAV9-VLCAD. Expression was detected in the liver, heart and muscle. Also substantial expression of VLCAD was noted in the brain, where it was expressed across different sections of the brain and in different cell types with different morphologies. Biochemical correction was observed in vector-treated mice beginning two weeks post-injection, as characterized by a significant drop in long chain fatty acyl accumulates in whole blood after an overnight fast. Changes persisted through the termination point around 20 weeks post injection. Magnetic resonance spectroscopy (MRS) and tandem mass spectrometry (MS/MS) revealed normalization of intramuscular lipids in treated animals. Correction was not observed in liver tissue extracts, but cardiac muscle extracts showed significant reduction of long chain metabolites. Disease-specific phenotypes were characterized, including thermoregulation and maintenance of euglycemia after a fasting cold challenge. Internal body temperatures of untreated VLCAD-/- mice dropped below 20℃ and the mice became lethargic, requiring euthanasia. In contrast all rAAV9-treated VLCAD-/- mice and the wild-type controls maintained body temperatures. rAAV9-treated VLCAD-/- mice maintained euglycemia, whereas untreated VLCAD-/- mice suffered hypoglycemia following a fasting cold challenge. These promising results suggest rAAV9 gene therapy as a potential treatment for VLCAD deficiency in humans.

TABLE OF CONTENTS

LIST OF TABLES

LIST OF FIGURES

LIST OF ABBREVIATIONS

FAO- Fatty-acid oxidation
CoA- Coenzyme A
Carnitine palmitoyltransferase-1 (CPT-1)
Carnitine palmitoyltransferase-2 (CPT-2)
Acyl-CoA dehydrogenases (ACADs)
Adenine Tri-phosphate (ATP)
Nicotinamide adenine dinucleotide (NAD+)
Flavin adenine dinucleotide(FAD)
Electron transferring flavoprotein (ETF)
Very long chain acyl-coA dehydrogenase (VLCAD)
Long chain acyl-coA dehydrogenase (LCAD)
Medium chain acyl-coA dehydrogenase (MCAD)
Short chain acyl-coA dehydrogenase (SCAD)
Tandem mass-spectrometry (MS/MS)
Sudden infant death syndrome (SIDS)
Medium-chain triglycerides (MCT)
Long-chain 3-hydroxyacyl CoA dehydrogenase (LCHAD)
Peroxisome proliferator-activated receptors (PPARs)
Messenger ribonucleic acid- (mRNA)
Mitochondrial trifunctional protein (mTFP)
Adeno associated virus (AAV)
Inverted terminal repeats (ITR)
Kilobases (kb)
Ribonucleic acid interference (RNAi)
Genomic deoxyribonucleic acid (gDNA)
Tibialis anterior (TA)
Chicken Beta Actin Promoter (CBA)
Phosphate Buffered Solution (PBS)
Vector genomes (vg)
Nuclear factor kappa-light-chain-enhancer of activated B cells (NFkB)
Blood brain barrier (BBB)
Green Fluorescent Protein (GFP)
Neuronal specific class III beta-tubulin (Tuj-1)
Single voxel proton magnetic resonance spectroscopy (1H-MRS)
Extensor digitorum longus (EDL)
Soleus (SOL)
Uncoupling protein 1 (UCP-1)
Cystic Fibrosis (CF)
Cystic fibrosis transmembrane regulator (CFTR)
Interleukin (IL)
Keratineocyte derived chemokine (KC)
Macrophage inflammatory protein-2 (MIP2)
Allergic broncho-pulmonary aspergillosis (ABPA)
T helper 2 lymphocyte (Th2)
Immunoglobulin (Ig)
Aspergillus fumigatus (Af)
Nuclear factor of activated T-cells (NFAT)

LIST OF MULTIMEDIA OBJECTS OR FILES

Video 5.1 Representative video of VLCAD-/- PBS control mouse after 18hr fast and 120 minutes at 4°C

Video 5.2 Representative video of VLCAD -/- rAAV9 treated mouse after 18hr fast and 120 minutes at 4°C

Video 5.3 Representative video of VLCAD +/+ PBS treated mouse after 18hr fast and 120 minutes at 4°C

PREFACE

Chapters II, IV, VI are all original unpublished works

Sections from Chapter I were published in:
Keeler AM, Flotte TR. *Cell and Gene Therapy for Genetic Diseases: Inherited disorders affecting the lung and those mimicking SIDS.* Hum Gene Ther. 2012

Sections from Chapter III and V were published in:

Keeler AM, C.T., Walter G, Zeng H, Shaffer SA, Dungtao F, Erger K, Cossette T, Tang Q, Mueller C, Flotte TR. *Long-term Correction of Very Long-chain Acyl-CoA Dehydrogenase Deficiency in Mice Using AAV9 Gene Therapy.* Mol Ther, 2012.

All qPCR from Chapter III, IV and V was preformed by Conlon T and anaylized and prepared by Keeler A, with the exception of Figure 4.11 which was preformed/analyzed /prepared by Keeler A, also parallel qPCR of different short-term data sets were preformed by A.Keeler in parallel but not presented here.

All immunohistochemistry from Chapter III, IV and V was preformed by Dungtao F, but images were analyzed/perpared by Keeler A.

Confocal Microscopy, in Chapter IV, staining was done by Dungtao F, but all microscopy/ image analysis and preparation was done by Keeler A.

All Magnetic Resonance Spectrometry from Chapter V was preformed/analyzed by Walter G and prepared by Keeler A.

All other technigues described were performed by Keeler A, unless otherwise noted.

Chapter VII was orginally published as:

Mueller C, Braag SA, Keeler A, Hodges C, Drumm M, Flotte TR. *Lack of cystic fibrosis transmembrane conductance regulator in CD3+ lymphocytes leads to aberrant cytokine secreation and hyperinflammatory adaptive immune responses.* Am J Respir Cell Mol Biol, 2011.44(6):922-9

Mueller C prepared: Figure 7.1& 2
Keeler A prepared: Figure 7.4,5,6
Mueller C and Keeler A prepared: Figure 7.3&7

Original ideas: Mueller C and Flotte TR, except relating to Figure 7.4 Keeler A

Manuscript was prepared by Mueller C and Flotte TR, except methods were Keeler A

Manuscript has been modified for this work

Chapter VIII was originally published as:
Mueller C, Keeler A, Braag S, Menz T, Tang Q, Flotte TR. *Modulation of exaggerated-IgE allergic responses by gene transger-mediated antagonism of IL-13 and IL-17e.* Mol Ther, 2010.18(3):511-8

Mueller C prepared: Figure 8.2,3,5
Keeler A prepared: Figure 8.1,6,7 (unpublished Figure 8.8)
Menz T prepared: Figure 8.4, Table 8.1

Original ideas: Mueller C and Flotte TR- receptor therapy, Keeler A- flow cytometry experiments relating to Figure 8.1,6,7,8

Manuscript was prepared by Mueller C, Keeler A and Flotte TR

Manuscript has been modified for this work

CHAPTER I: Introduction to Mitochondrial Fatty Acid Oxidation and Defects in Mitochondrial Fatty Acid Oxidation

Fatty-acid oxidation (FAO) is a cyclic process in which fatty acids are metabolized to produce energy. FAO is also important in removing toxic accumulations of certain fatty acids, such as short branched-chain fatty acids created by degradation of branched-chain amino acids. Under normal fed conditions, many organs preferentially derive their energy from glycolysis, but under certain conditions, such as fasting, exercise or metabolic stress, fatty-acid oxidation is an important source of energy. However, the heart's preferred energy source, from which it derives 70-95% of its energy, is FAO(1, 2). Skeletal muscle during low-intensity prolonged exercise can get 60% of its energy from FAO(3). In utero a fetus receives a constant supply of glucose from the placenta, but after birth 60% of it calories consumed from breast milk are fat, so highly oxidative tissues must rely on FAO for energy(4). During periods of fasting, the liver uses FAO to produce acetyl-CoA, which are further processed to produce ketones. The ketones can then be used for energy in the brain where glucose is the preferred energy source.

FAO can take place either in the mitochondria or in the peroxisomes, but generally peroxisomes only handle unusual fatty acid species and those containing chain-lengths larger than 20 carbons, which are shortened and oxidation is then finished in the mitochondria. Both α-oxidation and β-oxidation can occur in the peroxisomes but the mitochondria can only perform β-oxidation.

ω-oxidation occurs in the endoplasmic reticulum. The focus of this chapter will be on mitochondrial β-oxidation and disorders of β-oxidation primarily acyl-CoA dehydrogenase deficiencies.

In order for β-oxidation of fatty acids to occur, fatty acids must first be transported into the mitochondria as illustrated in Figure1.1. Free fatty acids are esterified with coenzyme-A to produce acyl-CoA's inside the cytosol, which are the precursors for β-oxidation. Long chain fatty acids, chain lengths of 12 carbons or more, are believed to be actively transported into the mitochondrial membrane. On the outer mitochondria membrane, carnitine palmitoyltransferase-1 (CPT-1) converts long chain acyl-CoA's to acyl-carnitine, translocating them to the inner mitochondria membrane. To cross the inner mitochondria membrane, carnitine acyl-carnitine translocase carries the acyl-carnitines in exchange for free carnitine. Finally carnitine palmitoyltransferase-2 (CPT-2) converts them back to acyl-CoAs. In order for FAO to occur transportation into the mitochondria is essential. In the case of defects of β oxidation the transport system also works in reverse, except the fatty acids remain as acyl-carnitines in the cytosol where they transfuse out of the cell and into the blood (Figure1.1).

Following mitochondrial transport, β oxidation occurs in the following four steps as illustrated in (Figure1.1): (1) dehydrogenation, in which acyl-CoA–dehydrogenases (ACADs) catalyzes a double bond between C-2 and C-3 and are noncovalently bound to flavin adenine dinucleotide (FAD) to accept electrons,

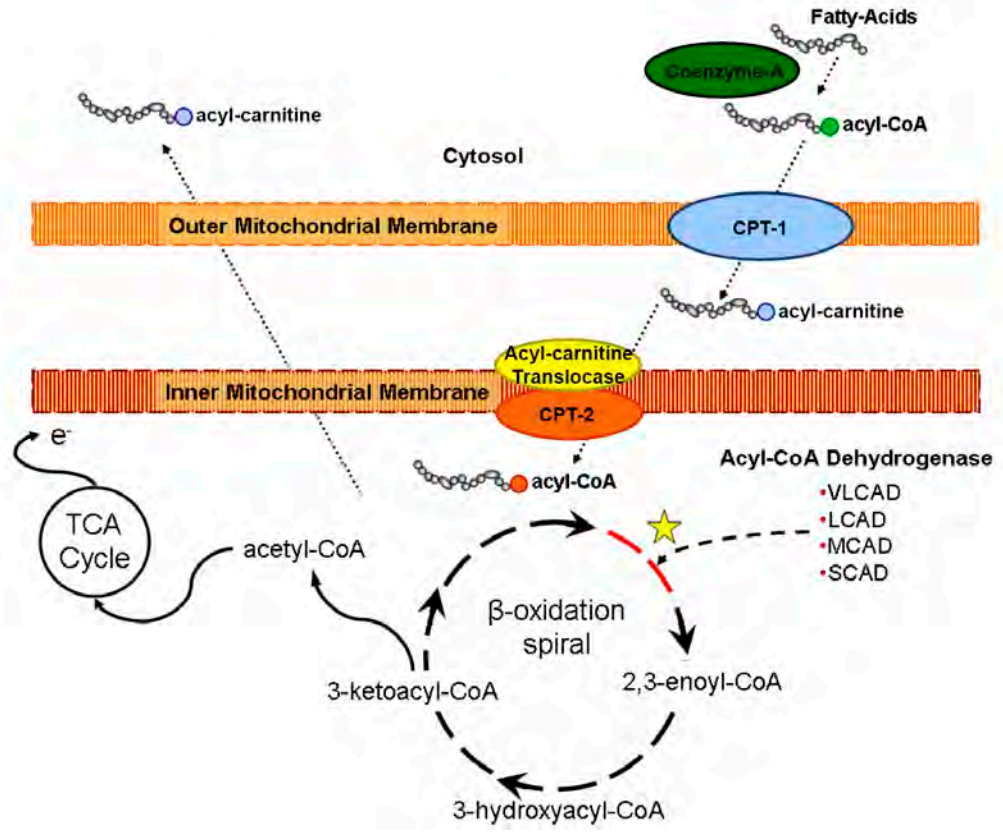

Figure 1.1 Transportation and Oxidation of Long Chain Fatty Acids in the Mitochondria

(2) hydration of the bond between C-2 and C-3 by enoyl CoA hydratase, which is stereospecific and forms only the L-isomer, (3) oxidation by L-β-hydroxyacyl-CoA-dehydrogenase converting the hydro group to a keto group and using NAD+ as an electron acceptor, and (4) thiolysis by β-ketothiolase cleaving the thiol group of CoA using free CoA. This results in an acetyl-CoA molecule and the acyl-CoA molecule that is two carbons shorter. This spiral continues shortening the acyl-CoA molecule two carbons at a time ultimately producing two final acetyl-CoAs. Acetyl-CoA can then go to the Citric Acid cycle and electron transport chain and produce 10 ATPs. Adding the additional electrons captured during step 1 and 3 of β-oxidation, more ATP is made from fatty acid oxidation than would be for the same carbon length glucose molecule. The electrons from the reduced FAD are removed from the ACADs by a mechanism, involving electron-transferring flavoprotein (ETF), which only recently has become better understood(5-7).

Alternative forms of oxidation such as α-oxidation and ω-oxidation are necessary if carbon 3 has a functional group, such as a methyl group. The rest of the introduction will focus on defects in mitochondrial fatty acid oxidation, and primarily acyl-CoA dehydrogenases.

Acyl-CoA dehydrogenases (ACADs) are a family of flavoenzymes that are responsible for catalyzing α, β-dehydrogenation of acyl-CoA and using use ETF to transfer elections. There are at least eleven known family members which function in either straight chain β-oxidation of fatty acids or metabolism of

branched-chain amino acids. All ACADs are processed into the mature form in the mitochondria, but encoded in the nuclear genome and translated in the cytoplasm. The enzymes involved in straight chain β-oxidation are: very long chain acyl-CoA dehydrogenase, (VLCAD), acyl-CoA dehydrogenase-9 (ACAD9), long chain acyl-CoA dehydrogenase (LCAD), medium chain acyl-CoA dehydrogenase (MCAD) and short chain acyl-CoA dehydrogenase (SCAD). They are responsible for catalyzing the first steps of mitochondrial fatty acid oxidation. As their names suggest each enzyme has specificity for a particular chain length of fatty acid for example VLCAD towards palmitoyl-CoA (C16) making it the rate-limiting enzyme of long chain FAO. All diseases of FAO described here are inherited recessive disorders caused by loss of protein function.

VLCAD Deficiency

VLCAD differs from the rest of the acyl-CoA's, in that it is structurally active in homodimer form as opposed to homotetramer, and is associated with the inner mitochondrial membrane instead of found within the inner mitochondrial space. VLCAD can catabolize long chain fatty acids from 24-14 carbons in size but it has optimal specificity for chain lengths of C14-18(8). The cavity depths of ACADs account for the specificity for particular chain lengths of acyl carnitine chains as well as VLCAD also has a binding pocket much wider then other ACADs. The gene is approximately 5.4kb with 20 introns located on chromosome 17 between bands p11.2 and p11.13105. The resulting protein

encoded is 67 kilodaltons in size. Incidence of VLCAD disorder has been reported to be from 1:30,000 to 1:85,000 live births (9, 10).

Disease Characteristics:

ACADs are responsible for catalyzing the first step in FAO and VLCAD is the rate limiting ACAD; in the absence of functional VLCAD enzyme long chain fatty acids are accumulated and an energy deficiency is created. There have been three phenotypes associated with VLCAD deficiency, which represent energy deficiencies in different highly metabolic organs. Of the three phenotypes, the earliest onset is also the most severe. It often presents as a cardiac phenotype, with cardiomyopathy as well as hepatomegaly, hypotonia and hypoglycemia within the first few months of life. The second phenotype presents during childhood and is associated with a liver phenotype, characterized by reoccurring hypoketotic hypoglycemia. The final phenotype is the most mild, occurring in late childhood/early adulthood as a mostly muscle phenotype presenting with rhabdomyolysis and myopathy. Since the establishment of better screening, patients with more severe phenotypes have increased lifespans surviving to adolescence, and are showing phenotypes of late onset disease such as exercise-induced rhabdomyolysis. There has been a genotype-phenotype correlation that has been recorded with VLCAD deficiency that is not detected with MCAD deficiency(11). Null mutations are more likely to present with severe symptoms in early-childhood while patients with missense mutations

present with milder phenotypes. However since VLCAD does not have a predominating mutation, and many different mutations have been identified, some missense mutations have been associated with severe disease. Residual enzyme activities of specific mutations have also been useful in predicting clinical outcomes. Patients with less than 10% activity will develop clinical features in absence of treatment, and patients with less than 20% activity may also be at risk for serious clinical disease(12). For example, one fatal case occurred in a patient with a genotype encoding a protein that retains residual activity. This mutation is often found in many asymptomatic patients(13). Because VLCAD has over 80 different pathological mutations identified it is difficult to determine how all the mutants inhibit functional activity but most are thought to disrupt protein stability.

Screening/Testing:

As stated earlier, in patients with a metabolic block the transport of fatty acid accumulates, as acyl-carnitines, out of the mitochondria and into the blood occurs at a high frequency. These acyl-carnitine species are readily detectable by tandem mass-spectrometry (MS/MS). Screening by MS/MS for specific chain length accumulations provides clear evidence of a metabolic disorder; in the case of VLCAD, C14:1, C14:2, C14 and C12:1 chain lengths accumulate. VLCAD screening has been added to the standard panel as part of the newborn screening program across all fifty states. Prior to newborn screening up to 5% of

sudden infant death syndrome (SIDS) were likely caused by a disorder of FAO(14). Accumulations of acyl-carnitines are measured from a dried blood spot taken shortly after birth. Confirmation can be made by analysis of VLCAD enzyme activity from various tissues as well as analysis of β-oxidation of fibroblasts. Since the advent of newborn screening, the prevalence of VLCAD deficiency has become higher than originally expected and many patients remain asymptomatic suggesting they would have gone undiagnosed prior to newborn screening.

Management:

During periods of metabolic derangement patients are given IV glucose, often with insulin. To prevent this metabolic status, patients are to avoid fasting, myocardial irritation, dehydration, high fat diets and anesthetics containing high doses of long chain fatty acids(15). Patients with the severe forms of VLCAD deficiency are placed on medium-chain triglyceride (MCT) supplementation and often have nocturnal gastric drip feedings. Although MCT supplementation is considered safe, many question its usage and long-term effects. Uncooked cornstarch is often given as a source of sustained release glucose.

Experimental Therapies:

MCT supplementation:

Several clinical papers have cited severe VLCAD deficient patients' reversal of cardiac symptoms after daily MCT supplementation, but long-term studies have not been done in humans(16, 17). However, work published in mouse studies reveals that long-term supplementation with MCTs increases serum free fatty acids, shifts in body triglyceride storage, as well as fat accumulation and oxidative stress in the liver(18). Spiekerkoetter and colleagues have published multiple mouse studies comparing different treatments of MCT in VLCAD deficient mouse models. They have demonstrated that MCT bolus prior to exercise did not cause steatosis or impaired lipid metabolism and decreased accumulates in skeletal muscle (19, 20). MCT supplementation before exercise has had promising results in recent clinical studies as well. Eleven patients who had long chain fatty acid oxidation disorders including: carnitine palmitoyltransferase-2 (CPT2) deficiency, long-chain 3-hydroxyacyl CoA dehydrogenase (LCHAD) deficiency and VLCAD deficiency, were given either isocaloric MCT or carbohydrate supplementation and then completed a 45 minute treadmill workout. At a different time, patients were given the other supplementation and the same exercise protocol was repeated. Following MCT supplementation, patients demonstrated altered substrate oxidation, resulting in increases in ketones as well as a decreased heart rate (21). However another clinical exercise study saw no benefit to either IV glucose or MCT supplementation, in terms of exercise tolerance, in two VLCAD deficient patients

(22). No clinical studies have been performed evaluating the dose of MCTs or when dosing should occur (23).

Carnitine supplementation:

Clinical case reports have demonstrated clinical improvement in VLCAD deficient patients after starting carnitine supplementation. In mouse models for VLCAD deficiency, studies looking at carnitine supplementation saw an increase of toxic acyl-carnitine accumulates in tissues without replenishment of free carnitine(24, 25). Clinically, carnitine is often supplemented in addition to MCT.

Triheptanoin:

A clinical study was preformed first testing *in vitro* with VLCAD deficient fibroblasts and then *in vivo* with three patients with VLCAD deficiency for supplementation with odd chain fatty acids. The hypothesis was that by replacing medium even chain fatty acids with medium odd chain fatty acids, allowing production of both acetyl-CoA and anaplerotic propionyl-CoA, would result in improved cardiac and skeletal muscle function and energy production by allowing for replacement of catalytic intermediates of the citric acid cycle(26). Odd chain fatty acids of different chain lengths (C15, C9 and C7) were tested in VLCAD deficient patient fibroblasts and heptanoate (C7) was found to be the best potential therapy as normal amounts of propionyl carnitine (C3) were produced without a significant accumulation of heptanoyl carnitine (C7). Three patients

were switched from MCT therapy after three days of testing to triheptanoin. In comparison to MCT treatment, patients treated with triheptanoin produced both four and five carbon ketone bodies, not just four-carbon ketone bodies, and plasma heptanoate accumulates were no more than octanoate after MCT treatment. Patients 1 and 2 were on the therapy for 26 months and 22 months respectively, and only patient 2 had one hospitalization for rhabdomyolysis after 15 months on therapy. Significant improvement was observed in muscle strength almost immediately after treatment as well as reduction of hepatomegaly and cardiomyopathy in all patients.

Bezafibrate:

Bezafibrate has only been tested so far *in vitro* for VLCAD deficiency, but is widely prescribed for hyperlipidemia. The hypothesized mechanism is that fibrates may stimulate FAO by being an agonist of peroxisome proliferator-activated receptors (PPARs)(27). Increase of FAO capabilities of patient fibroblasts from myopathic forms of VLCAD deficiency, but not severe forms, was observed after exposure to bezafibrate. Another study tested 33 different fibroblast cell lines, with 45 different mutations, from VLCAD patients and was able to show phenotypic correction of 21 different genotypes(28). No difference was detected in VLCAD RNA expression between the 33 different phenotypes but in the 11 genotypes related to severe phenotypes little to no residual VLCAD activity was observed after treatment. A pilot trial of bezafibrate was performed

in 6 patients with related CPT-1 and CPT-2 deficiency resulting in improvement of conditions with increased physical activity and decreased muscle pain(29).

Dantrolene Sodium:

The benefit of adjunctive muscular relaxant dantrolene sodium was shown in a clinical case in one VLCAD patient with recurrent rhabdomyolysis(30).

Resveratrol:

In a study using fibroblasts from mild forms of VLCAD and CPT-2 deficient patients, a dose and time dependent increase of FAO flux was demonstrated after resveratrol treatment, suggesting a possible therapy for mild forms of VLCAD and CPT-2(31).

In conclusion, therapeutic options are very limited, including the current standard treatment of MCTs, as patients are still hospitalized with recurrent periods of hypoglycemia and rhabdomyolysis while taking MCTs and long-term effects have not been studied. Most experimental therapies focus on augmenting VLCAD protein such as bezafibrate and resveratrol, which do not work for severe cases of VLCAD deficiency where better therapeutic options are needed most.

ACAD9 Deficiency

ACAD9 has only recently been discovered with the gene identified in 2002(32) and reports of patients with ACAD9 deficiency in 2007(33). ACAD9 has an overlapping specificity with VLCAD from metabolizing fatty acids of C14 to C20, as well as sharing very similar sequence homology(34). Interestingly, it also is a functional dimer much like VLCAD, but unlike other ACADS. Unlike VLCAD, it is highly expressed in the brain with primarily neuronal expression(33). ACAD9 and VLCAD have similar expression levels in the liver, but the muscle is dominated by VLCAD expression. The role of mitochondrial β-oxidation in the human CNS is controversial as neurological problems are usually not present in patients with these ACAD deficiencies. However, of the three patients reported with ACAD9 deficiency all had neuronal abnormalities such as moderate to severe reduction of neurons in the neocortex, cerebellum and hippocampus(33). It has been suggested that ACAD9 plays a role in oxidative phosphorylation, and mutations in ACAD9 could be responsible for some causes of mitochondrial complex I deficiency which is linked to many neurological diseases(35, 36).

LCAD

No cases of LCAD deficiency have been reported in humans, and patients originally diagnosed with LCAD deficiency were found to have VLCAD deficiency after the VLCAD protein was discovered in 1992. In vitro, LCAD's activity ranges from C20-C6 with optimal activity at C12(8). Therefore VLCAD and LCAD would

have an overlapping specificity for certain lengths of long chain fatty acids. However, in vivo activity for LCAD shows specificity for branched chain fatty acid oxidation. Also unlike VLCAD and MCAD, which are highly expressed in liver, heart and skeletal muscle, LCAD's mRNA and protein expression is very low in these highly metabolic tissues in humans(37, 38). Interestingly in rodent models LCAD is highly expressed within these tissues, and LCAD deficient mice have a more severe phenotype than VLCAD deficient mice(37).

MCAD Deficiency

MCAD deficiency is the most common disorder of fatty acid oxidation with a disease frequency of approximately 1:10,000 (39). The human MCAD gene is 44kb long located on chromosome 1. A 421 amino acid precursor protein is encoded which is responsible for importation into the mitochondria, protein folding and assembly into the mature homotetramer form. It catalyzes fatty acids from C12-C4, with an optimal activity at C8. In MCAD deficiency, the most common mutation is a guanine instead of an adenine at position 985 (985A/G) which caused a lysine to be translated instead of glutamic acid at position 304 (K304E). It has been reported that at least 90% of patients are at least heterozygous for this mutation and 80% of those patients are homozygous for the K304E mutation(40). Newborn screening has revealed more information on less common mutations and now more than 54 variants of MCAD deficiency

have been characterized(40). Interestingly, MCAD has a clinically variable phenotype like VLCAD even though it has a relatively homozygous genotype unlike VLCAD. It is possible that environmental and epigenetic factors play a role in clinical outcomes, as patients carrying the K304E mutation, which is considered a severe mutation can remain asymptomatic(41). A mild phenotype of MCAD has emerged since newborn screening, which generally correlates to a heterozygous K304E mutation or two non-K304E mutations. However, patients with less severe mutations with high residual activity have still developed hypoglycemia and become comatose during metabolic decomposition and should still be considered at risk for clinical manifestations(42-44).

Disease Characteristics:

MCAD is regarded as mild in comparison to VLCAD deficiency, however in undiagnosed patients 25% die suddenly with the first presentation of disease. Of the survivors 30-40% show developmental delay and irreversible neurological impairment(45). Even with the early asymptomatic detection through newborn screening, deaths have been reported in MCAD patients and at least 20 patients who had previous clinical knowledge of the disorder have died suddenly(46). Patients usually present between three and 24 months, but adult presentations are possible and can result in sudden death(47, 48). The most common presenting symptom is hypoglycemia, often in combination with hypoketosis, hepatomegaly, hyperuricemia and elevated liver transaminases. Autopsies after

patient sudden death reveal cerebral edema, and fatty infiltrates in liver, kidneys and heart(49). In long-term studies, patients complain of fatigue, muscle pain and exercise intolerance(50).

Screening:

MCAD is part of the standard newborn screening program in all 50 states. MCAD is diagnosed by plasma accumulations of C6-C10, or accumulations in urine organic acids or acylglycines. Confirmation can be determined by fatty acid oxidation or MCAD enzyme activity in fibroblasts as well as molecular genetic testing.

Management:

During disease manifestations, simple carbohydrates or IV infusion of glucose may be necessary. Treatment for MCAD is mostly avoidance of fasting, and a relatively low fat diet. Uncooked cornstarch is often given at night for overnight glucose supply during infancy. Supplemental L-carnitine is still being evaluated for its clinical significance.

SCAD Deficiency

SCAD is the last enzyme in the acyl-CoA dehydrogenase cycle, and unlike the other disorders results in almost normal amounts of acetyl-CoA. Its prevalence has been found to be 1:50,000 in the Netherlands(51). It catalyzes

fatty acyl chain lengths from C4. It is caused usually by missense mutations that disrupt proper protein folding(52). There are two susceptibility missense variants often associated with SCAD, 511C>T and 625G>A. Compound heterozygosity with a severe mutation is likely to produce an SCAD deficiency. Biallelic susceptibility variants may also cause a clinical phenotype, but is generally thought not to be a significant risk due to how common the variants are within the general population.

Disease Characteristics:

Unlike VLCAD and MCAD, sufficient energy can be produced from the preceding steps of fatty acid oxidation. Hypoglycemia is rare in SCAD patients and they generally have normal ketogenesis(53, 54).The accumulation of butyric acid (C4) and its derivatives are not toxic to the heart and liver. However neurological symptoms of SCAD can be attributed to butyric acid and its derivatives, mainly ethylmalonic acid, accumulating within the central nervous system. Almost all patients present with clinical symptoms in early life, generally before the age of five. SCAD has an extremely broad clinical phenotype with many patients remaining normal while others show severe symptoms including dysmorphic facial features, failure to thrive, metabolic acidosis, ketotic hypoglycemia, lethargy, developmental delay, seizures, hypotonia, dystonia and myopathy(55). In the largest study to date of 114 patients, three groups emerged encompassing most of the patients with: 30% presenting with developmental

delay and hypotonia without seizures, 25% with developmental delay and seizures and 20% with failure to thrive and hypotonia(56). Overlapping phenotypes of failure to thrive, developmental delay and hypotonia were observed in 14% of patients. The remaining patients either had a mixture of symptoms including dysmorphic features, cardiomyopathy, myopathy and hepatic steatosis (7%) or remained asymptomatic (4%). However, symptoms often disappear after initial diagnosis and can often be explained by other causes.

Testing/Screening:

SCAD is not specifically tested for by the state of Massachusetts as part of the newborn screening process, but through testing for VLCAD and MCAD, which are mandated, patients who potentially have SCAD are potentially recognizable. SCAD deficient patients have elevated levels of butyryl carinitine (C4) in blood or plasma spots or increased concentrations of ethylmalonic acid in their urine. SCAD deficient patients may have either a mutation/mutation or mutation/susceptibility variant or variant/variant in both ACADS alleles(51). SCAD enzyme levels are not clinically helpful, but skin fibroblast fatty acid oxidation studies can reflect enzyme levels and can confirm diagnosis(57).

Management:

The need for treatment of these patients is unclear because most patients are asymptomatic when healthy. However, like VLCAD and MCAD, prevention of symptoms is maintained by avoidance of fasting. There are no accepted recommendations as far as dietary manipulations. During periods of metabolic acidosis, or hypoglycemia, which is uncommon in SCAD, treatment is similar to other disorders of fatty acid oxidation with intravenous fluids therapy of high dextrose solutions to promote anabolism. Supplementation of riboflavin has been suggested as a possible therapy as it is the precursor to flavin adenine dinucleotide (FAD) which is an essential cofactor for SCAD(58).

Other disorders of Fatty Acid Oxidation

With 21 genes encoding at least 17 different enzymes for mitochondrial β oxidation, mutations in most genes associated with mitochondrial β oxidation correlate with human disease(4). There are also diseases associated with peroxisomal oxidation, however symptoms originate more from toxic accumulations than from energy deficiencies. Here the focus is on four disorders that have similar presentations and symptoms to acyl-CoA dehydrogenase deficiencies, particularly VLCAD, two also involved in oxidation of long chain fatty acids and two involved in transportation into the mitochondria.

CPTI:

Carnitine palmitoyltransferase-1, the enzyme responsible for bringing long-chain fatty acids into the mitochondria, is made by three distinct genes to produce a CPT-1a liver isoform, CPT-1b skeletal/cardiac muscle isoform and CPT-1c brain isoform. Only CPT-1a has been associated with human disease, with patients presenting with hypoketotic hypoglycemia, but with little to no cardiac or skeletal involvement as CPT-1b is the predominant isoform in skeletal/cardiac tissue. CPT-1a and CPT-1b knock-out mice are embryonic lethal, interestingly the CPT-1c brain isoform is viable and its function is not well understood as it does not possess palmitoyltransferase activity(59).

CPTII:

CPTII is responsible for converting the long chain fatty acid back to the acyl-CoA form during transport into the inner membrane of the mitochondria. Patients deficient in this enzyme have very similar phenotypes to VLCAD deficient patients with the most severe forms presenting at infancy with hypoketotic hypoglycemia, cardiomyopathy and sudden death. Patients with adolescent to adult presentation have exercise-induced pain and weakness and myoglobinuria.

mTFP and LCHAD:

The mitochondrial trifunctional protein (mTFP), consists of 4 α subunits and 4 β subunits and carries out steps 2-4 of FAO for long chain fatty acids. The α units are responsible for steps 2 and 3 and the β for step 4. LCHAD, long chain 3-hydroxyacyl-CoA dehydrogenase, activity is contained in the α subunit, and mutations within this result in hypoketotic hypoglycemia. Mutations can also affect all three enzymatic activities, mTFP deficiency, and result in cardiomyopathy. Interestingly mTFP and LCHAD deficiency present with two additional phenotypes not associated with other defects in long-chain fatty acid metabolism. In mTFP patients, 80% present with neuropathy, but only 5-10% of patients with LCHAD(60, 61). Conversely, 30-50% of LCHAD patients present with retinopathy, whereas only 5-13% of mTFP patients have retinopathy(60-63). Neuropathy and retinopathy are not generally associated with the other disorders of long chain fatty acid oxidation.

In summary, mitochondrial FAO has an essential function in energy production, especially in highly metabolic organs such as the liver, heart and skeletal muscle, as well as in degrading toxic accumulates. There are multiple disorders associated with mitochondrial FAO that are clinically important and most are detected as part of the Newborn Screening program. To date no definitive therapy exists for these diseases.

CHAPTER II: Gene Therapy for Beta-Oxidation Disorders

Gene Therapy

In principle, using a genetic therapy to correct a single gene disorder is very simple. Augmentation of protein expression for autosomal recessive disorders caused by loss of function or silencing protein expression for dominant disorders caused by gain of function can provide therapies for a multitude of diseases. However the technological hurdles associated with the practical correction of these diseases are intrinsically more challenging. Safety as well as efficiency must be evaluated; while a given vector may excel in one aspect it may also disappoint in another.

The first hurdle to overcome is the vector's ability to transport the genetic material into the targeted cells. Either cells can be removed and the therapy can be preformed *ex vivo*, or the targeted cells can be treated *in vivo*. Several methods have been proposed, for *in vivo* gene transfer including: plasmids, viral vectors, and liposomes.

Among viral vectors, adeno associated virus (AAV) has stood out in terms of both efficiency and safety. AAV, was originally discovered as a contaminant of Adenovirus preparations, which is where it derives its name but is not related genetically to Adenovirus. It is a member of the parvovirus family of the genus *dependovirus*, and as its name suggests it is replication deficient depending on other viral genes in order to replicate. Because of this natural life cycle, AAV remains latent in infected cells predominantly in extra chromosomal concatemers

until provided with proteins for replication by another virus such as adeno or herpes virus(64, 65). AAV is associated with no known human disease, and many of the serotypes are widespread throughout the human population, with up to 90% of the adult humans seropositive for at least one known serotype(66). These innate wtAAV viral attributes allow for AAV to be a safe and efficient viral vector *in vivo*.

AAV Virology

The 4.7kb single stranded DNA viral genome is very simple in structure, consisting of two open reading frames, *rep* and *cap* and two non-coding 145 nucleotide inverted terminal repeat (ITR) sequences at the 5' and 3' end(67, 68). The *rep* gene is transcribed from two different promoters to allow for production of 4 Rep proteins. The *cap* gene is transcribed from one promoter to produce a total of three proteins through alternative splicing and a non-canonical ACG start codon. The capsid structure is T=1 icosahedral particle, with a total of 60 copies of the three viral proteins at a ratio of 1:1:8 of VP1:VP2:VP3. Recently another protein was found to be encoded within the *cap* gene responsible for trafficking cap proteins to the nucleolus for assembly as well as playing a role in viral assembly(69).

Over 100 novel serotypes have been discovered largely by Gao and Wilson(70), at least ten have been well classified. Although differing AAV's are commonly referred to as "serotypes" they are not true serotypes in that they are

not immunologically distinguished. AAVs are now classified using HIV taxonomy to segregate AAV into six “clades” based on sequence diversity so that they share overall structure, serology and functional aspects(70-72).

AAV enters the cell through receptor-mediated endocytosis, allowing for cellular specificity. Different AAV serotypes have been associated with different receptors: AAV1 binding α2-3- and α2-6-N-linked sialic acid(73-75), AAV2&3 binding heparin sulfate proteoglycan receptor, with a co-receptor of either fibroblast growth factor receptor or αv-β5 integrin(76-79), AAV4 binding α2-3-O-linked sialic acids(80), AAV5 binding α2-3N linked sialic acid with platelet derived growth factor receptor(73, 80, 81), AAV6 binding both heparin sulfate proteoglycan and sialic acid(75, 82), and AAV8&9 associated with the widespread laminin receptor but the primary receptor for AAV9 is N-linked galactose (83, 84). The varied AAV serotype receptor specificities allow for differing tropism between cell types and within different organisms.

AAV Gene Therapy

To construct recombinant AAV (rAAV) vectors all viral coding regions are deleted and only the ITRs are retained for packaging. *Rep* and *cap* genes are provided *in trans* as well as additional adenoviral helper genes. Often viruses are transcapsidated by using the AAV2 ITRs but differing capsid sequences as they determine tropism, and packaged using AAV2 *rep* gene. Additional vector manipulation has allowed for normal single stranded AAV (ssAAV) genome to be

converted into a transcriptionally-active self complementary double stranded genome (scAAV) by mutations in the ITRs(85). Although packaging capacity is halved, these vectors have been shown to be more efficient since they skip the rate-limiting steps of transduction of either second-strand synthesis or opposite strand self-annealing(86, 87).

By using different capsid genes, rAAV's can be targeted to specific tissues for different therapeutic effects. The route of administration also plays a role in efficiently targeting specific tissues. rAAV9 has been found to have a very broad distribution when injected intravenously showing expression in tissues such as the liver, heart, muscle, brain, and lung in rodents with more robust expression than many other vectors(88, 89). rAAV9 has also shown robust expression when injected locally, whether in the eye by subretinal injection(90) or brain by intracranial injection(91). Modifications have also been made to enhance tissue transduction of rAAV vectors. Specific tyrosines in the AAV capsid have been identified which can be phosphorylated causing impaired transduction and trafficking, however making point mutations to these tyrosines allows for high efficiency transduction by avoiding ubiquitination and proteasome-mediated degradation(92). By avoiding proteasome degradation these vectors are also less immunogenic.

Because some AAV's such as AAV9, have broad transductions, modifications have been made to rAAV vectors to be more tissue specific. The modifications can be split into two groups: modifying the capsid to change the

tissue tropism or modifying the genome sequence to limit expression in certain tissues. One method of changing the capsids specificity is by inserting peptide ligand sequences into the capsid(93, 94). DNA shuffling from multiple serotypes has also been used to alter tropism(95-97). In addition, specific mutations can be made to the capsid structure, primarily at known receptors or co-receptors, to alter viral tropism(98). In order to change the expression of the transgene rather than the viral tropism two different strategies have been employed. One strategy involves using tissue specific promoters to drive expression in only the target tissues. The other strategy, uses RNAi to de-target expression in unwanted tissues. Xie *et al.* put microRNA binding sites for miR-122, which has high prevalence in the liver, and miR-1, which has high prevalence in the heart and skeletal muscle, within the 3' untranslated region of their reporter gene to downregulate expression in the liver, heart and skeletal muscle, in order to get more specific CNS expression(99). Future directions for further specificity in targeted tissue transduction can be foreseen by combining techniques for a more tropic virus as well as specific promoter targeting and RNAi de-targeting within the same vector, or by combining multiple vectors.

AAV Gene Therapy Trials

rAAV vectors were first approved in 1994 for airway delivery in a human trial for cystic fibrosis, which subsequently began in November 1995(100). This study progressed to enroll over 100 patients and went on to a Phase 2b. The

first published trials, were for hepatic and intramuscular delivery of Factor IX in Hemophilia B patients(100). The hepatic delivery however was hampered by transient increase in hepatocellular enzymes and an immune response resulting in loss of expression(101). Immune responses have been detected against either the capsid or the transgene, but they are not always associated with clearance of expression(102). A Phase 2 trial for α-1-Antitrypsin deficiency has had promising results in spite of inflammatory infiltrates, although therapeutic levels of protein have not yet been reached(103). In all, over 25 different clinical trials have been approved treating over 13 different disease including Parkinson's disease, Canavan's disease, α-1-Antitrypsin deficiency, muscular dystrophies and retinal degeneration(100). Differing routes such as intracranial, intracardiac and intraocular administration, and differing serotypes AAV1, 2, 5 and 6 have all been approved.

Gene Therapy for Disorders of Fatty Acid Oxidation

In 1997, Kelly *et al.* created a liver specific SCAD knock-in by microinjection of SCAD-minigene within the SCAD deficient mouse model. They were able to observe decreased lipid accumulates in the liver by oil-red-o staining and systemic correction of decreased accumulation of butyryl carnitine in the urine(104). These studies provided a foundation that gene therapy through specific tissue targeting is possible for disorders of fatty oxidation, and also detected overexpression of the therapeutic protein was not detrimental. Holm *et*

al. next observed gene transfer to livers of SCAD deficient mice by hydrodynamic transfer(105). Although gene transfer occurred and 5% of liver cells expressed functional SCAD proteins 31 days post injection, systemic correction by reduced blood butryrl carnitine after fasting was not detected. Conlon *et al.* published on gene therapy for SCAD disorder using intramuscular injection of rAAV1 and rAAV2 encoding SCAD providing both correction *in vitro* of SCAD deficient patient cells and *in vivo* in SCAD deficient mice(106). This targeted muscle gene therapy showed systemic correction of serum butyryl carnitine levels after fasting, using rAAV1 ten weeks post injection. Also, a method of detecting lipid accumulates within specific tissues non-invasively *in vivo* was validated using Magnetic Resonance Spectrometry (MRS). Next Beattie *et al.* used a liver directed approach, like Kelly *et al*, but using rAAV5 and rAAV8 for gene therapy in the SCAD deficient mouse(107). Using portal vein injections of rAAV8, protein expression was targeted to the liver where a decrease in lipid accumulates was observed by both oil-red-o staining and MRS 10 weeks post injection. Systemic correction was also observed by reduction of serum butyryl carnitines after fasting.

In vitro correction of MCAD deficiency using a recombinant adenoviral vector has been performed but so far no gene therapy *in vivo* has been published for MCAD deficiency. MCAD deficient human fibroblasts were infected with recombinant adenoviral vectors encoding MCAD, and whole cell medium showed

reduction of C6, C8 and C10(108). These results are promising for future studies of an *in vivo* MCAD gene therapy.

Although there is no known disease caused by LCAD deficiency in humans, an LCAD deficient mouse model exists. Unlike humans, mice express LCAD at high levels in metabolically active tissues such as liver, skeletal and cardiac muscle(37, 38). The LCAD mouse model has a more severe phenotype then VLCAD mice, which mimics the severe clinical phenotype of VLCAD deficient patients(109). Correction of LCAD +/- mice, which display an intermediate phenotype, was shown by both a muscle-targeted, rAAV1 injected intramuscularly, and a liver-targeted, rAAV8 through the portal vein, approach(110). Reduction of the lipid peak by MRS was observed in the muscle 10 weeks after intramuscular injection or rAAV1 as well as a systemic effect on decreased macrosteatosis in the liver by oil-red-o staining in female mice. Muscle-targeted transduction however was not able to reduce acyl-carnitine accumulates in the serum. Reduction of both macrosteatosis and microsteatosis was observed by oil-red-o staining after portal vein injection of rAAV8.

Hydrodynamic injection of VLCAD into VLCAD deficient mice was able to show expression of functional VLCAD protein, as well as correction *in vitro* observed in human VLCAD deficient fibroblast cells by reduction of acyl-carnitine accumulates(111). rAAV8 gene therapy using the CMV promoter delivered by systemic tail vein injection, was published by the same group (112). Expression was shown in the liver of these mice at an early time-point, 11 days post-

injection, but was not detected at a later time-point of 102 days post-injection, although vector genomes were still present. Expression of VLCAD in the heart increased between 11 and 102 days, but muscle transduction was generally poor. Correction of acyl-carnitine accumulations in the blood was observed throughout the study as well as fasting induced hypoglycemia. Based on the previous work, we hypothesized that we could obtain correction of clinically relevant phenotypes of VLCAD deficiency in VLCAD deficient mice if we had long-term expression of VLCAD protein in the liver, cardiac and skeletal muscle by systemic injection of rAAV9 expressing VLCAD protein driven by a cytomegalovirus enhancer/chicken β-actin promoter (CBA) promoter. The following chapters will discuss this study of long-term expression of VLCAD protein after systemic injection of rAAV9-VLCAD(113). As well as addressing the important expression of VLCAD also observed in the brain after systemic injection suggesting that rAAV9-VLCAD crossed the blood brain barrier. Systemic correction was observed in reduction of blood acyl-carnitine accumulates, but tissue specific accumulates were measured in the liver, heart and muscle *ex vivo*, and in the liver and muscle *in vivo* by MRS. For the first time, correction of disease specific phenotypes, such as cold intolerance, induced hypoglycemia and hypotonia, were observed in animals receiving rAAV9-expressing VLCAD. This study shows significant proof-of-principle for gene therapy to correct VLCAD deficiency, and taken together these studies have important clinical applications for diseases of mitochondrial fatty acid oxidation.

Chapter III: Gene Therapy for VLCAD- Transduction and Expression

Introduction

A large number of different serotypes of AAV have recently been discovered(71), and each have unique properties, giving gene therapists a diverse toolbox from which to chose their vectors. VLCAD deficiency presents with different phenotypes each relating to highly metabolic tissues: a severe heart phenotype presents early in life with cardiomyopathy, a liver phenotype characterized by hypoketotic hypoglycemia, and a muscle phenotype characterized by rhabdomyolysis and exercised-induced muscle pain and intolerance. Some patients experience symptoms from multiple phenotypes and as patients age they often shift from early onset heart and liver phenotypes to the muscle phenotype(114).

In the previous attempt using gene therapy for treatment of VLCAD deficiency, rAAV8 serotype was used(112). VLCAD expression was not detected long-term in the liver, nor was VLCAD protein highly expressed in the muscle. In order to target each tissue associated with disease in VLCAD, long-term and efficient expression must be achieved in the liver, cardiac and skeletal muscle. This treatment could effectively treat all phenotypes of VLCAD deficiency, as well as phenotypes that would develop with age. rAAV8 is usually associated with long-term transduction of the liver, however in the previous study the

cytomegalovirus (CMV) promoter was used, which is known to be turned off in the liver(115). In this study rAAV9 was used as it efficiently targets the liver, cardiac and skeletal muscle(89, 116), along with the hybrid chicken beta actin (CB) promoter, which does not get shutdown in the liver. Using these tools we hypothesize that long-term expression of VLCAD will be observed in the liver, cardiac and skeletal muscle, which will in turn provide therapeutic benefit to all tissues associated with VLCAD deficient phenotypes.

Methods

Animals:

VLCAD -/- mice were created by Exil *et al.* and purchased from Mutant Mouse Regional Resource Centers (MMRC, University of Missouri, MO). VLCAD-/- animals were created by breeding VLCAD-/+ animals producing VLCAD-/- and VLCAD+/+ littermate controls, as well as VLCAD-/+ for future breeding. Mice were maintained in a pathogen-free facility with 12hr light and dark schedule. Mice were fed PicoLab Mouse Diet 20 5058 (LabDiet, Richmond IN) until two weeks post-injection and then were placed on a standard chow. Mice received both diets and water *ad libitum*.

All animal procedures were approved by University of Massachusetts Medical School Institutional Animal Care and Use Committee as well as University of Florida Institutional Animal Care and Use Committee in accordance with the Association for Assessment and Accreditation of Laboratory Animal Care International specifications.

rAAV vectors:

rAAV2/9 pseudotyped vectors were generated to express human VLCAD under the transcriptional control of the cytomegalovirus enhancer/chicken β-actin promoter (CBA) (115). rAAV vectors were produced, purified and tittered as previously described (UMMS Gene Therapy Center, Worcester MA)(117).

Genomic DNA extraction and Quantitative PCR:

DNA was extracted and quantified as previously described(118). Animals were sacrificed at indicated time points and tissues were harvested in a manner to avoid cross-contamination, snap frozen in liquid nitrogen and stored at -80°C. Genomic DNA (gDNA) was extracted using a DNeasy blood and tissue kit (Qiagen Inc., Valencia, CA, USA) according to the manufacturer's instructions. gDNA concentrations were determined using an Eppendorf Biophotometer (Eppendorf, Hamburg, Germany).

rAAV genome copies in the gDNA from heart, liver, tibialis anterior (TA) muscle, gonands, lung, spleen, lymph nodes, brain and brown fat were quantified by qPCR with an ABI 7900 HT sequence detection system (Applied Biosystems, Carlsbad, CA, USA) according to the manufacturer's instructions and results were analyzed using SDS 2.3 software. Briefly, primers and probe were designed to amplify SV40 poly-A tail of the rAAV9-CBA-VLCAD vector. A standard curve was generated using plasmid DNA containing the same SV40 poly-A target sequence. PCR reactions contained a total volume of 100µL and

were run at the following conditions: 50°C for 2 minutes, 95°C for 10 minutes, and 45 cycles of 95°C for 15 seconds and 60°C for one minute.

DNA samples were assayed in triplicate. In order to assay PCR inhibition, the third replicate was spiked with plasmid DNA at a ratio of 100-copies/µg gDNA. If this replicate was greater than 40-copies/µg gDNA then the results were considered acceptable. If a sample contained greater than or equal to 100-copies/µg gDNA it was considered positive for vector genomes. If a sample contained less than 100 copies/µg gDNA it was considered negative for vector genomes. If less than 1µg of gDNA was analyzed to avoid PCR inhibition, the vector copy number reported was normalized per µg gDNA and the plasmid spike in was reduced to maintain the ratio of 100-copies/µg gDNA.

Immunohistochemistry:

Tissues were fixed in 10% neutral buffered formalin, and embedded in paraffin. Immunohistochemistry was carried out by the Molecular Pathology and Immunology Core at University of Florida using the DAKO Autostainer plus protocol. Briefly, 4 µm serial sections were removed of paraffin and incubated with 3% H_2O_2 in methanol to block endogenous peroxidase activity. Sections were treated with Trilogy (Cell Marque, Rocklin, California) at 95^0 C for 25 minutes and blocked with Sniper (Biocare Medical, Walnut Creek, CA) to reduce non-specific background staining. Sections were incubated with rabbit anti-mouse VLCAD at room temperature for 1 hour. Then sections were incubated

with Mach2 Gt x Rb HRP polymer (Biocare Medical, Walnut Creek, CA) for 30 minutes. Staining was visualized with DAB chromagen (Biocare Medical, Walnut Creek, CA).

Results

To assess the transduction and expression of rAAV9-VLCAD cDNA delivery, 6-8 week-old male VLCAD-/- or VLCAD+/+ littermate controls were injected into the tail vein with either rAAV9-CBA-VLCAD ($1x10^{12}$vg) as a therapeutic agent or rAAV9-CBA GFP or PBS as controls. Quantitative real-time PCR was performed on gDNA isolated from multiple tissues at 22-26 weeks post injection to determine tissue distribution of vector genomes (Fig. 3.1). All tissues were negative for vector genomes in PBS VLCAD-/- or PBS VLCAD+/+ controls. In mice injected with rAAV9-VLCAD, the highest vector genome concentration in tissues associated with fatty acid oxidation, was observed in the liver followed by heart, skeletal muscle and brown fat. Expression is shown by hVLCAD antibody staining of the liver, heart, TA muscle and brown fat (Fig. 3.2a-h). Also vector genomes were found present in tissues not associated with fatty acid oxidation including gonads, lung, spleen and lymph nodes (Fig. 3.1). Surprisingly a large amount of vector genomes were found in the brain, which will be discussed in depth in Chapter 4 (Fig 3.1). Although transduction of the liver had the highest transduction among the tissues, liver expression was not widespread, with numerous cells expressing VLCAD at high levels while others did not express

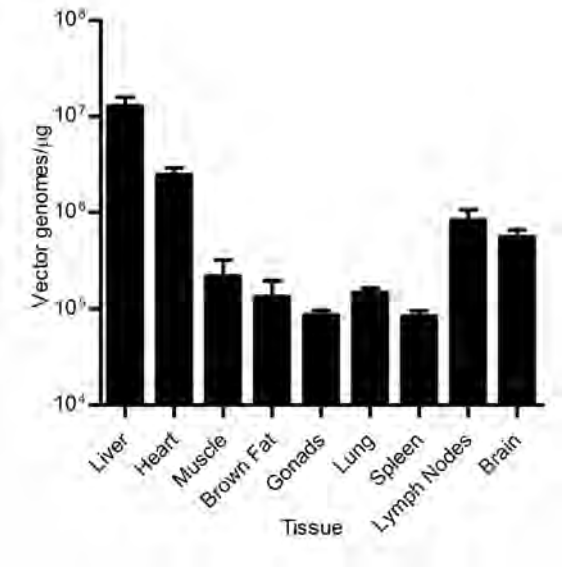

Figure 3.1 Transduction of rAAV9-VLCAD

Quantitative PCR of vector genomes. Means of 3 separate assays± SEM (error bars) are shown for each organ. *n*=7 for VLCAD-/- PBS Control, 6 for VLCAD-/- rAAV9-VLCAD treated and VLCAD +/+ PBS Control. Only VLCAD-/- rAAV9 treated are shown, as PBS Controls were all negative.

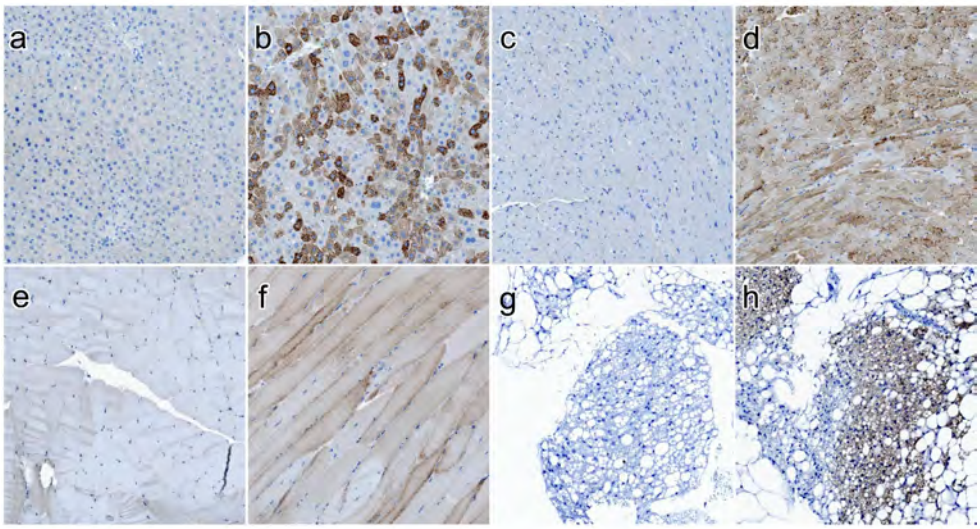

Figure 3.2 Expression of rAAV9-VLCAD

Representative images at 5x magnification of VLCAD antibody staining in VLCAD-/- mice, sacrificed at range between 21-26 weeks post injection. The tissues are labeled as follows: (a) Liver PBS Control (b) Liver, rAAV9-VLCAD treated (c) Heart, PBS Control (d) Heart, rAAV9-VLCAD treated (e) Tibialis anterior (TA) muscle, PBS Control (f) TA, rAAV9-VLCAD treated (g) Brown fat, PBS Control and (h) Brown fat, rAAV9-VLCAD treated.

VLCAD, which may be related to the perivascular (Fig. 3.2 b). Expression of VLCAD in the heart and TA was widespread (Figs. 3.2d, f). Interestingly, transduction and expression was detected in the brown fat (Figs. 3.2h).

Liver and muscle were also stained with hematoxylin and eosin and scored by pathologist, who was blinded to the treatment groups, for inflammation as well as macrosteatosis and microsteatosis (Fig 3.3). Some inflammation in the liver was observed across all groups but no significant difference was observed in inflammation between AAV9-VLCAD treated VLCAD-/- mice or PBS controls. Surprisingly, low levels of portal vein inflammation and macrosteatosis were observed in VLCAD+/+ PBS animals that were not observed in the treated or untreated VLCAD-/- animals. No inflammation was detected in any group within the muscle. Taken together, these results indicate that rAAV9-VLCAD vectors were able to sufficiently transduce and express for over 6 months in vital organs, which rely on fatty acid oxidation.

However, female VLCAD-/- mice injected with the same vector, rAAV9-CB-VLCAD, at the same dose $1x10^{12}$vg did not display the same expression patterns as the male mice. In Figure 3.4, it is apparent that expression within the liver is markedly reduced, with little to no expression, the converse of what is observed in male mice. This finding is not surprising, as it has been previously published that in mice AAV transduction in the liver is testosterone dependent(119). Expression within other tissues, such as the heart and muscle, seem not to be affected and is similar to expression in male mice(Figure 3.4).

Figure 3.3: Inflammation of Liver Post-injection

Liver sections from 22-26 weeks post injection were stained with hematoxylin and eosin and scored on a 0-4 scale, with 4 being the most severe inflammation, by a blinded pathologist for (a) parenchymal inflammation (b) portal inflammation (c) macrosteatosis (lipid vesicles that distort the nucleus) and (d) microsteatosis (lipid vesicles present but do not distort the nucleus). N=7 for VLCAD-/- PBS Control and n=6 for both AAV9 treated and VLCAD+/+ PBS Control.

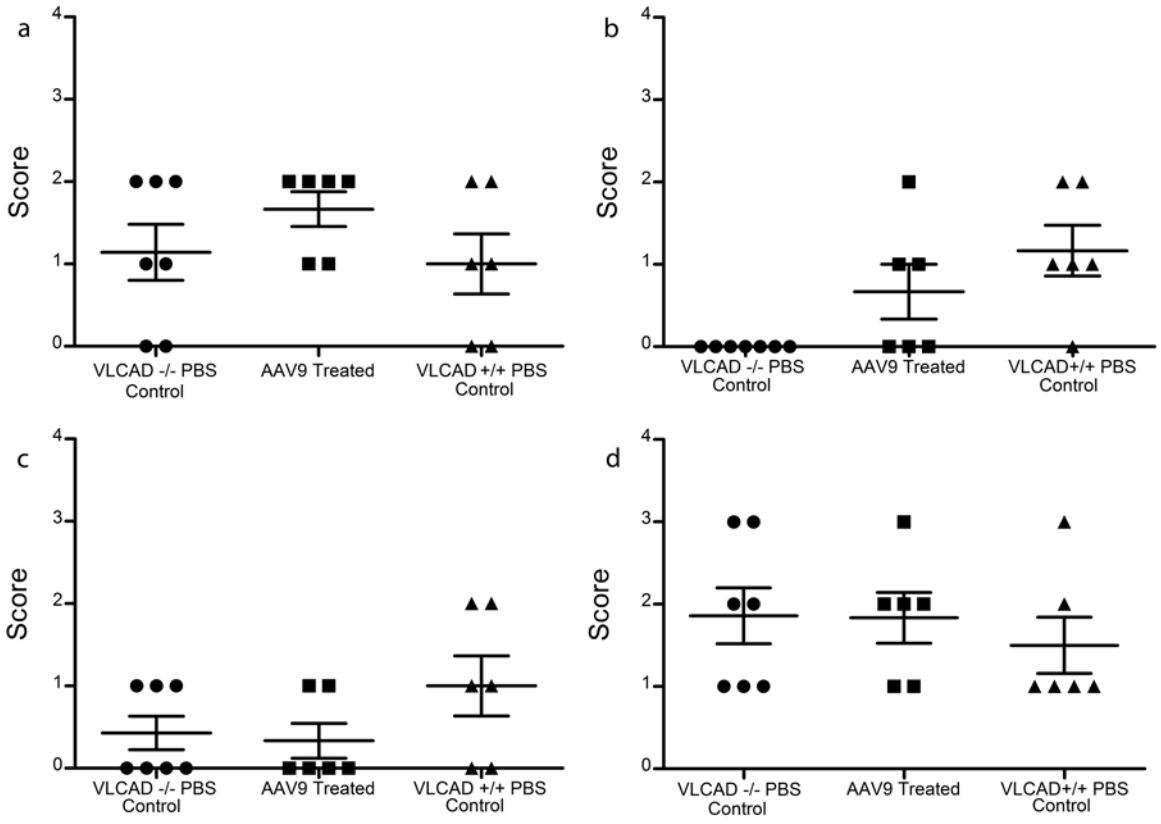

Figure 3-3: Inflammation of Liver Post-injection

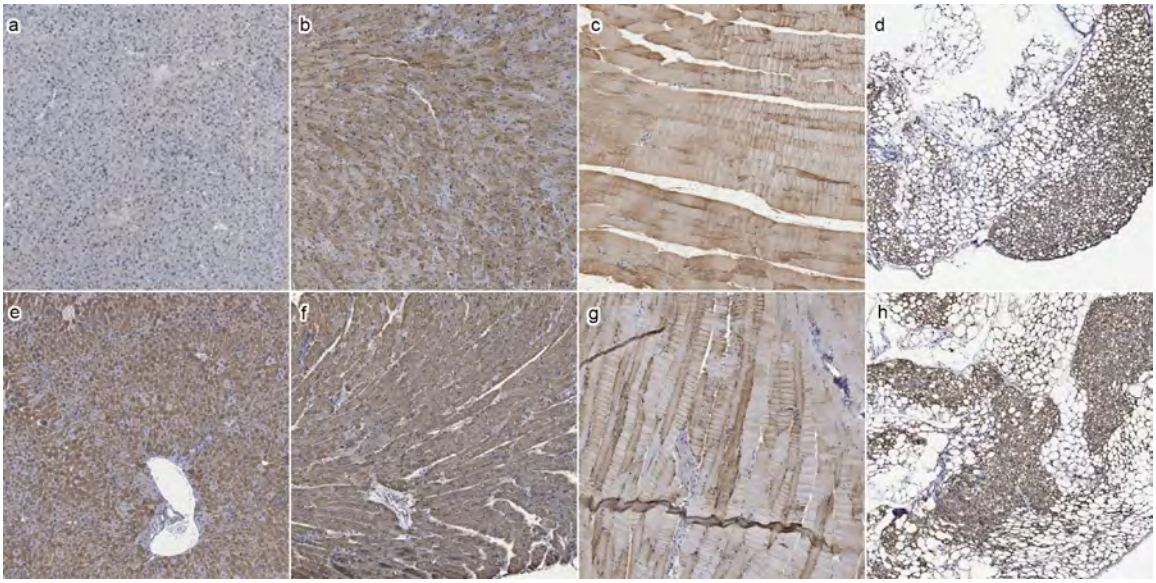

Figure 3.4 Expression differences of rAAV9-VLCAD in Male and Female mice

Representative images at 4x magnification of VLCAD antibody staining in male and female mice VLCAD-/- mice 12 weeks post injection of rAAV9-VLCAD. Panels a-d represent female mice: (a) Liver (b) Heart (c) Muscle (d) Brown Fat. Panels e-f represent male mice: (e) Liver (f) Heart (g) Muscle (h) Brown Fat.

Discussion

Unlike the previous work by Merritt and colleagues(112), we were able to show long-term expression of VLCAD in all targeted tissues including liver, brown fat, cardiac and skeletal muscle. The difference in long-term expression in the liver could have been due to the use of the CBA expression cassette over the CMV promoter, the latter of which is known to be inactivated in the liver in the absence of NFkB(115). Efficient, long-term transduction and expression in the muscle can be attributed to rAAV9's tropism(89).

Expression of VLCAD in brown fat after systemic injection is novel. To our knowledge, there have been no reports that have shown transduction of brown adipose tissue and only two reports attempting to target white adipose tissue. Both reports used AAV1 and required an enhancing agent in order to get efficient transduction(120, 121). In this report, we were primarily concerned with brown adipose tissue because of its important role in thermogenesis, which will be discussed in depth in Chapter 5. Brown fat differs from white adipose tissue in that it is highly vascularized, which gives rAAV9 easy access to brown adipose tissue when given systemically. However that does not necessarily imply transduction or expression. Transduction was also detected in other tissues including the brain, lung, lymph nodes, spleen and gonads. De-targeting strategies such as capsid mutations and tissue specific promoters and microRNAs may be employed to minimize transduction and expression in unwanted tissues, if this ultimately proves to be necessary. The expression

pattern of little to no transduction observed in female mice in the liver, however normal expression was detected in other tissues. However it can easily be explained through androgen-dependent liver expression by AAV already documented in mice(119). Although different serotypes experience more or less of this effect, rAAV9 sex-dependent expression has not been well characterized(122). Sex-dependent expression has not been detected in non-human primates. The expression pattern observed in female mice presents a potential tool for studying the liver's role in correction of disease-specific phenotypes and will be discussed more in further chapters.

CHAPTER IV: Transduction of Brain after Systemic Injection

Introduction

Foust *et al.* were able to first show self complementary AAV9's (scAAV9) (described in Chapter II) ability to cross the blood brain barrier (BBB) and transduce cells in the brain after systemic delivery(123). After systemic injection with scAAV9, broad transduction was observed in neonates, whereas in adult mice expression was mostly in astrocytes of the brain. They hypothesized that differences in transduction patterns were due to the underdeveloped BBB in neonates. However tight junctions which are responsible for some of the barrier function of the BBB, are fully developed during early development(124). But it has been suggested that astrocytes' endfeet are not fully developed, and are also present at low levels which may have an effect on transduction pattern differences reported between neonates and adults(124, 125). Interestingly, when AAV9 is directly injected into the brain of adult mice it has little specificity for astrocytes. Another possibility is that AAV is able to cross the BBB by receptor-mediated transcytosis, as some AAVs have been shown to cross barrier endothelial and epithelial cells. As the brain develops different receptors are expressed potentially accounting for differences in transduction patterns between neonates and adults(126).

Other groups have shown single-stranded vectors are also able to cross the BBB; however, very limited results have been shown in adult mice(126, 127). All these studies used GFP as reporter gene for expression. Currently only one

therapeutic study has been conducted by Fu *et al.,* using single stranded rAAV9 vectors in adult mice to treat mucopolysaccharidosis IIIB deficiency. This study, although does not specifically assay for transduction since the therapeutic protein is secreted, did see significant reduction of disease specific phenotypes within different areas of the brain(128). The mucopolysaccharidosis IIIB protein is unable to cross the BBB on its own, causing recombinant protein therapy to be unavailable for these patients. But the rAAV could have transduced the brain vasculature, allowing for the protein to be secreted directly into the brain. Although some studies suggest that single stranded rAAV9 is unable to efficiently cross the BBB in adult mice(127) Fu's work suggests that there may be enough expression for correction(128).

In this study, we confirm expression of VLCAD protein after intravenous administration of single stranded rAAV9 in the brain of adult mice after our initial observation of surprising amounts of vector genomes in the brain. Here, VLCAD is used as reporter gene rather then a therapeutic gene as VLCAD protein is not highly expressed in the brain and does not play a known role in VLCAD deficiency in patients. VLCAD expression is compared to the traditional reporter GFP, and found to be much easier to detect. This study suggests that brain transduction after intravenous delivery of single stranded rAAV9 may currently be underestimated.

Materials and Methods

Animals:

VLCAD -/- mice were created by Exil *et al.* and purchased from Mutant Mouse Regional Resource Centers (MMRC, University of Missouri, MO). VLCAD-/- was created by breeding VLCAD-/+ animals creating VLCAD-/- and VLCAD+/+ littermate controls. Balb/c and C57/B6 mice were purchased from Jackson Laboratories (Bar Harbor, ME). Mice were maintained in a pathogen-free facility with 12hr light and dark schedule. Mice were fed a standard chow and water *ad libitum*.

All animal procedures were approved by University of Massachusetts Medical School Institutional Animal Care and Use Committee as well as University of Florida Institutional Animal Care and Use Committee in accordance with the Association for Assessment and Accreditation of Laboratory Animal Care International specifications.

rAAV vectors:

rAAV2/9 pseudotyped vectors were generated to express human VLCAD, of GFP under the transcriptional control of the cytomegalovirus enhancer/chicken β-actin promoter (CBA) (115). rAAV vectors were produced, purified and tittered as previously described (UMMS Gene Therapy Center, Worcester MA)(117).

Genomic DNA extraction and Quantitative PCR:

DNA was extracted and quantified as previously described(118). Animals were sacrificed at indicated time points and tissues were harvested in a manner to avoid cross-contamination, snap frozen in liquid nitrogen and stored at -80°C. Genomic DNA (gDNA) was extracted using a DNeasy blood and tissue kit (Qiagen Inc., Valencia, CA, USA) according to the manufacturer's instructions. gDNA concentrations were determined using an Eppendorf Biophotometer (Eppendorf, Hamburg, Germany).

rAAV genome copies in the gDNA from brain, heart, liver, and tibialis anterior (TA) were quantified by qPCR with an ABI 7900 HT sequence detection system (Applied Biosystems, Carlsbad, CA, USA) according to the manufacturer's instructions and results were analyzed using SDS 2.3 software. Briefly, primers and probe were designed to amplify SV40 poly-A tail of the rAAV9-CBA-VLCAD vector. A standard curve was generated using plasmid DNA containing the same SV40 poly-A target sequence. PCR reactions contained a total volume of 100µL and were run at the following conditions: 50°C for 2 minutes, 95°C for 10 minutes, and 45 cycles of 95°C for 15 seconds and 60°C for one minute.

DNA samples were assayed in triplicate. In order to assay PCR inhibition, the third replicate was spiked with plasmid DNA at a ratio of 100-copies/µg gDNA. If this replicate was greater than 40-copies/µg gDNA then the results were considered acceptable. If a sample contained greater than or equal to 100-

copies/µg gDNA it was considered positive for vector genomes. If a sample contained less than 100 copies/µg gDNA it was considered negative for vector genomes. If less than 1µg of gDNA was analyzed to avoid PCR inhibition, the vector copy number reported was normalized per µg gDNA and the plasmid spike in was reduced to maintain the ratio of 100-copies/µg gDNA.

Immunohistochemistry:

Tissues were fixed in 10% neutral buffered formalin, and embedded in paraffin. Immunohistochemistry was carried out by the Molecular Pathology and Immunology Core at University of Florida. Briefly, 4 µm serial sections were removed of paraffin and incubated with 3% H_2O_2 in methanol to block endogenous peroxidase activity. Sections were treated with Trilogy (Cell Marque, Rocklin, California) at 95° C for 25 minutes and blocked with Sniper (Biocare Medical, Walnut Creek, CA) to reduce non-specific background staining. For GFP staining, several different antigen retrieval (AR) methods were tested including: no AR, Trilogy at 95°C for 25 minutes, Citrate at 95°C for 25 minutes, DAKO high at 95°C for 20 minutes and 20 minutes cool down on bench, DAKO low 95°C for 20 minutes and 20 minutes cool down on bench and Trypsin at 37°C for 5 minutes. Sections were incubated with rabbit anti-mouse VLCAD at room temperature for 1 hour. For GFP staining the following antibodies were tested: GFP raised in Rabbit (Cat#290, Abcam, Cambridge, MA); GFP raised in chicken (Cat#3839, Abcam, Cambridge, MA); AF488-conjugated GFP (Cat# A-

21311, Invitrogen, Grand Island, NY). Then sections were incubated with Mach2 Gt x Rb HRP polymer (Biocare Medical, Walnut Creek, CA) for 30 minutes. Staining was visualized with DAB chromagen (Biocare Medical, Walnut Creek, CA).

Confocal Microscopy:

Slides were de-paraffinized with xylene and re-hydrated through decreasing concentrations of ethanol to water. For heat-induced antigen retrieval, sections were heated in a water bath at 95°C while submerged in Trilogy buffer (Cell Marque, Hot Springs, AR) for 25 minutes. Slides were subsequently rinsed in 1X tris-buffered saline (TBS) and sections were blocked for 20 min at room temperature with 10% normal goat serum. Next, sections were incubated with VLCAD (1:1000 dilution, homemade) overnight at 4°C followed by incubation with AF594 goat anti-rabbit IgG (Vector Laboratories, Inc.). Avidin and Biotin kit (Vector Laboratories, Inc.) was used for 15 min to block endogenous avidin and biotin, separately. Then MOM kit (Vector Laboratories, Inc.) was used to block endogenous mouse IgG. A 1:400 dilution of B3-Tubulin antibody (Invitrogen, NY) was added to the samples for overnight incubation at 4°C. Then samples were washed twice with TBS, treated with the 1:200 dilution of a biotinylated anti-mouse IgG and incubated at room temperature for 30 min. After washing with TBS, the sections were incubated with Fluorescein Avidin DCS (Vector Laboratories, Inc.) for 5 min. After being

washed twice with TBS for 5 min each, the slides were mounted with DAPI (Vector Laboratories, Inc.). Slides were stored at 4°C until imaged using Perkin Elmer Ultraview spinning disc confocal microscope: Zeiss Axiovert 200M, ×10 Plan-Apocromat NA 1.4 Oil objective, or ×63 Plan-Apocromat NA 1.4 Oil objective and Hamamatsu ORCA-ER camera.

Results

VLCAD-/- mice were tail vein injected with 200µl of single stranded rAAV9-CB-VLCAD at $1x10^{12}$ vector genomes in per mouse and were sacrificed after 12 weeks to look at long-term expression. Brains were removed, sectioned and stained for VLCAD. Our initial observation of expression of VLCAD in cells with different morphologies (Figure 4.1) as well as throughout different sections of the brain is demonstrated by VLCAD staining in the Hippocampus (Figure 4.2) in cells with morphology similar to neurons and astrocytes, Cerebellum (Figure 4.3) in cells with morphology appearing to be purkinjie neurons and Choroid Plexus (Figure 4.4).

In order to test if the expression detected was a result of a more permeable BBB in VLCAD-/- mice, different mouse strains: VLCAD+/+ background strain, C57/B6 and Balb/c mice were tested for transduction of VLCAD, 12 weeks post rAAV9 injection. Brains were sliced in coronal sections for both qPCR of vector genomes (Figure 4.6) and for histology (Figure 4-5). VLCAD+/+, C57/B6, and Balb/c mice all possess the VLCAD gene, however

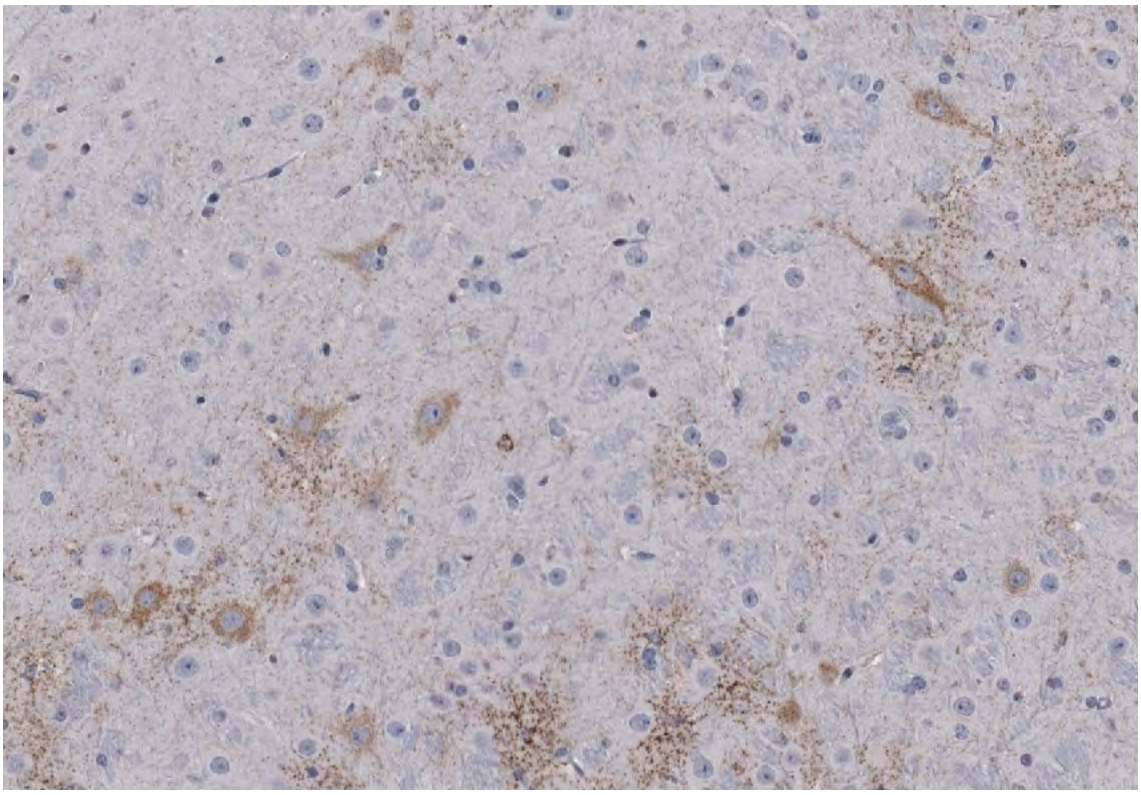

Figure 4.1 AAV9 mediated VLCAD Expression in Cell types with Different Morphologies in the Brain

Image of 10x magnification of VLCAD-/- mouse stained with VLCAD antibody 12 weeks post-injection with rAAV9-VLCAD by systemic administration. Staining can be observed in cell types with different morphologies suggesting both astrocytes and neurons are being transduced.

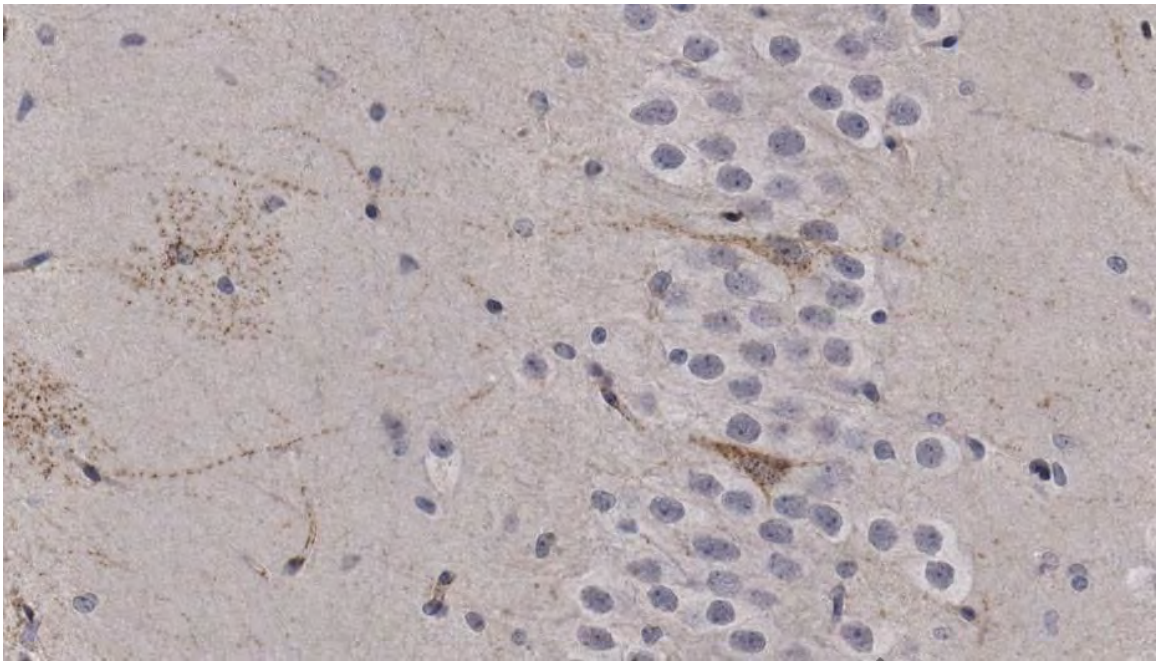

Figure 4.2 AAV9 mediated VLCAD Expression in the Hippocampus

Representative image at 10x magnification of the hippocampus of VLCAD-/- mouse brain stained with VLCAD antibody, 12 weeks post injection with rAAV9-VLCAD by systemic administration. Punctate staining is observed corresponding to mitochondrial expression.

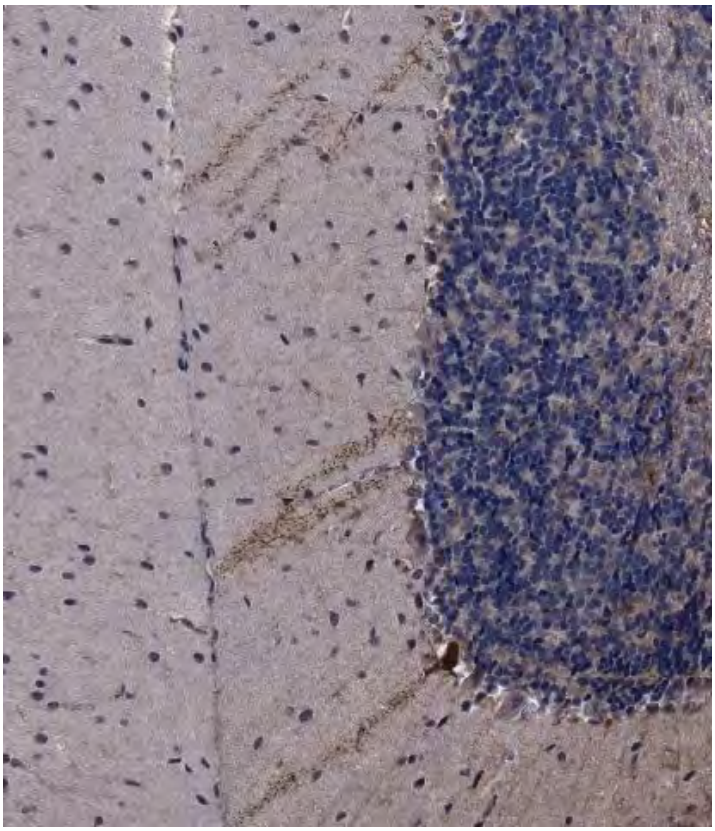

Figure 4.3 AAV9 Mediated VLCAD Expression in the Cerebellum

Representative image of the cerebellum at 10x magnification of a VLCAD-/- mouse stained with VLCAD antibody 12 weeks post-injection with rAAV9-VLCAD.

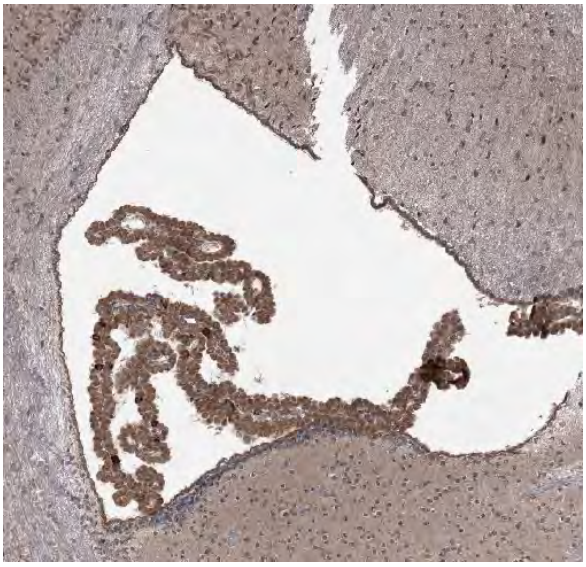

Figure 4.4 AAV9 mediated VLCAD Expression in the Choroid Plexus

Representative image of the Choroid Plexus at 20x magnification of a VLCAD-/- mouse stained with VLCAD antibody 12 weeks post injection with rAAV9-VLCAD by systemic administration..

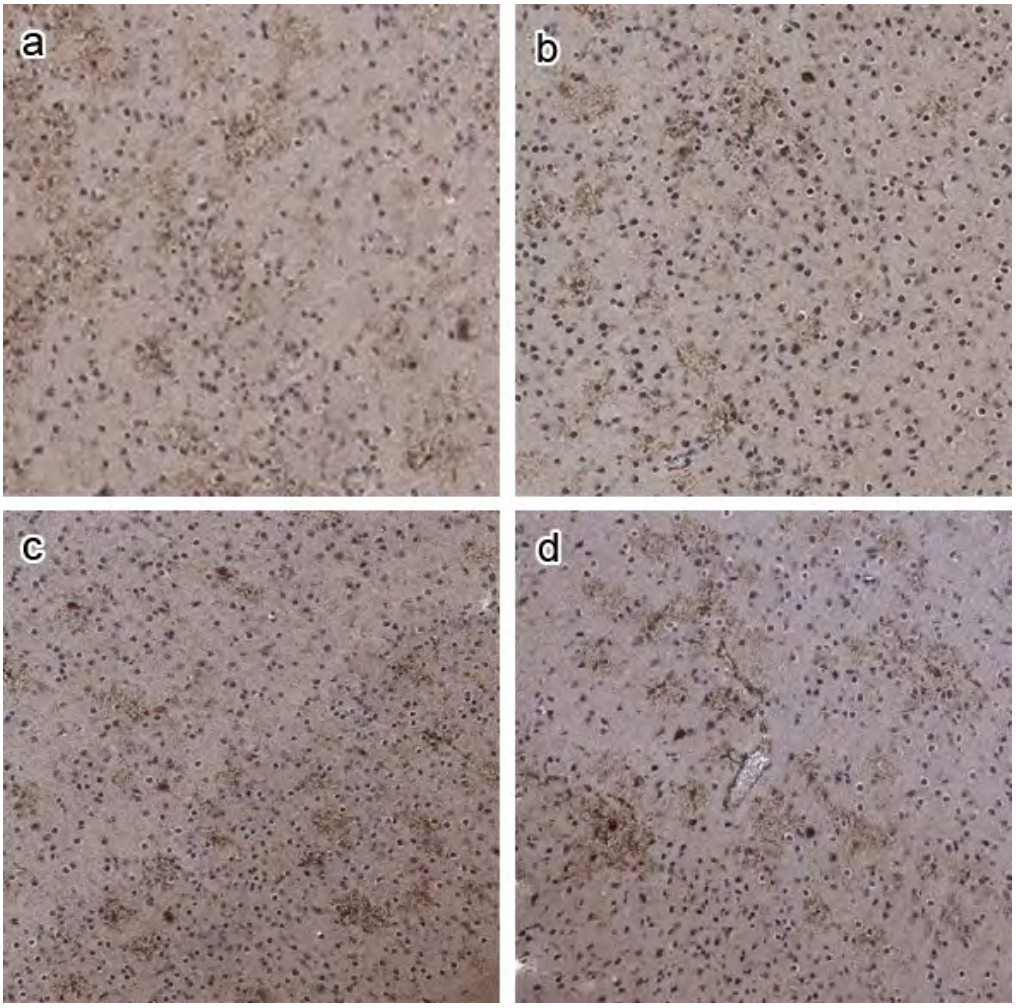

Figure 4.5 Expression of VLCAD in different Mouse Strains in the Brain

Representative images of primary motor cortex at 10x magnification of Different mouse strains were injected with rAAV9-VLCAD. VLCAD staining was performed 12 weeks post-injection. Panel (a) depicts VLCAD -/- (b) depicts VLCAD+/+ (c) depicts Balb/c and (d) C57/B6. n=4 from each group.

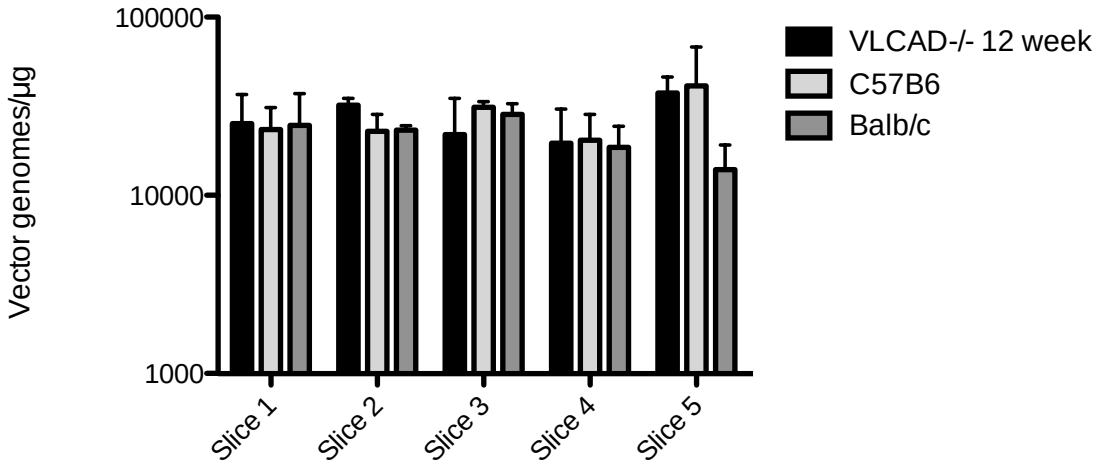

Figure 4.6 AAV9 mediated VLCAD Transduction in the Brain of different Mouse Strains

Different mouse strains were injected with AAV9-VLCAD and sacrificed 12 weeks post-injection. Brains were sliced into coronal blocks 2.0mm thick numbered 1-5, rostral-caudal. Black bars depict VLCAD-/-, C57/B6 depicted by light gray bars and Balb/c depicted by dark gray bars. Error bars denote SEM, and n=3 for each group.

VLCAD expression in the brain is very limited and only found at moderately low levels in the endothelial cells in the frontal cortex(33). Very low background staining was observed in VLCAD +/+ mouse strains. All four strains of mice had similar staining patterns and vector genomes of VLCAD throughout differing regions of the brain. Overall there were no significant differences detected in either vector genomes, strain of mouse or different sections of the brain.

To test if expression was time dependent, mice sacrificed at an earlier time point of 5 weeks post-injection were compared to animals sacrificed at 12 weeks post injection. Less staining overall in the cerebellum was observed at 5 weeks post-injection in comparison to mice 12 weeks post-injection (Figure 4.7).

Next to test if the increased expression in the brain was transgene specific, we injected VLCAD -/- mice with either vectors containing GFP or VLCAD. Vector genomes to measure transduction were detected at approximately the same amount in mice injected with either GFP or VLCAD across all sections of the brain (Figure 4.8). Interestingly, no GFP staining could be discerned across any of the brain sections, whereas VLCAD staining was readily observed in all sections and in many morphologically distinct cells (Figure 4.1-4.9). Six different antigen-retrieval protocols were tested as well as three different GFP antibodies, but no protocol or antibody produced reliable staining, however different fixations, such as frozen sections were not tested by may yield better results. When GFP and VLCAD transduction and expression were compared in other tissues, vector genomes were comparable in liver, TA muscle

a

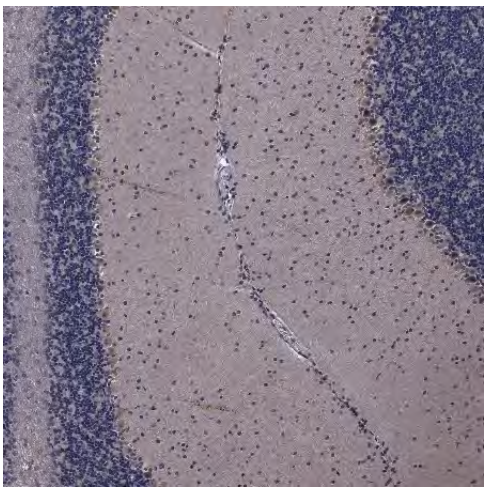

b

Figure 4.7 AAV9 mediated VLCAD Expression at different time points post-injection

Representative VLCAD staining of Cerebellum sections at 5x magnification of VLCAD-/- mice after injection with AAV9-VLCAD. Panel (a) depicts 5 weeks post-injection 5x, and panel (b) depicts 12 weeks post-injection. n=4 for both time points.

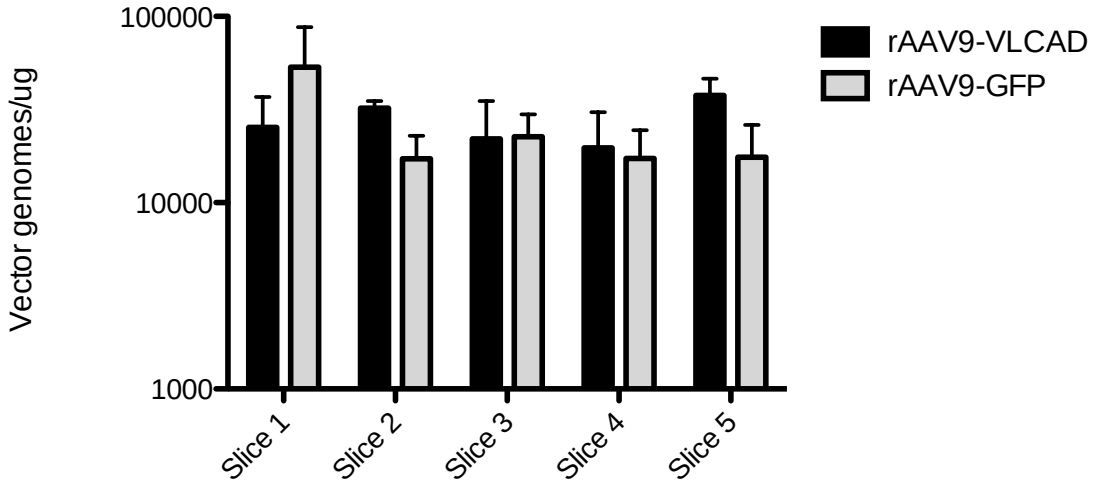

Figure 4.8 Comparison of Transduction in mice injected with different transgenes

Vector genomes were quantified from brains collected at 12 weeks post-injection from VLCAD-/- mice injected with either rAAV9-GFP or VLCAD. Coronal 2.0mm sections of brains numbered 1-5, rostral-caudal. Black bars represent VLCAD-/- mice injected with rAAV9-VLCAD and gray bars AAV9-GFP. Error bars indicate SEM. n=3 for rAAV9-VLCAD and n=4 for rAAV9-GFP.

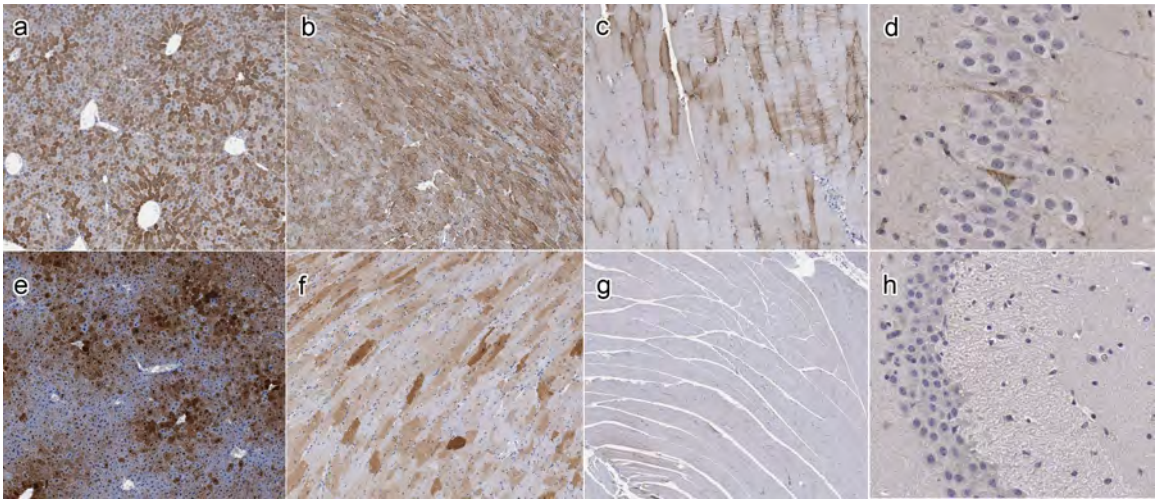

Figure 4.9 VLCAD and GFP expression in different tissues

Tissues from VLCAD-/- mice were harvested at 12 weeks post-injection from either rAAV9-GFP or VLCAD injected animals. Tissues were stained with either GFP or VLCAD antibodies respectively. Representative images are shown from an n=4 for both groups. Magnification of liver, heart and muscle shown at 4x, Hippocampus at 20x. a-d VLCAD expression in rAAV9-VLCAD injected animals (a) Liver (b) Heart (c) Muscle (d) Hippocampus, e-h GFP expression in rAAV9-GFP injected animals (e) Liver (f) Heart (g) Muscle (h) Hippocampus

and brain (Figure 4.9-4.10). Importantly in the liver, where average vector genomes were $1.3x10^7$, GFP expression was readily detectable by immunohistochemistry (Figure 4.9,10). However in the muscle, where average vector genomes of GFP were $1.8x10^5$ lower than the $4.8x10^5$ average vector genomes in the brain, no GFP staining was detected (Figure 4.10).

Finally, to confirm that neurons in the brain were being transduced after single-stranded AAV9 injection into adult mice, confocal microscopy was performed. Sections from the hippocampus were fluorescently stained for using VLCAD and Tuj-1, neuronal specific class III beta-tubulin, antibodies. Confocal microscopy confirmed the presence of transduced neurons (VLCAD+, Tuj-1+) within the hippocampus (Figure 4.11).

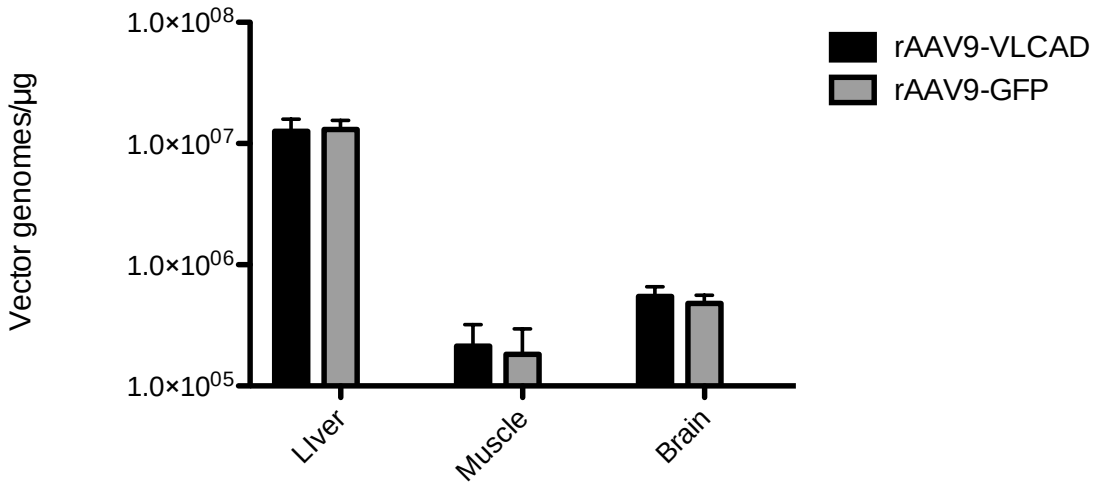

Figure 4.10 AAV9 Transduction comparison of VLCAD and GFP in different tissues

Liver, TA muscle and brain were collected from mice 12 weeks post-injection with either rAAV9-VLCAD or rAAV9-GFP for vector genome quantification. Black bars represent mice injected with rAAV9-VLCAD and Gray bars represent mice injected with rAAV9-GFP. Error bars represent SEM. n=7 for rAAV9-VLCAD, n=5 for rAAV9-GFP.

Figure 4.11 Neuronal Expression of VLCAD by Confocal Microscopy

Hippocampus section of VLCAD-/- mouse injected with $1x10^{12}$vg AAV9-VLCAD 12 weeks post injection. Panel represents (a) 20x magnification and panel (b) 63x magnification. DAPI stain is blue. VLCAD stain is red, and Tuj-1, neuronal specific class III beta-tubulin, is green.

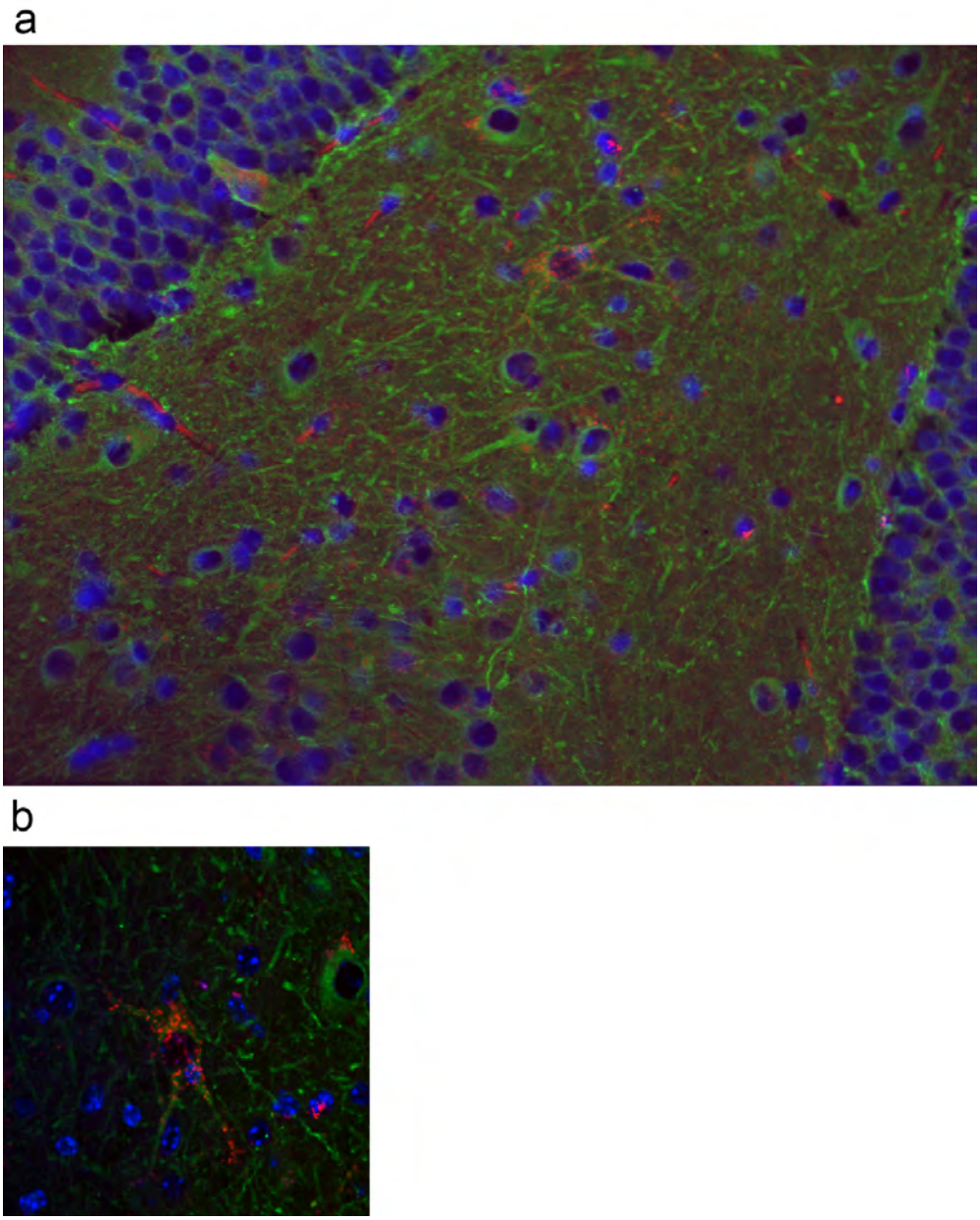

Figure 4.11 Neuronal Expression of VLCAD by Confocal Microscopy

Discussion

Miyake *et al.*, suggest that rAAV9 vectors are unable to cross the BBB if injected after 42 days post birth(127). Here we show that rAAV9 vectors expressing VLCAD, injected systemically, are able to cross the BBB and transduce cells in the brain including neurons. Our results may differ from the previous studies for multiple reasons: timeframe post-injection, mouse model used, vector dosage, and transgene expressed by rAAV9. Miyake *et al.* detected no expression two weeks post-injection, and Gray et al. saw very limited transduction four weeks post-injection. While this timeframe may be reasonable for self-complementary vectors, which can efficiently skip either the second strand synthesis or the self-annealing step, single stranded vectors may need more time before efficient expression can be observed. Our data supports this argument as lower expression was observed five weeks post-injection compared to twelve weeks post-injection, as well as the work by Fu et al. where correction of the phenotype was assayed 6-9 months post-injection.

Since the initial observation was made using VLCAD deficient mice, it was important to determine if the VLCAD deficient mice have an intrinsically more permeable BBB. However, expression and transduction after systemic injection with rAAV9-VLCAD were similar in both C57/B6 mice, used in other studies, as well as Balb/c mice. Our vector dosage of $1x10^{12}$vg, although higher than $5x10^{11}$vg used by Gray *et al.,* is a lower dose than the $1.5x10^{12}$vg dose used by Miyake *et al*. Given that $1x10^{12}$vg is a relatively high dose, neither study, even at

the highest dose of $1.5x10^{12}$vg, was able to observe the extent of transduction and expression reported here.

Finally, neuronal expression was confirmed by confocal microscopy. However expression of GFP, in spite of equivalent amounts of transduction distributed throughout the brain, was undetectable after several different strategies were attempted. However different processing and fixation of tissue may yield better results for GFP staining. Neither Gray *et al.*, nor Miyake *et al.,* quantified vector genomes, and only Gray *at el.* observed very low levels of GFP staining after enhancing the signal by an avidin-biotinylated enzyme complex, which was not used in these experiments.

The discrepancies between GFP and VLCAD expression could simply be explained by the antibody sensitivity, but alternative possibilities exist. Unlike GFP, which resides in the cytosol, VLCAD is expressed at the inner mitochondrial membrane producing a well-defined punctate pattern of staining throughout the brain. This expression pattern may concentrate signal, over the diffuse expression of GFP. Clearance of GFP may be even higher than VLCAD. Even though VLCAD is being used as a reporter gene as it is not expressed in the brain for therapeutic benefit(33), it is still a self gene, has a role, and is compartmentalized in the mitochondria even if not expressed in VLCAD-/- mice. Expression of GFP can be toxic and Gray *et al.,* showed that GFP expression caused transient liver toxicity after systemic injection(126). Also, the half-life of GFP is approximately 26 hours, which could also cause the staining to be less

apparent. In these studies mRNA levels for either GFP or VLCAD were not studied, nor were in situ hybridizations used. Therefore low levels of expression of GFP protein in the brain could also account for the differences observed, even though vector genomes are approximately the same between GFP and VLCAD.

Taken together, regardless of mechanistic explanations of why GFP expression is undetectable at low transduction efficiencies, these studies suggest GFP reporter assays in the brain may underestimate expression of other transgenes. In the only study using a single stranded vector encoding a therapeutic gene rather than a reporter gene, Fu *et al.* was able to see remarkable correction of the mucopolysaccharidosis IIIB phenotype even at a low dose. The results presented here allow for more potential therapeutic options by using single stranded vectors, that have more packing space then self-complementary, and adult administration for diseases that will not be diagnosed or treated until adulthood. It is currently unknown whether rAAV9 or any of the other serotypes will be able to cross the BBB in humans after systemic injection, but work with self-complementary vectors crossing the BBB in adult nonhuman primate and large animal models is promising(126, 129). If rAAV is able to cross the BBB in humans, there are numerous therapeutic applications for these vectors.

CHAPTER V: Gene Therapy for VLCAD- Biochemical and Phenotypic Correction

Introduction

VLCAD deficiency is the most common disorder of long chain fatty acid metabolism, with a regional incidence in the United States of 1 in 30,000 births, and second in frequency only to MCAD deficiency among disorders of fatty acid oxidation. (130, 131) Characterized by the most severe phenotype within the acyl-CoA dehydrogenase deficiency family, patients generally present with one of three distinct clinical phenotypes. Of these three phenotypes the earliest onset presentation during infancy is the most severe, presenting with cardiomyopathy and hepatopathy and are often fatal(132). A less severe hepatic phenotype presenting with recurrent hypoketotic hypoglycemia, also occurs in infancy to early childhood. The third phenotype is a mild, myopathic form presenting in adolescence or adulthood with muscle weakness, myalgia and myoglobinuria(133, 134).

VLCAD is responsible for catabolism of long chain fatty acids, with highest specificity for carbon lengths C14-C18, as part of the mitochondrial beta-oxidation spiral. It is the rate-limiting enzyme in the process, causing an energy deficiency as well as accumulations of long chain fatty acids. Beta-oxidation is an important source of energy for liver and muscle, especially cardiac muscle. The disease is associated with a lack of energy caused by the inability to

breakdown long chain fatty acids but the accumulates of these long chain fatty acids can also be detrimental(135, 136). The amassments of these metabolites are exploited for diagnostic purposes as part of the newborn screening by analyzing for acyl carnitine metabolite accumulations in the blood by tandem mass spectrometry (MS/MS). Although newborn screening has reduced mortality, the current treatment is limited to fasting avoidance, and supplementation of medium chain triglycerides (MCT), which remains controversial since supplementation of MCT in excess of the immediate caloric demand will induce the production of longer chain fatty acids for storage as triglycerides(18). These in turn will add to the total load of longer chain fatty acids, which cannot be subsequently metabolized when caloric restriction occurs. Therefore, VLCAD deficiency is a candidate for gene therapy because of its limited treatment options as well as its potentially fatal phenotype.

The Flotte laboratory has previously shown biochemical correction of SCAD deficiency by targeting muscle with rAAV1 and rAAV2, and liver with rAAV8 as well as LCAD deficiency by targeting the muscle with rAAV1(106, 107, 110). New AAV serotypes, such as AAV9, have improved expression and wider transduction profiles(89, 116). Merritt and colleagues showed limited biochemical correction of VLCAD deficiency using systemic injections with AAV8. Here we present the first evidence of a genetic therapy that systemically targets major tissues involved in beta-oxidation, has long term expression and corrects several disease-specific phenotypes in a VLCAD deficient mouse model.

Materials and Methods

Mass Spectrometry:

Blood acyl carnitines were extracted, derivatized and analyzed as described previously(137). The following labeled carnitine standards (Cambridge Isotope Laboratories, Andover MA) were used for quantification: L-carnitine (N-trimethyl-D_9), L-Acetylcarnitine (N-methyl-D_3), L-propionylcarnitine (N-methyl-D_3), L-Butyrylcarnitine (N-methyl-D_3), L-Isovalerylcarnitine (N-trimethyl-D_9), L-Octanoylcarnitine (N-methyl-D_3), L-Myristoylcarnitine (N-trimethyl-D_9) and L-Palmitoylcarnitine (N-methyl-D_3). Blood acyl carnitine samples were analyzed as butyl esters on a Micromass Quattro II (Manchester UK) with an electrospray ionization source operating in the positive ion mode by direct infusion. Tissue samples were processed as previously described(138). In brief, frozen tissue samples were ground into powder and resuspended in 80% acetonitrile containing carnitine standards described above at a concentration of 60mg/ml. Samples were homogenized and centrifuged, supernatants were dried under nitrogen. Samples were then resuspended in 10% acetyl chloride in 1-butanol and heated at 65°C for 15 minutes, dried under nitrogen and brought up in 80% acetonitrile for analysis. Samples were run in triplicate on a Waters (Milford, MA) Premier XE triple quadrupole mass spectrometer similarly to the blood samples.

^{1}H-MRS:

Single voxel ^{1}H-MRS was obtained from the TA muscle and liver at 11.1T and 4.7T respectively. 11.1T localized proton muscle spectra were obtained using a Bruker spectrometer (PV3) as described previously(106). A custom-made loop gap coil with 1.4-cm inner diameter tuned to 470.5 MHz was used. Localizer anatomical proton magnetic resonance images were acquired using FLASH (matrix, 256 x 256; echo time (TE)=4.3 msec; repetition time(TR)=207 msec, FOV=20X20mm^{2}) were acquired in three orthogonal directions for the precise localization of a volume of interest (VOI) from which proton MRS would be obtained. Water suppression was optimized by chemical shift-selective (CHESS) water suppression. Localized spectra were acquired by point-resolved spatially localized spectroscopy (PRESS) (TE=18 msec; TR=3,000 msec; number of excitations (NEX)=512, bandwidth=8013Hz, number of complex points=2,048). Data were processed using jMRUI(http://www.mrui.uab.es/mrui/mrui_Overview.shtml). Similarly localized single voxel proton liver spectra were obtained at 4.7T using PRESS (TE=14 msec; TR=2,500 msec; NEX=16, bandwidth=3,005Hz, number of complex points=8,196) on a Varian/Agilent spectrometer (VnmrJ). Liver MRS was processed using in house software (IDL; ITT) in order to determine the integral of water and lipid resonances.

Animals were fasted for 18-24 hours before bleeds, magnetic resonance spectrometry or cold fast challenge. For cold fast challenge, after the 18 hour

fast, mice were singly housed in minimal bedding cages and placed in a 4°C cold room for 150 minutes or until rectal temperatures were below 20°C. Blood glucose levels were measured by Nova Max Glucose Monitor and Strips (Nova Biomedical Corporation, Waltham MA).

All animal procedures were approved by University of Massachusetts Medical School Institutional Animal Care and Use Committee as well as University of Florida Institutional Animal Care and Use Committee in accordance with the Association for Assessment and Accreditation of Laboratory Animal Care International specifications.

Results

Because VLCAD deficient patients have a greater magnitude of accumulation of long chain acyl carnitines in the blood, it was essential to demonstrate biochemical correction of whole blood by measuring acyl carnitine accumulates by electrospray tandem mass spectrometry (MS/MS). Prior to treatment, and on days 14, 42 and 140 post-injection, male mice were subjected to a 24-hour fast followed by whole blood collection. Metabolic stress such as fasting was required to observe optimal response. Large accumulations of long chain metabolites were found in VLCAD-/- PBS controls and reductions of the levels of C14, C16:1, C16, C18:2, C18:1 and C18 were revealed 14 days post-injection in rAAV9-treated VLCAD-/- animals when compared to VLCAD-/- PBS controls (Fig. 5.1). There were no significant differences between controls, AAV9-GFP or PBS, so PBS was used as a control for subsequent experiments

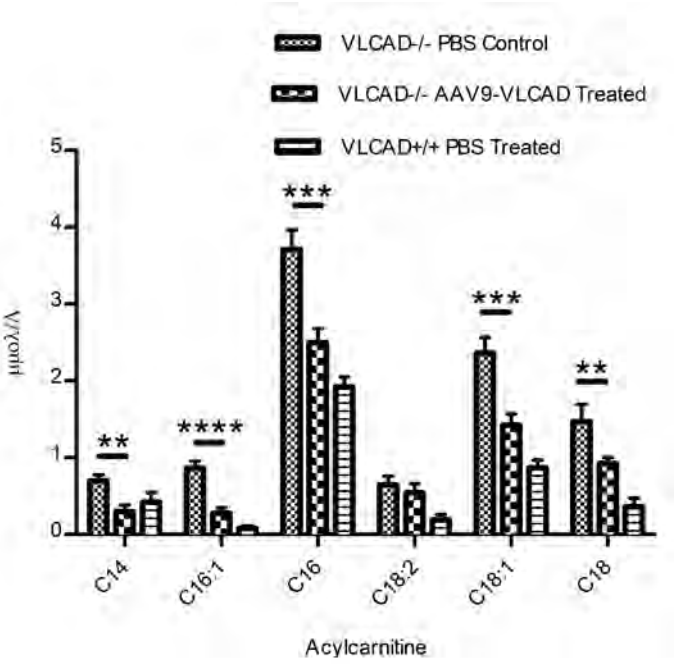

Figure 5.1 Reduction of Acyl Carnitines in the blood of rAAV9-VLCAD treated mice

All animals were fasted 24 hours prior to bleeding. Designates p< 0.05, **p<0.01, ***p<0.001, ****p<0.0001. Quantities of acyl carnitine species were assessed by mass spectrometry of whole blood day 14-post injection. *n*=7 untreated VLCAD-/- controls, *n*=6 rAAV9 treated VLCAD-/- mice; and *n*=6 in wildtype controls. Error bars are SEM. P-values are as follows: C14 p=0.002, C16:1 p=<0.0001 C16 p=0.0008 C18:2 p=0.005, C18:1 p=0.005, C18 p=0.04

(Figs. 5.2a-c). It was noted that reductions in blood acyl carnitines were observed across all groups between the first and second 24-hour fasting time points, regardless of treatment, age, or if mice remained uninjected (Fig. 5.3,4,5,6), a phenomena that is also observed in our MCAD mice. Significant reductions in levels of C16, C18:1, C18 (Figs. 5.4,5,6), $P<0.0006$, in whole blood persisted for over 140 days post-injection of rAAV9-VLCAD when compared to the PBS controls. These reductions, which were observed out to 140 days post injection, infer biochemical correction of the whole blood.

Biochemical correction within the liver tissue itself was assessed by an *in vivo* and *ex vivo* approach. Using single voxel proton magnetic resonance spectroscopy (1H-MRS), lipid accumulations in the liver were measured in live animals 17 weeks post- injection. Figure 5-7A shows representative liver spectra from VLCAD-/- PBS control, VLCAD-/- AAV9 treated and VLCAD+/+ PBS control mice. A measure of total lipid, the ratio of the area under the lipid peak divided by the area under the water peak, as an internal control is shown in Figure 5.7B. No significant differences were detected in accumulations measured by MRS between the VLCAD-/- and VLCAD+/+ or rAAV9-treated groups. *Ex vivo* acyl carnitine accumulations were measured by MS/MS of the liver tissue in Figure 5.8. Significant differences in C16, C18:2, C18:1 and C18 were

Figure 5.2 Levels of Acyl Carnitines in rAAV9-VLCAD with GFP Control

All mice were fasted 24 hours before blood collection. n=3 for VLCAD-/- PBS, n=3 for VLCAD-/- AAV9-GFP control, n=4 VLCAD-/- AAV9 VLCAD treated, n=4 for VLCAD+/+ (a) Mass Spectrometric quantification of C16 in whole blood. 2-way ANOVA Between PBS Control and AAV9-GFP p=0.67(b) Mass Spectrometric quantification of C18 in whole blood. 2-way ANOVA Between PBS Control and AAV9-GFP p=0.94 (c) Mass Spectrometric quantification of C18:1 in whole blood. 2-way ANOVA Between PBS Control and AAV9-GFP p=0.64

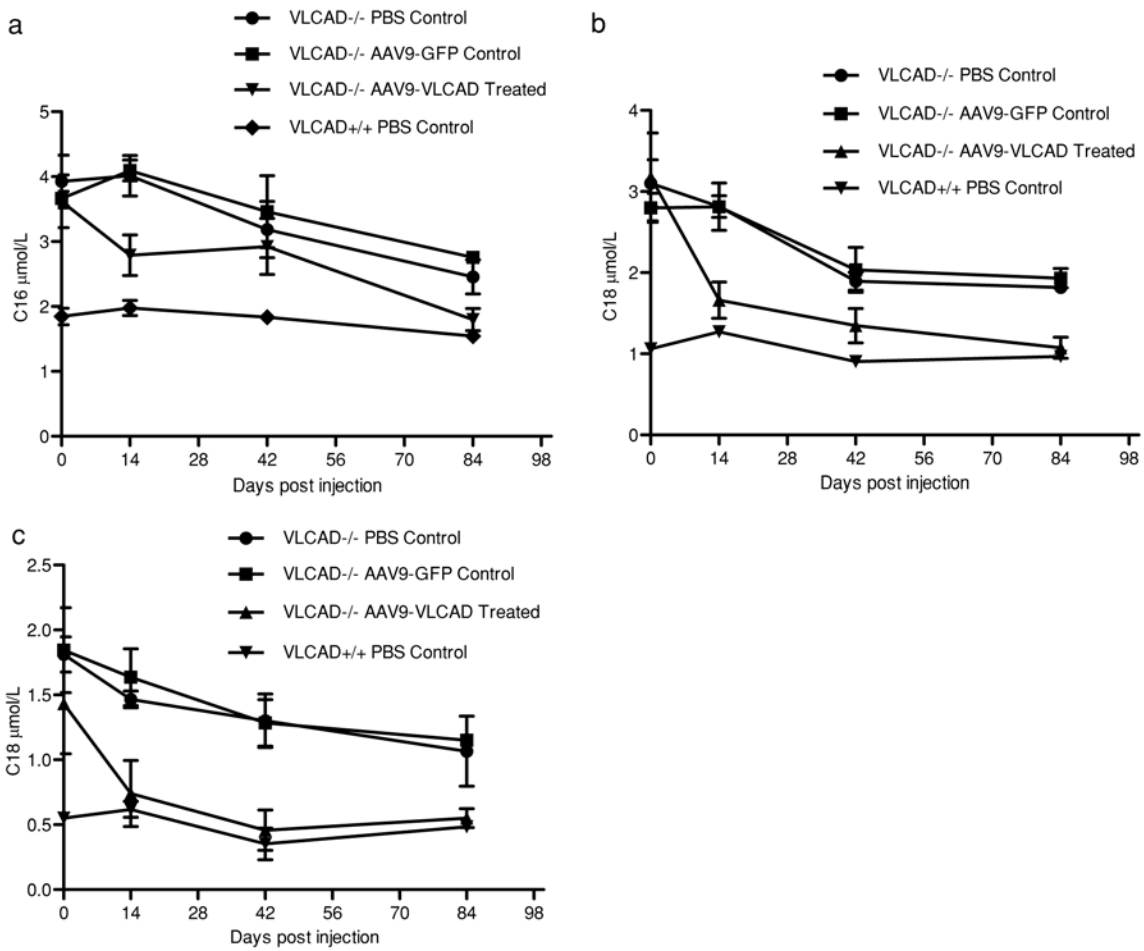

Figure 5.2 Levels of Acyl Carnitines in rAAV9-VLCAD with GFP Control

Figure 5.3 Acyl Carnitine Profiles in blood of uninjected mice over time

All mice were uninjected, and fasted for 24-hours prior to blood collection. Panels a,b and c had an n of 4 for VLCAD+/+ and an n of 5 for VLCAD-/-. Panels d, e and f had an n of 2 for 6-8 week old VLCAD+/+, n of 2 for 16-18 weeks old VLCAD +/+, n of 2 for 6-8 weeks old VLCAD-/- and n of 3 for 16-18 week old VLCAD-/-. Age is designated by age at first fasting-bleed. (a) Mass Spectrometric analysis of accumulations of C16 in whole blood over 12 weeks. (b) Mass Spectrometric analysis of accumulations of C18:1 in whole blood over 12 weeks. (c) Mass Spectrometric analysis of accumulations of C18 over 12 weeks. (d) Mass Spectrometric analysis of accumulations of C16 in whole blood over 12 weeks. (e) Mass Spectrometric analysis of accumulations of C18:1 in whole blood over 12 weeks. (f) Mass Spectrometric analysis of accumulations of C18 over 12 weeks.

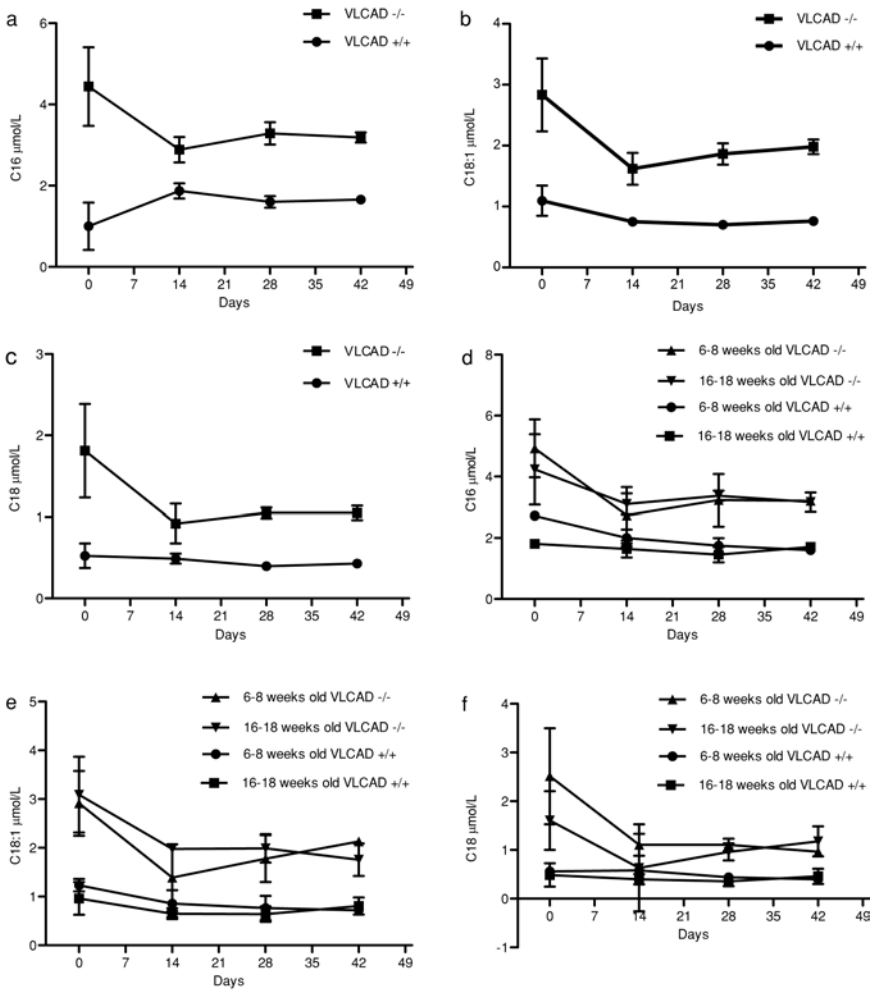

Figure 5.3 Acyl Carnitine Profiles in blood of uninjected mice over time

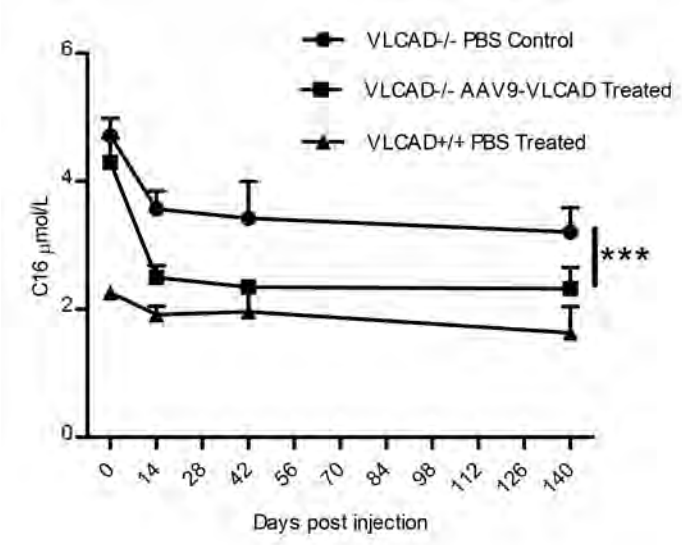

Figure 5.4 MS/MS quantification of C16 in the whole blood over time

All animals were fasted 24 hours prior to bleeding. ***Designates p<0.001. Untreated VLCAD-/- controls Day 0 and 14 *n*=11; Day 6 *n*=3; D140 *n*=7. rAAV9 Treated VLCAD-/- mice Day 0 and 14 *n*=11; Day 6 *n*=5; D140 *n*=6. Wildtype control mice Day 0,14 *n*=11; Day 6 *n*=5; D140 *n*=6. Error bars are SEM. A 2-way ANOVA was preformed on data from Day 14-Day 140 with p= 0.0006.

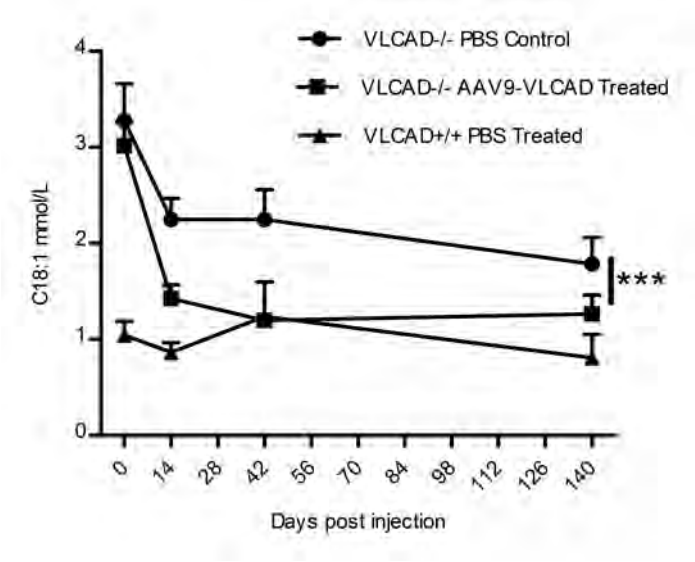

Figure 5.5 MS/MS quantification of C18:1 in the whole blood over time

All animals were fasted 24 hours prior to bleeding. ***Designates p<0.001. Mass Spectrometric quantification of C18:1 over time. Untreated VLCAD-/- controls Day 0 and 14 *n*=11; Day 6 *n*=3; D140 *n*=7. rAAV9 Treated VLCAD-/- mice Day 0 and 14 *n*=11; Day 6 *n*=5; D140 *n*=6. Wildtype control mice Day 0,14 *n*=11; Day 6 *n*=5; D140 *n*=6.Error bars are SEM. A 2-way ANOVA was preformed on data from Day 14-Day 140 with p= 0.0003

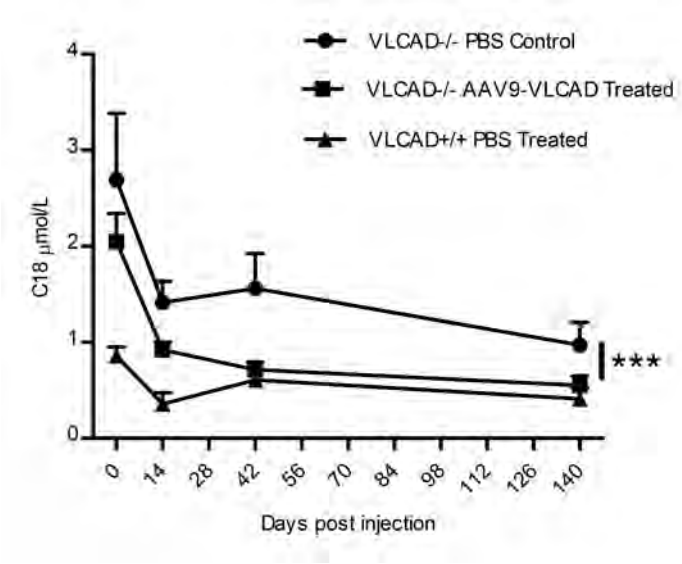

Figure 5.6 MS/MS quantification of C18 in the whole blood over time

All animals were fasted 24 hours prior to bleeding. Designates ***p<0.001. Mass Spectrometric quantification of C18 over time. Untreated VLCAD-/- controls Day 0 and 14 *n*=11; Day 6 *n*=3; D140 *n*=7. rAAV9 Treated VLCAD-/- mice Day 0 and 14 *n*=11; Day 6 *n*=5; D140 *n*=6. Wildtype control mice Day 0,14 *n*=11; Day 6 *n*=5; D140 *n*=6.Error bars are SEM. A 2-way ANOVA was preformed on data from Day 14-Day 140 with p= 0.0014.

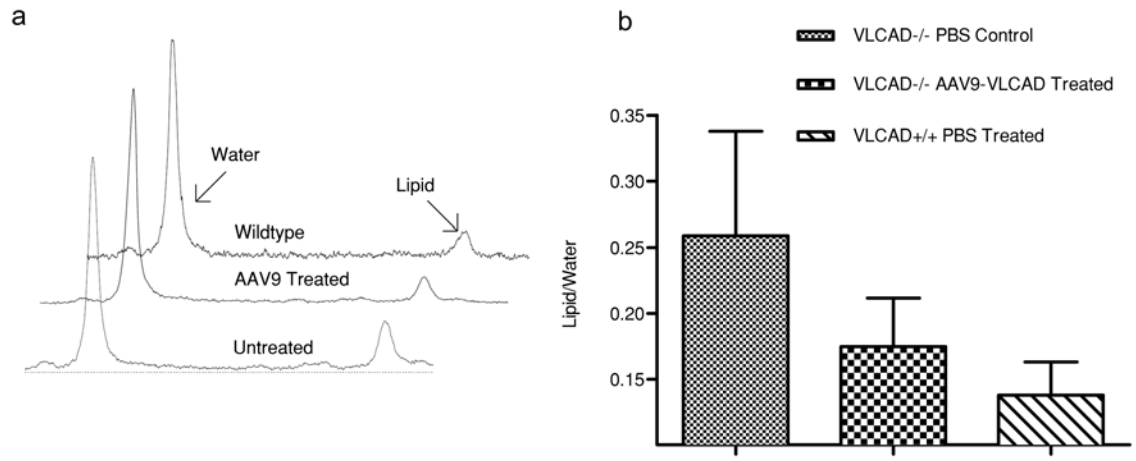

Figure 5.7 Biochemical analysis of lipids in the liver *in vivo*

(a) Representative spectra from magnetic resonance spectrometry of liver *in vivo*. 17–18 weeks post-injection. (b) Quantification of the ratio of the area of the lipid peak/area of the water peak. Error bars are SEM. *n* = 3.

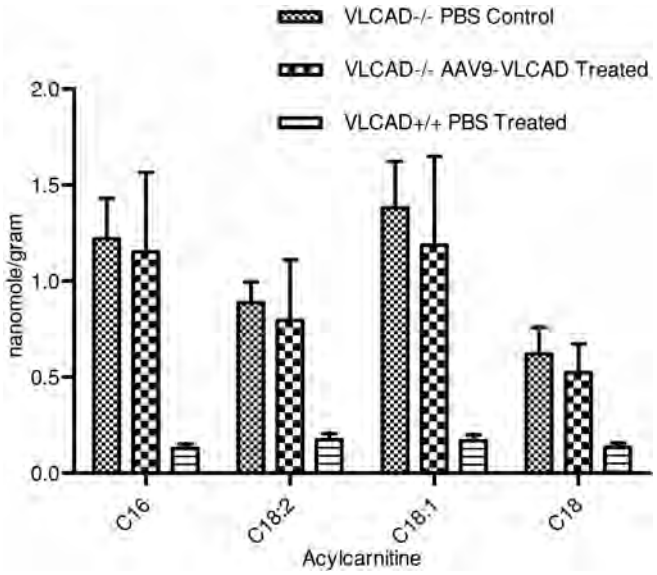

Figure 5.8 Biochemical analysis of Acyl Carnitines in the liver *ex vivo*

Mass spectrometric analysis of liver tissue *ex vivo*, 21–25 weeks post-injection; n = 7 untreated VLCAD$^{-/-}$ controls, n = 6 rAAV9-treated VLCAD$^{-/-}$ and wild-type controls. Error bars are SEM. Samples were analyzed in triplicate. No significant difference between any of the groups.

observed between the VLCAD-/- PBS control and VLCAD+/+ mice (Figure 5.8). Unexpectedly, reductions were not distinguished in the liver of the VLCAD-/- rAAV9-treated animals, despite the significant reductions observed in whole blood.

Analogously, we assessed biochemical correction in the muscle tissue employing the same *in vivo/ex vivo* approach. Figure 5-9a is an MRI image of a representative muscle where the 1H-MRS spectrum was taken. Representative spectra from VLCAD-/- PBS control, VLCAD-/- rAAV9-treated and VLCAD+/+ PBS control mice are shown in Figure 5.9b. The ratio of the area under the lipid peak was divided by the area under the taurine, tri-methyl ammonium and creatine total peak, as the internal control for muscle. Comparison of VLCAD-/- PBS control, VLCAD-/- rAAV9-treated and VLCAD+/+ PBS control mice, lipid peak ratios are shown in Figure 5.9c. The VLCAD-/- PBS control mice had accumulation of lipids within the muscle whereas the VLCAD-/- rAAV9 treated exhibited reduced lipid content similar to wildtype mice. Acyl carnitine accumulations were observed from *ex vivo* tissue by MS/MS for both the extensor digitorum longus (EDL), primarily composed of fast twitch muscle, and the soleus (SOL), primarily composed of slow twitch fibers. Reductions of long chain accumulations were observed in both the EDL (Figure 5.10a) and SOL (Figure 5.10b) in the rAAV9 treated animals. Furthermore, expression of VLCAD in the skeletal muscle reduced accumulations of acyl carnitines within the tissue.

Figure 5.9 Biochemical analysis of lipids in the muscle *in vivo*

(a) Magnetic resonance image (MRI) of hindlimb muscle 12–14 weeks post-injection. (b) Representative spectra from MRS of muscle *in vivo.* (C) Quantification of the ratio of the area of the lipid peak/area of the taurine–creatine peak. *n* = 7 untreated VLCAD$^{-/-}$ controls, *n* = 6 rAAV9-treated VLCAD$^{-/-}$ animals and wild-type controls. No statistical difference between any groups. Error bars are SEM.

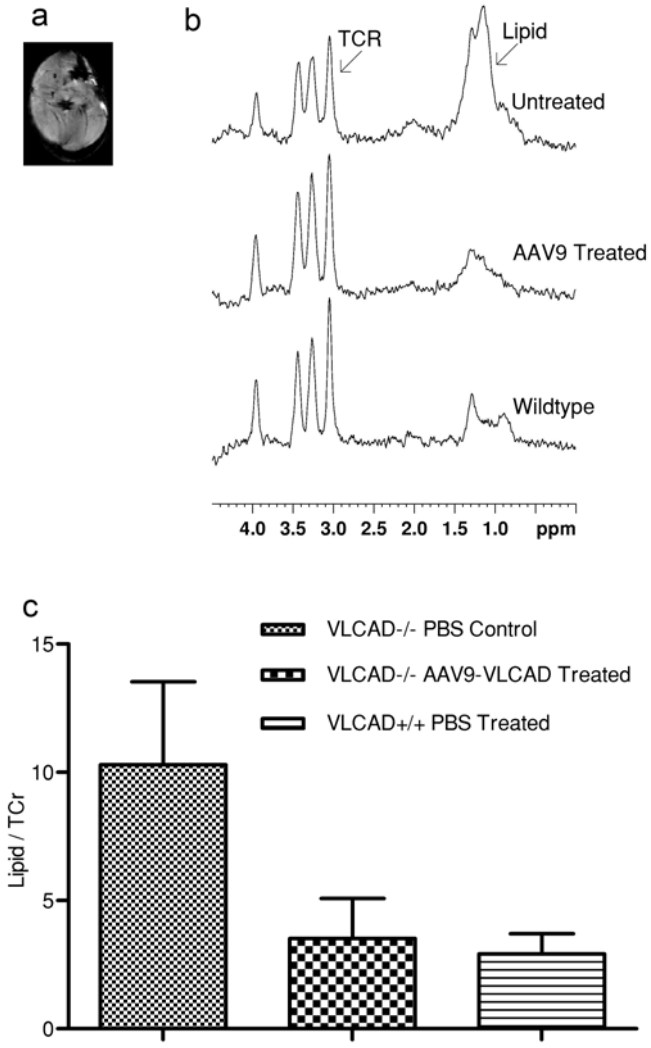

Figure 5.9 Biochemical analysis of lipids in the muscle *in vivo*

Figure 5.10 Biochemical analysis of Acyl Carnitines in the muscle *ex vivo*

(a) Mass spectrometry of extensor digitorum longus (EDL) *ex vivo* 21–25 weeks post-injection. *n* = 7 untreated VLCAD$^{-/-}$ controls, *n* = 6 AAV9-treated VLCAD$^{-/-}$ and wild-type controls. Error bars are SEM. Differences were as follows: C16 *P* = 0.09, C18:2 *P* = 0.06 C18:1 *P* = 0.06 C18 *P* = 0.05. Samples were run in triplicate. (b) Mass spectrometry of soleus (SOL) *ex vivo* 21–25 weeks post-injection. *n* = 7 untreated VLCAD$^{-/-}$ controls, 6 rAAV9 VLCAD$^{-/-}$ and wild-type controls. Error bars are SEM. Statistics were as follows: C16 NS, C18:2 *P* = 0.001, C18:1 *P* = NS, C18p = NS.

a

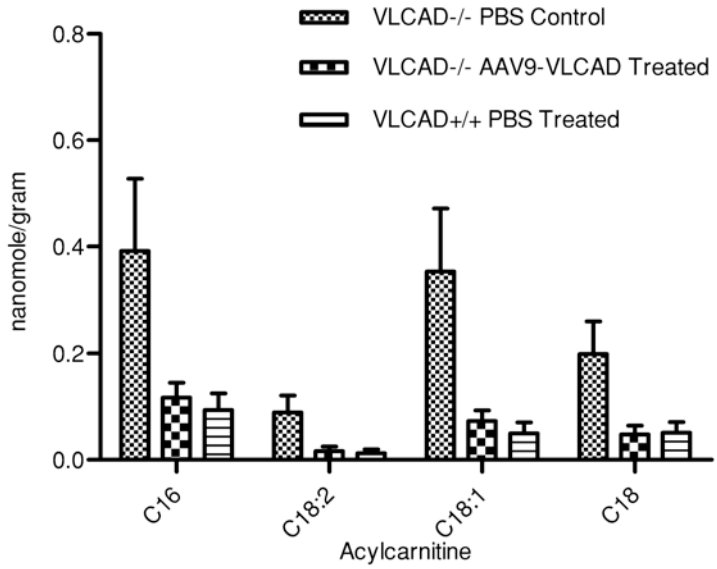

b

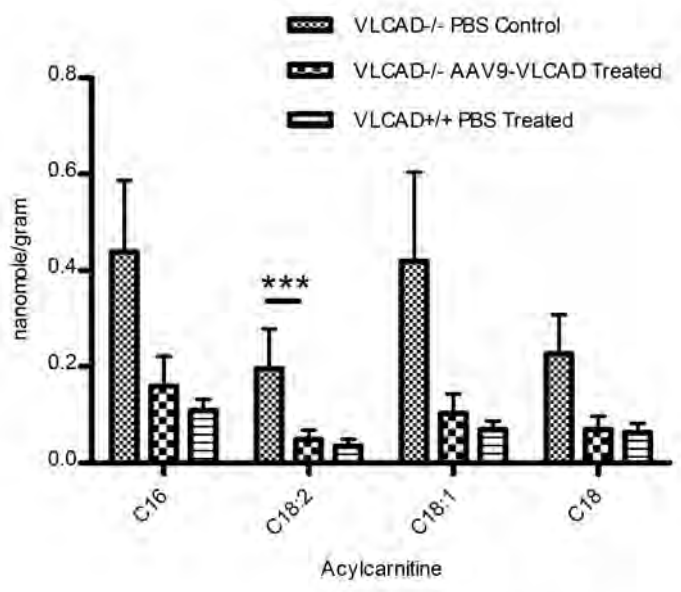

Figure 5.10 Biochemical analysis of Acyl Carnitines in the muscle *ex vivo*

Cardiomyopathy can be a presenting symptom in patients with VLCAD deficiency(139, 140). Since expression was widespread in the heart (Figure 2.2), a question remained if biochemical correction of the cardiac tissue had occurred. Cardiac tissue was analyzed by MS/MS of acyl carnitines extracted from *ex vivo* tissue. Acyl carnitines in cardiac muscle were at or below wildtype levels in rAAV9-treated mice whereas VLCAD-/- PBS controls had large accumulations (Figure 5.11). Expression of VLCAD in cardiac muscle, facilitated by rAAV9, was able to correct VLCAD-/- animals to wild-type levels of acyl carnitines in the cardiac tissue instead of large accumulations observed in VLCAD -/- animals.

Cold can induce metabolic derangement in VLCAD deficiency patients, as production of heat requires fatty acid oxidation especially after dietary fat stores have been used up (141). VLCAD deficient mice are also unable to maintain body temperatures during a cold challenge, and it has been shown to be fatal especially when combined with fasting (142). To assay for disease specific phenotypic correction, a cold fast challenge was utilized, in which the mice are fasted for 18 hours followed by a cold challenge in a 4°C room for 2.5 hours. During the challenge, a humane sacrifice was performed for animals with a body temperature below 20°C as determined by IACUC. In Figure 5.12a, the VLCAD-/- AAV9-treated and wildtype animals were able to maintain average body temperatures of 26.15°C and 26.4°C respectively for 150 minutes.

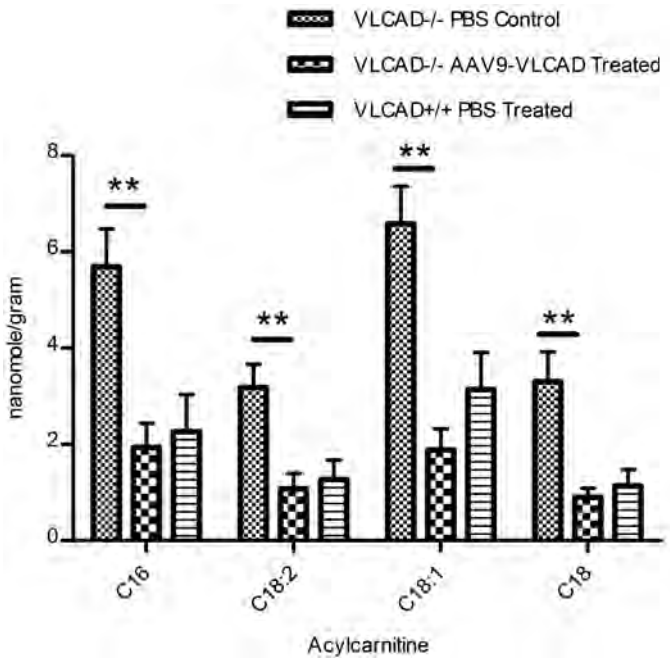

Figure 5.11 Reduction of Acyl Carnitines in the heart

Mass spectrometry of heart tissue *ex vivo* at 21–25 weeks post-injection. n = 7 untreated VLCAD$^{-/-}$ controls, n = 6 AAV9 VCLAD$^{-/-}$ and wild-type controls. Error bars are SEM. Statistics were as follows: C16 P = 0.003 C18:2 P = 0.005 C18:1 P = 0.004 C18 P = 0.005.

Figure 5.12 Temperature maintenance and survival of rAAV9- VLCAD treated mice after cold fast challenge

(a) Core body temperature of mice undergoing cold fast challenge, temperatures were recorded every 20 minutes by rectal thermometer. Mice were humanely sacrificed if body temperatures dropped below 20 °C, $n = 4$. Error bars are SEM. $P \leq 0.0001$ by two-way analysis of variance (ANOVA) of temperature and time (starting at 20 minutes in cold until 150 minutes) between VLCAD-/- PBS Control and VLCAD-/- AAV0-VLCAD Treated. (b) Survival of cold fast challenge.

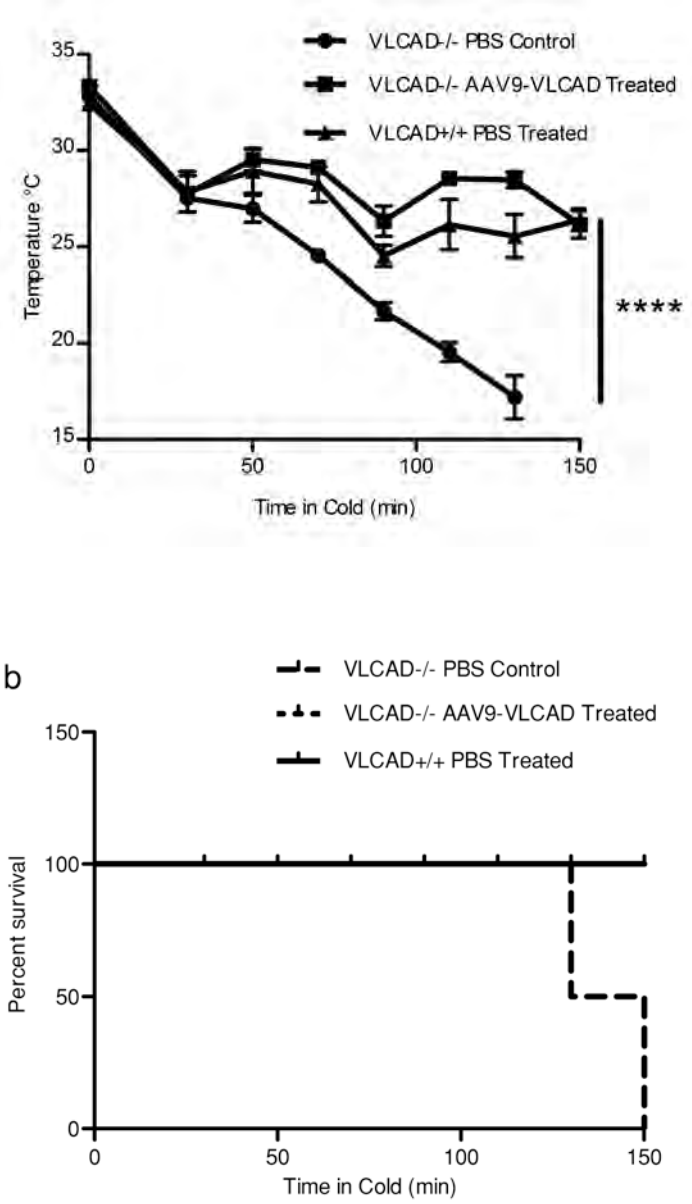

Figure 5.12 Temperature maintenance and survival of rAAV9-VLCAD treated mice after cold fast challenge

However, PBS control VLCAD-/- animals were unable to maintain body temperatures above 20°C, with two animals being euthanized at 110 minutes the remaining two animals at 130 minutes. To summarize, by 150 minutes into the cold challenge all of the PBS control VLCAD-/- animals had internal temperatures that dropped below the humane sacrifice point, whereas all the VLCAD -/- AAV9 treated, and wildtype animals survived (Fig. 5.12B). Lethargy and hypotonia are often a presenting symptom when VLCAD deficient patients are undergoing a period of metabolic crisis(136). PBS control VLCAD deficient animals became lethargic and hypotonic during the cold fast challenge (Video 5.1). In contrast, rAAV9-treated animals as well as the wildtype animals did not display lethargy and hypotonia as can be appreciated (Video 5.2 and 5.3).

Hypoketotic hypoglycemia is a primary presenting symptom in VLCAD deficient patients. Blood glucose levels were compared in all three strains, in fed, fasted and cold challenge state. There were no significant differences between any of the groups at the fed levels, however blood glucose levels were significantly reduced following both fasting and cold challenge in the PBS control VLCAD deficient animals when compared to the wild type mice (Fig. 5.13). In contrast, the rAAV9-VLCAD treated animals fully corrected glucose levels to that of wildtype under both fasted and cold conditions. One wildtype mouse out of four had a blood glucose level of 278mg/dl, which drove the average up in the wildtype after the cold fast challenge. However, blood glucose levels after the

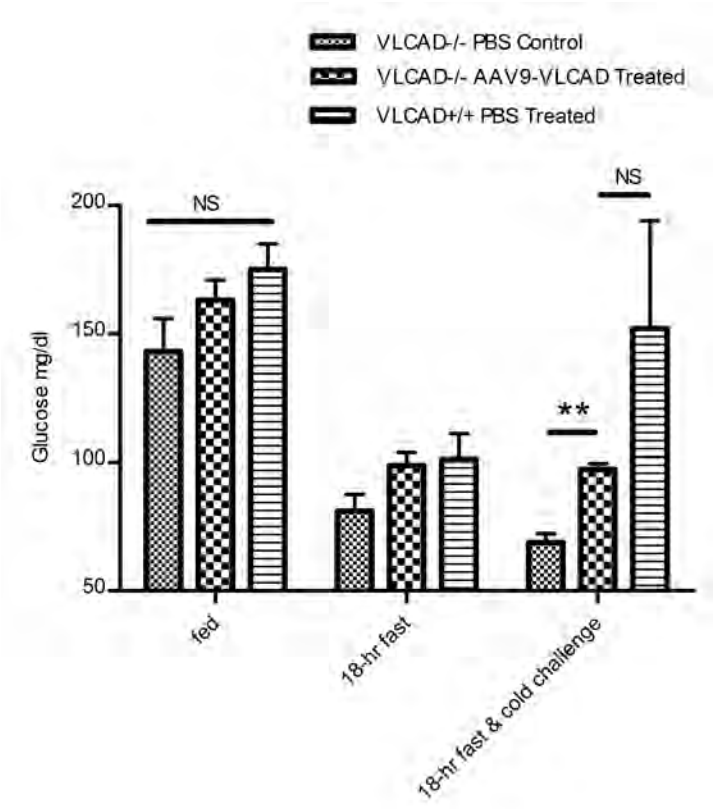

Figure 5.13 Maintenance of blood glucose in rAAV9-VLCAD treated mice after cold fasting challenge

Blood glucose levels during fed, fasted and fasted plus cold challenge conditions, *n* = 4. Error bars are SEM. No significant difference at fed state between all groups or between rAAV9-treated animals and wild-type under any condition, Significant differences were observed between rAAV9-treated VLCAD-/- animals and PBS treated VLCAD -/- after cold fast challenge *P* = 0.005.

cold fast challenge, were not significantly different from the VLCAD-/- rAAV9-treated and the wildtype mice, whereas VLCAD-/- animals blood glucose levels were significantly reduced.

Interestingly rAAV9-VLCAD treated female mice, which received the same vector and dose but had little to no VLCAD expression in the liver, did not show reduction of accumulates of long chain acyl carnitine after fast like the male counterparts(Figure 5.14). Although an initial drop is reported two weeks post injection in VLCAD-/- VLCAD treated mice, which is commonly observed across all groups and even in uninjected mice (Figure 5.3), the accumulation levels return to what is observed VLCAD-/- PBS controls. Opposite of the levels detected in male mice, which were corrected and were more similar to VLCAD +/+ mice after VLCAD injection. The female mice did however have similar levels of expression of VLCAD in other tissues (Figure 3.4).

When the rAAV9-VLCAD treated female mice underwent the cold fasting challenge on one hand, they were able to better maintain body temperatures then VLCAD-/- PBS treated females, like their male counterparts (Figure 5.15). On the other hand they were unable to maintain temperatures as well as wildtype, unlike the male counterparts. rAAV9-VLCAD treated female mice were able to maintain temperatures at wildtype levels for 90 minutes, at which point one VLCAD-/- PBS treated mouse's temperature dropped below the critical temperature. However, by the end of the study at 150 minutes, two out of three

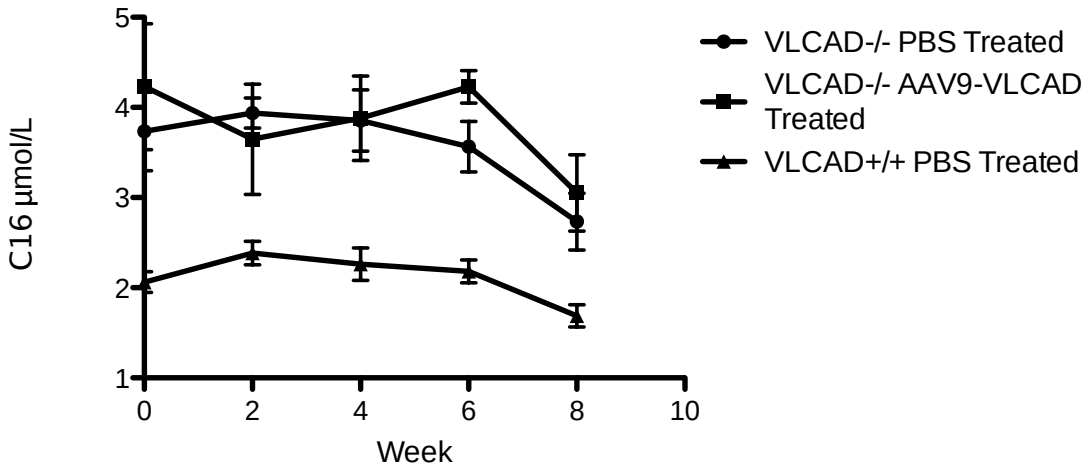

Figure 5.14 MS/MS quantification of C16 in the whole blood over time in female mice

All animals were fasted 24 hours prior to bleeding. Mass Spectrometric quantification of C18:1 over time. n=10 for week 0 & 2 and n=4 for weeks 4 & 8 for all groups.

Figure 5.15 Temperature and survival of female rAAV9-VLCAD treated mice after cold fast challenge

(a) Core body temperature of mice undergoing cold fast challenge, temperatures were recorded every 20 minutes by rectal thermometer. Mice were humanely sacrificed if body temperatures dropped below 20 °C, *n* = 4. Error bars are SEM. (b) Survival of cold fast challenge

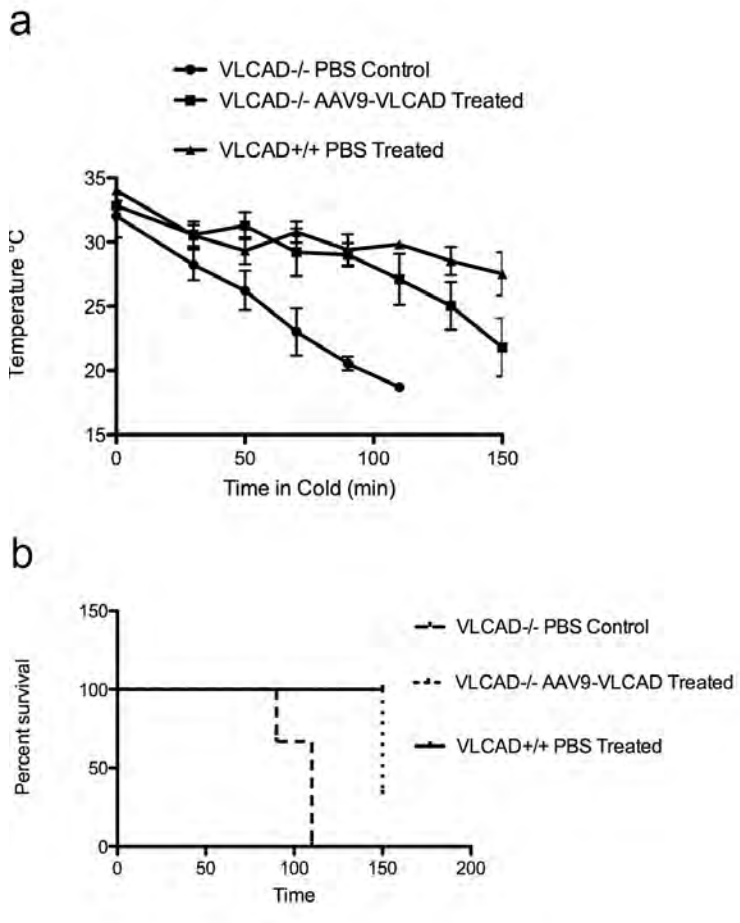

Figure 5.15 Temperature and survival of female rAAV9-VLCAD treated mice after cold fast challenge

rAAV9-VLCAD treated females temperatures dropped below the humane point and had also become lethargic. It should be noted that female VLCAD-/- mice in general were more susceptible to the cold fast challenge, as their temperatures dropped below 20°C from 90-110 minutes whereas the male mice did not drop below 20°C before 130 minutes. The difference may be accounted for by males have significantly larger body weight and insulating fat stores. rAAV9-VLCAD treated female mice also became hypoglycemic after fasting and the cold fast challenge, similarly to VLCAD-/- PBS controls (Figure 5.16). Unlike the male rAAV9-VLCAD treated mice they were not able to maintain glucose levels through a fast or cold fast challenge, and behaved more similarly to untreated VLCAD -/- mice.

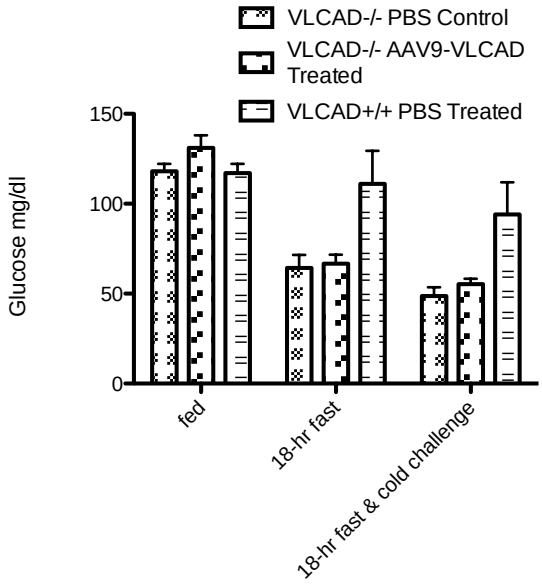

Figure 5.16 Blood glucose in female rAAV9-VLCAD treated mice after cold fast challenge

Blood glucose levels during fed, fasted and fasted plus cold challenge conditions, *n* = 3. Error bars are SEM.

Discussion

Phenotypic correction of multiple disease-specific phenotypes, including blood acyl carnitines, thermoregulation, resistance to lethargy, and blood glucose maintenance was demonstrated here using rAAV9-mediated gene therapy in a male mouse model of VLCAD deficiency. A clinically translatable non-invasive technique, MRS, was employed to measure correction within the muscle and liver. *In vivo* MRS results confirmed the MS/MS findings *ex vivo* in the tissues. Within the liver tissue, lipid accumulates were mildly reduced as detected by MRS and MS/MS but not to the extent distinguished in other tissues such as skeletal muscle. No previous work concerning correction of disorders of fatty acid oxidation have employed MS/MS of tissue samples to measure accumulations of acyl carnitines within tissues themselves. Correction of SCAD using rAAV8 demonstrated reduction of liver accumulates by MRS but used a liver targeted approach injecting into the portal vein(107). Expression within the liver was observed after systemic injection used in this study. The VLCAD staining pattern in the liver is different from that within the cardiac and skeletal muscle where it is widespread but at a low level of expression. Within the liver, it appeared that certain cells expressed VLCAD at very high levels, while other cells did not express at all. However without efficient targeting of the liver, reduction of accumulates in the blood as well as maintenance of blood glucose levels would not be expected, as noted in the female mice. This variable VLCAD expression pattern may cause the correction discrepancy between whole liver

extract accumulations and the impact of the liver on reducing whole blood accumulates and maintaining blood glucose levels. It was noted that expression within the liver directly correlated with reduction of acyl-carnitine accumulates within in the tissue itself. Individual mice with the most expression displayed the most reduction, whereas individual mice with the least expression had large accumulations within the liver. Also as androgen-dependent transduction of the liver was shown to be important in female mice, differential expression of testosterone may account for variable levels of expression across mice, however these levels were not tested. This phenomenon of variable expression in the liver has been previously reported using rAAV8(143).

Brown fat plays an important role in non-shivering thermogenesis by expressing UCP-1 protein, which allows uncoupling of oxidative phosphorylation and the production of heat. Brown fat has a vital role in thermogenesis in human newborns, and is present and functional in adult humans although to a lesser extent(144). The pronounced ability of rAAV9-treated VLCAD-/- mice to thermoregulate body temperature in a cold environment compared to the untreated mice clearly demonstrates correction of the cold sensitive phenotype. The role brown fat plays in the phenotypic correction of these mice has yet to be determined; however it is suspected that brown fat is not solely responsible for temperature maintenance during the cold fast challenge as the female mice were unable to maintain body temperatures at wildtype levels in spite of brown fat transduction. However, they were not as susceptible to cold temperatures as the

VLCAD-/- mice were, suggesting that brown fat, cardiac or skeletal muscle or even multiple systems also play important roles in thermogenesis. Work by Skilling and colleagues(145) suggests that brown fat does not play as strong a role in VLCAD deficient sensitivity to cold as it does in shorter chain deficient animals such as SCAD. They suggest that rapid consumption of glycogen in the liver and muscle as well as impaired ability to shiver and decreased cardiac function is responsible for cold sensitivity(145). Unlike other disorders of fatty acid oxidation no energy can be produced by fatty acid oxidation in VLCAD deficient individuals, as VLCAD is the rate-limiting enzyme. Exil and colleagues(146) reported that VLCAD deficient animals succumb to bradycardia during the cold fast challenge. Therefore both shivering, heat produced through muscle contraction, and non-shivering, heat produced through uncoupling of oxidative phosphorylation in the brown fat, thermogenesis may play a role in the defect in thermoregulation in these mice. rAAV mediated expression of VLCAD in liver, allowing the animal to produce ketones which can go on to produce energy in other tissues, may have a larger impact on thermogenesis than expression of VLCAD in the brown fat as VLCAD deficient mice retain 80% residual activity in the brown fat(145). Also rAAV-mediated expression of VLCAD in the muscle may allow for heat production through shivering. Interestingly, carnitine palmityoltransferase 1a (CPT1a) heterozygous mice, the liver isoform of CPT enzyme, are not cold intolerant but heterozygous (CPT1b), the muscle/heart isoform (CPT1b) are cold intolerant suggesting the importance of long chain fatty

acid oxidation in the muscle and heart for thermogenesis(4). Correction of multiple tissues, as demonstrated in the male mice, may be necessary in order to see correction of this phenotype.

Current standard of care for VLCAD patients is primarily dietary, limiting long chain fatty acids and supplementing with medium chains as well as avoidance of fasting. Studies have shown effectiveness, especially when administered prior to exercise(20, 21). However, even with screening and treatment, approximately 10-20% of patients suffer episodic rhabdomyolysis(147). Supplementation of medium chain triglycerides has come under question since patients can suffer myopathic symptoms despite treatment and studies in VLCAD-deficient mice have shown muscle phenotypes after exercise on fat-reduced carbohydrate-enriched diets(148). Also mice fed a diet of medium chain triglycerides had accumulations of visceral fat, liver lipids and tissue fat composition changed significantly(18). Although patients diagnosed by newborn screening have greatly reduced mortality associated with all disorders of fatty acid oxidation, sudden death has still been reported(46). Having a therapy rather than treatment options could vastly improve patients' quality of life. This work provides proof-of-concept for rAAV9-mediated gene therapy for VLCAD deficiency.

CHAPTER VI: Discussion

Taken together the work presented here has significant implications for both clinical and basic sciences. We have presented not only a potential therapy for VLCAD deficiency, but also more generally developed useful tools for the basic understanding of the roles specific tissues play in mitochondrial fatty acid oxidation. Also in the course of this work, a novel method for transduction of brown fat by single-stranded rAAV9 was discovered, as well as efficient expression across the brain in cells of different morphologies, after systemic injection in adult mice. The therapeutic benefits of efficient brain transduction after non-invasive administration have a number of potential clinical applications. Clinical applications of brown fat expression have yet to be explored. However, rAAV9-VLCAD expression may also have a therapeutic benefit of increasing levels of fatty acid oxidation for different disorders where fatty acid oxidation rates are low. One group recently showed that in mice, rAAV1 delivery to the liver of carnitine palmitoyltransferase 1A (CPT1A) and a permanently activated form of CPT1A protected against weight gain, steatosis, diabetes and obesity-induced insulin resistance after induction of a high fat diet; and moreover in a genetically obese mouse model, reported reduced glucose and insulin levels and liver steatosis(149).

VLCAD deficiency is a recessive single gene disorder that affects multiple organs and is detectable by newborn screening but yet has no known definitive treatment. Moreover it has a heterogeneous phenotype with some patients

presenting with a cardiomyopic phenotype, others with a liver phenotype and still others with a muscle phenotype. The presenting symptoms are not exclusive between phenotypes and can often change with time. With the advent of better therapeutic vectors, the possibility of targeting multiple tissues with one vector is now available. Multiple tissue targets were desirable here as an important proof-of-concept that biochemical correction could be achieved in all three organ tissue targets.

Moving forward a more targeted gene therapy approach may be possible. Vector selection is generally based on the target tissue for expression of the therapeutic protein. In the case of secreted proteins, the tissue targeted for transduction and expression of the therapeutic protein is not always the tissue where the protein will have the therapeutic benefit. The muscle is an ideal clinical candidate for ectopic expression as it is easily accessible, has a large mass, and potentially less detrimental if a severe side effect occurred. For example, a recent clinical trial by Flotte *et al*. uses the muscle to express the secreted alpha-1 anti-trypsin protein where the therapeutic effect is in the lungs of the patients(103).

In the work described here, VLCAD is associated with the inner mitochondria membrane, and therefore not secreted, however VLCAD's substrate, long-chain fatty acids, are able to freely enter into and out of cells, but must be transported into and out of the mitochondria. In a disorder like SCAD or disorders of peroxisomal degradation, where disease phenotypes are generally

associated with toxic accumulates and not with energy deficiencies, it could be suggested that one organ could act as a metabolic sink for a systemic therapeutic effect. SCAD also benefits from short and medium chains not requiring active translocation across the mitochondria membrane. Conlon *et al.* and Beattie *et al.,* were both able to show systemic reduction of blood acyl-carnitine accumulations after targeting the muscle and liver respectively, in SCAD deficiency(106, 107). However the disease phenotype for long chain fatty acid disorders is not only associated with toxic accumulations but more importantly an energy deficiency. When Beattie *et al.* tried to target muscle in LCAD deficient mice using rAAV1, correction of blood acyl-carnitine accumulations were not detected, although reduced hepatic microsteatosis was reported in female mice(110). In studies presented here, female mice suggest that muscle correction alone, although expression of VLCAD was measured in many other tissues besides skeletal muscle, was not sufficient for reduction of acyl-carnitine accumulations, maintenance of temperature or blood glucose under fasting and cold conditions. Even if the muscle correction would show biochemical correction of accumulates, it is unlikely that it could treat the energy deficiency suffered in other organs such as heart or liver, as once long-chain fatty acids have started beta-oxidation they are unlikely to leave the treated muscle cell and travel to an untreated liver or heart cell. All VLCAD deficient patients have the ability to break down long chain fatty acids in their peroxisomes, which is capable of oxidizing fatty acids until they reach a chain size of eight carbons,

but yet a phenotype for this disease still exists in deficient patients. Severity of disease and wide heterogeneous phenotype in these patients may be related to the amount of compensation peroxisomal oxidation can provide. Alternatively, muscle expression may not have been high enough in female mice to produce systemic correction in the female mice and a more targeted muscle approach may be able to show systemic correction.

Interestingly, there is an organ that can produce energy that can subsequently be transferred systemically. The liver's ability to produce ketones, which can be broken down to produce energy in other tissues, allows for hope of a tissue-specific correction of VLCAD by potentially treating both the energy deficiency and toxic accumulations. Long chain fatty acids could be metabolized in the corrected cells of the liver, thus removing toxic accumulations, and also producing ketones. From the liver those ketones released into the blood which can go to the heart, whose preferred energy source is fatty acid oxidation, or the brain which prefers glucose for energy production but uses ketones under glucose limiting conditions. Tissue specific expression restricted to the liver was not studied in this work, but could have important therapeutic relevance in the future.

Defense of Gene Therapy for VLCAD Deficiency

A large number of genetic therapy targets are often diseases with devastating outcomes and where patients have little hope. Although VLCAD

deficiency is not associated with drastically reduced lifespan and quality of life it is highly associated with sudden death. With the advent of newborn screening for these disorders infant sudden death has been drastically decreased, but has been by no means eliminated. VLCAD can still be fatal during early infancy in spite of newborn screening(147). There have been 20 reported cases of sudden death in MCAD deficienct patients, which is less severe then VLCAD deficiency, even when MCAD deficient status was known and 3 of the patients were 19 years or older at death(46). Also mild adult onset phenotypes can sometimes become more severe. One VLCAD case report describes a 32 year old patient, who previously had recurrent muscular weakness and a family history of a brother who died of Reye's syndrome at 17 years of age, presented with coma, persistent hypoglycemia, rhabdomyolysis and acute cardiomyopathy requiring 20 days in intensive care unit, but was successfully discharged after 13 weeks(150). Any period of metabolic decomposition in a patient with a FAO disorder, although acute, can be fatal and severely detrimental.

Current treatments for VLCAD deficiency other than low-fat dietary restrictions and avoidance of fasting, are not well studied and inefficient. Many severe patients must be fed through gastrostomy tubes especially at young ages. Also as patients are usually exercise restricted and told to eat regularly on a frequent schedule, patients often have excessive weight gain in spite of low-fat diets. Non-compliance is also often an issue with these disorders since under normal conditions these patients can appear perfectly healthy. However any

seemingly mild illness can cause rapid metabolic decomposition. Extra care must also be taken in any perioperative period, as patients can have severe complications(15).

On current standard MCT treatment, 10-20% of patients still experience rhabdomyolysis. The three patients described in the triheptanoin study, who were currently on MCT therapy given by gastrostomy were described as: 5 years old patient unable to stand from sitting, climb stairs or open heavy doors without assistance, hepatomegaly and symptoms of mild cardiomyopathy, 9 year old who had very limited exercise capacity due to pain, attention deficient disorder and mild hepatomegaly, and a 2 year old who was unable to support his own weight when lifted through his arms and could not run for more then 10-15 feet without stumbling(26). The last two patients would be considered in the mild muscle phenotype because no hypoglycemia or cardiomyopathy was reported. Moreover the standard treatment of MCT supplementation has not been well studied in the long-term and mouse studies have produced concerning results. Studies have shown that supplementation prior to exercise has benefits but long-term supplementation leads to hepatic steatosis, oxidative stress, disrupted fat distribution and composition (18, 20, 148, 151)

Even among the experimental therapies outlined in Chapter I, very limited therapies have been suggested that could treat all VLCAD phenotypes. Bezafibrate and resveratrol only help patients with mild disease and some enzyme activity. Other treatments are mostly palliative and are not well studied.

Gene therapy for VLCAD, as well as other long-chain FAO defects and acyl-CoA deficiencies, would allow for curative therapies for all phenotypes associated with disease as well as phenotypes that might develop with age. Retinopathies associated with mTFP and LCHAD may be able to be corrected through gene therapy approaches as rAAV eye gene therapies have had clinical success(152). Through these proof-of-concept studies, non-invasive evaluative tools such Magnetic Resonance Spectrometry were performed which would allow for potential tracking of clinical outcomes in patients.

Perhaps most importantly, this work demonstrated that correction of biochemical and defects correlated with disease-specific phenotypes under conditions of physiologic stress, such as the cold fasting challenge. The type of phenotypic correction is crucial for demonstrating the feasibility of therapeutic benefits for VLCAD gene therapy in a clinical setting. Based on these findings, gene therapy for these disorders may have a clear clinical benefit for affected patients. Future steps toward clinical gene therapy are already in progress, as a collaboration is being formed with a leading clinical group in this field at Oregon Health Sciences University. Formal pharmacology and toxicology studies will be needed to satisfy FDA requirements, but these should provide a straightforward path to the clinic for this disorder.

CHAPTER 7: Additional Projects: Aberrant Immune Responses in CFTR-/- mice

Introduction

Cystic fibrosis (CF) is the most common autosomal recessive genetic disease in the US, affecting 1 in 3,300 live births; and the result of mutations in CFTR, a chloride channel and regulator of other ion channels. CF patients suffer a wide range of clinical consequences from the disease, including pancreatic insufficiency, with subsequent malabsorption and impaired nutrition, and chronic airway infection with *Pseudomonas aeruginosa* and other pathogens(153). The mechanisms by which CFTR mutations cause chronic lung disease in CF are not fully defined, but may include the combined effects of altered ion and water transport across the airway epithelium(154-156), increased binding or decreased clearance of *Pseudomonas aeruginosa* (157, 158) as well as increased pro-inflammatory cytokine production in the CF airway (159-163). CF cell lines demonstrate increased NFkB activation and increased IL-8 secretion in response to *P. aeruginosa* exposure, as compared with control cells (163, 164). Furthermore, CFTR mutant mice demonstrate a greater cytokine response (KC, MIP2, IL-1beta), greater mortality, and weight loss after airway challenge with a *P. aeruginosa*-agarose bead slurry, as compared with control mice (165-168).

Allergic broncho-pulmonary aspergillosis (ABPA) is a clinical syndrome characterized by recurrent wheezing and pulmonary infiltrates, an excessively

high total serum IgE, and high IgE and IgG antibodies directed against *Aspergillus fumigatus* (Af), which is usually found to be colonizing the airways of these patients. ABPA is common in CF, affecting approximately 15% of all patients (169, 170). It is occasionally recognized in patients with asthma, although some studies have shown that up to 50% of asthma patients with ABPA have at least one mutation in the CFTR gene (171-174). The immune response in ABPA appears to be an IL-4-driven, Th2-predominant response that is observed in CF patients and in the Cftr mutant mouse expression profiling studies (175-178). Based on this observation, our laboratory has recently described an ABPA-like model in CF mice (179). In subsequent studies we observed divergent cytokine production in splenocytes from the *Cftr* mutant mice challenged with Af antigen (180). This led us to question whether the differences in inflammatory signaling in CF mice are due to the direct or indirect effects of *Cftr* mutations within lymphocytes.

This question has been raised in previous work (181, 182). Studies conducted immediately following the discovery of CFTR indicated that lymphocyte chloride transport was defective in CF and could affect function under certain circumstances (183). A number of other studies have shown that *CFTR* gene replacement could restore lymphocyte channel activity to normal (184, 185). Finally, the Th2-bias of CF lymphocytes have been confirmed by a number of investigators (176, 177). In this report, we investigated whether there are primary defects in lymphocytes lacking CFTR function. Furthermore, we

propose a possible mechanism for this increased response in lymphocytes, in which aberrant calcium fluxes lead to an increase in the nuclear localization of NFAT, a transcriptional regulator of cytokines driving the Th2-biased response.

Materials and Methods

Mouse strains:

The *Cftr* knock-out strain used for these studies was the CFTR S489X -/- neo insertion in C57BL/6 mice developed initially at the University of North Carolina (186) and then modified with the transgenic over expression of gut-specific expression of human *CFTR* from the fatty acid binding protein (FABP)-promoter in order to prevent intestinal obstruction and improve viability (187). The other mouse strain used is *Cftr*-Δ*F508* mouse, both mouse strains have been backcrossed 10 generations onto a C57BL/6 mouse. For experiments on conditional knockout mice the recently developed floxed *Cftr* mouse (188) was crossed with the C57BL/6 mice expressing CRE recombinase under the control of the leukocyte-specific protein tyrosine kinase (LCK) promoter.

Aspergillus sensitization and challenge:

Animals were sensitized to Aspergillus fumigatus crude protein extract (Af-cpe) (Greer Laboratories). Briefly, animals were administered with intraperitoneal (i.p.) injections of 200ug of Af-cpe extract dissolved in 100ul of PBS on days 0 and 14. Aerosol challenge was performed with 0.25 % Af-cpe for 20 min in a

30x30x20 cm acrylic chamber using a jet nebulizer Pari model LC-D with an air flow of 6 liters/min on days 28, 29 and 30.

Adoptive Transfers:

Adoptive transfers were performed by harvesting either Af-cpe sensitized or naïve splenocytes from *Cftr-ΔF508* (Cftr-/-) or wildtype littermate controls. Briefly, spleens were disaggregated in Hank's buffer saline and passed through a 20um mesh. Cells were then resuspended in PBS at a concentration of $4.5x10^8$ cell/ml. Rag-/- mice on a C57BL/6 background were then injected intra-peritoneally with 100ul of the suspension. Eight weeks were allowed for engraftment before either challenging or sensitizing and challenging Rag-/- mice.

Antigen Recall:

Spleens were harvested and CD4 T cells and CD11b cells were separated using the AutoMACs pro (Miltenyi Biotec). Cells were counted and plated in 96 well round bottom plates so that there were 1×10^5 CD4 T cells and 1×10^5 CD11b positive cells for a total of 2×10^5 cells per well. Cells were cultured in media that contained 10mg/ml albumin (Sigma). After 3 days supernatants were removed and frozen for cytokine analysis using Luminex Technology (Bio-Rad, Hercules CA).

Intracellular Calcium Flux:

Spleens were harvested and CD4 T cells were separated using AutoMACS pro (Miltenyi Biotec). Intracellular Calcium staining was carried out as previously described (189).

NFAT Studies:

Splenocytes from *Cftr*-Δ*F508* (*Cftr*-/-) or wildtype littermate controls were plated on paired round bottom 96 well plates with RPMI 1640 10% FBS and 1% Pen/Strep at a concentration of $1x10^5$ cells/well. The cells were then stimulated with CD3/CD28 antibody cocktail and wells from one plate were harvested at (10, 30 and 90 min.). For nuclear protein extraction while the other was used to obtain cell culture supernatants at (1.5, 3, 6 and 24 hrs) for cytokine analysis. Nuclear NFAT translocation was assayed from the nuclear extracts using the modified kit TransAM NFATc1 (Active Motif). Cell culture supernatants were analyzed for cytokine secretion profiles using Luminex Technology (Bio-Rad, Hercules CA).

Results

In previous studies, we have shown that *Cftr*-/- mice on a mixed background had IgE levels that were 2-5 fold higher than their controls when sensitized and airway challenged with *Aspergillus fumigatus* crude protein extract (Af-cpe)(179). Furthermore, this phenotype was partially corrected after *Cftr* gene replacement with recombinant adeno-associated vectors(180). Here we further establish the phenotype by comparing total serum IgE levels in *Cftr*-/- mice that are on a congenic C57BL6 background. *Cftr*-/- and *Cftr*+/+ littermates were sensitized and challenged with Af-cpe as previously described. Total serum IgE from congenic mice littermates challenged with Af-cpe were on average two-fold higher for *Cftr*-/- mice (Figure 7.1).

To determine if *Cftr*-/- lung epithelial cells were responsible for higher IgE response towards Af-cpe, we designed adoptive transfer experiments transferring Cftr-/- immune cells into Rag-/- mice hosts that where otherwise normal for *Cftr*. In the first set of experiments, *Cftr*-/- mice with a deletion of phenylalanine at amino acid position 508 of the *Cftr* gene (ΔF508, the most common mutation in the CF population) were sensitized but not airway challenged with Af-cpe. We then harvested splenocytes from these mice and their wildtype littermate controls and adoptively transferred them via an intra-peritoneal injection into Rag-/- mice of the same C57BL6 genetic background. Eight weeks post transfer the Rag-/- mice were airway challenged with aerosolized Af-cpe. Since Rag-/- are deficient in T and B cells and can not

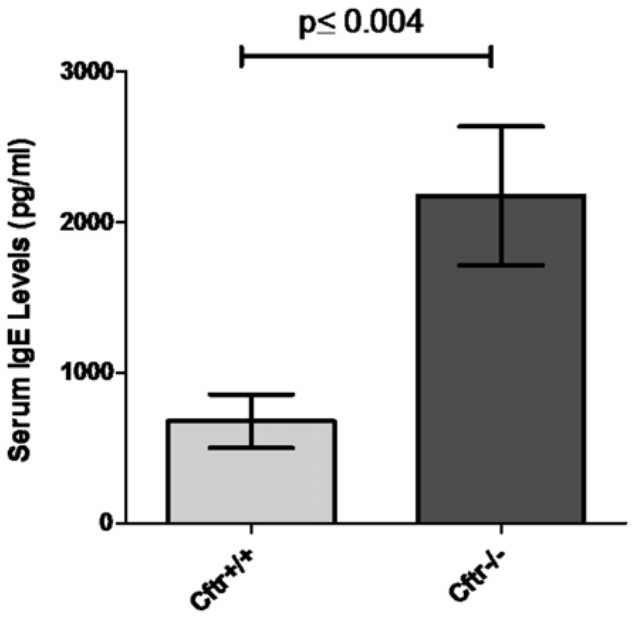

Figure 7.1 Total serum IgE levels in congenic C57B6 CFTR−/− mice and their littermates after Af sensitization and challenge

Mice were sensitized with 200 µg of Af crude extract dissolved in 100 µl of PBS on Days 1 and 14. Blood samples were collected on Day 32, 48 hours after the third aerosol Af challenge. Total serum IgE in the Af-sensitized mice was measured by ELISA. Data are shown as group averages (±SEM).

produce IgM, total circulating IgM levels were measured to verify engraftment (Figure 7.2B). In order to determine if sensitized splenocytes from CF mice alone were able to recapitulate the high IgE phenotype in a wildtype (*Cftr*+/+) airway, sera from the adoptively transferred Rag-/- mice was checked for IgE levels. The two-fold enhanced IgE phenotype is transferred into the host by the adoptive transfer of sensitized splenocytes (Figure 7.2A). To rule out the possibility of other *Cftr*-deficient tissues having an effect on the sensitization of the immune cells that were transferred, we repeated these experiments by transferring naïve splenocytes into naive Rag-/- mice. Eight weeks after the naïve splenocyte transfer, Rag-/- mice were sensitized and airway challenged with Af-cpe. Again the experiments recapitulated the hyper-IgE phenotype as serum levels of Rag-/- mice receiving CF splenocytes were also two-fold higher than Rag-/- mice receiving wildtype splenocytes (Figure 7.2C). In contrast, IgM levels in these two groups were not different, confirming that the difference in IgE antibodies levels was not due to differences in B-cell engraftment (Figure 7.2D).

We then designed a series of antigen recall experiments in order to determine what cell population of the splenocytes was responsible for polarizing the adaptive Th2 immune responses. In these experiments, splenocytes from mice that had been sensitized to ovalbumin (OVA) were magnetically sorted into either CD4+ lymphocytes or CD11b+ monocytes. The rationale for using OVA stimulation was that *in vitro* the monocytes would process the antigen and present it to the OVA specific T cells, allowing one to monitor the cytokine

Figure 7.2 Adoptive transfer of CF splenocytes confers elevated IgE phenotype

CFTR-ΔF508 (CFTR−/−) mice on the C57BL/6 background or matched control C57BL/6 mice (CFTR+/+) were used as donors for splenocyte adoptive transfer into B6-Rag−/− mice. Total serum IgE (A and C) and IgM (B and D) were measured after Af challenge. (A and B) CFTR-ΔF508 (n = 6) and C57BL/6 littermates (n = 6) were sensitized with Af–crude protein extract (Af-cpe), and 2 weeks after sensitization their splenocytes were transferred into Rag−/− mice, where they were allowed to engraft for 8 weeks before airway challenging the mice. (C and D) Naive CFTR-ΔF508 (n = 10) and naive C57BL/6 littermates (n = 10) were used to harvest naive splenocytes for transfer into Rag−/− mice. Splenocytes were allowed to engraft for 8 weeks, and then Rag−/− mice were sensitized and airway challenged with Af-cpe.

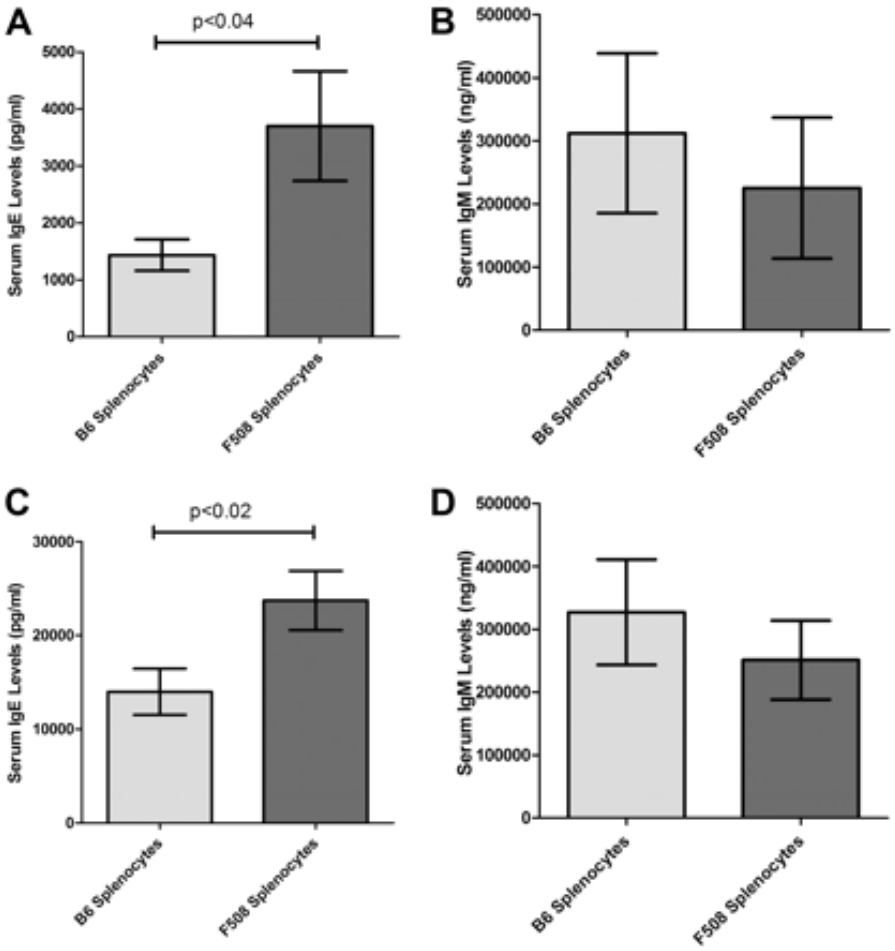

Figure 7.2 Adoptive transfer of CF splenocytes confers elevated IgE phenotype

profiles secreted in response to a specific antigen. To determine if the Th2 polarization was due to either antigen presentation or to the antigen-specific response by T-cells the cell populations were paired in the following configuration; CF monocytes with CF T-cells, CF monocytes with wildtype T-cells, wildtype monocytes with CF T-cells or wildtype monocytes with wildtype T-cells. These experiments uncovered three main cytokine secretion patterns. First elevated secretion of Th2 cytokines IL-4 and IL-13 was dependent on whether the stimulated cells had CF CD4+ T cells and was independent of the monocyte source (Figure 7.3A-B). A different cytokine secretion pattern was observed for IL-17 and IL-5; this one was synergistic and dependent on whether both the antigen presenting cell population (Cd11b+) and the effector cell population (CD4+) were *Cftr*-/- (Figure 7.3C-D). Finally IL-2 secretion was similar among all combinations demonstrating that the altered cytokine secretion patterns are not an experimental artifact resulting from the cell mixtures (Figure 7.3E).

To confirm the hypothesis that deficiency in functional CFTR in T cells results in Th2 biased adaptive immune response and leads to higher IgE levels, we used conditional *Cftr* knockout mice. These studies were carried out by crossing the recently described *Cftr* floxed mice (188) with mice expressing Cre recombinase under the control of the leukocyte-specific protein tyrosine kinase (Lck) promoter, which drives expression of Cre recombinase in CD3+ lymphocytes, resulting in the knockout of the *Cftr* gene in both CD4+ and CD8+ T-cells.

Figure 7.3 *In vitro* antigen recall with mixed cell populations

Splenocytes from congenic CFTR−/− or CFTR+/+ mice sensitized to ovalbumin (OVA) were separated into both CD11b+ and CD4+ cell populations with magnetic beads. Cells were mixed and “crossed” to make four groups of cell preparations: (1) CF CD11b+ with CF CD4+ cells; (2) CF CD11b+ with wild-type (WT) CD4+ cells; (3) WT CD11b+ with CF CD4+ cells; and (4) WT CD11b+ with WT CD4+ cells. Cells were then stimulated with OVA for 5 days. The cell culture supernatants were analyzed for cytokine profiles at Day 5. Data are shown as group averages (±SEM).

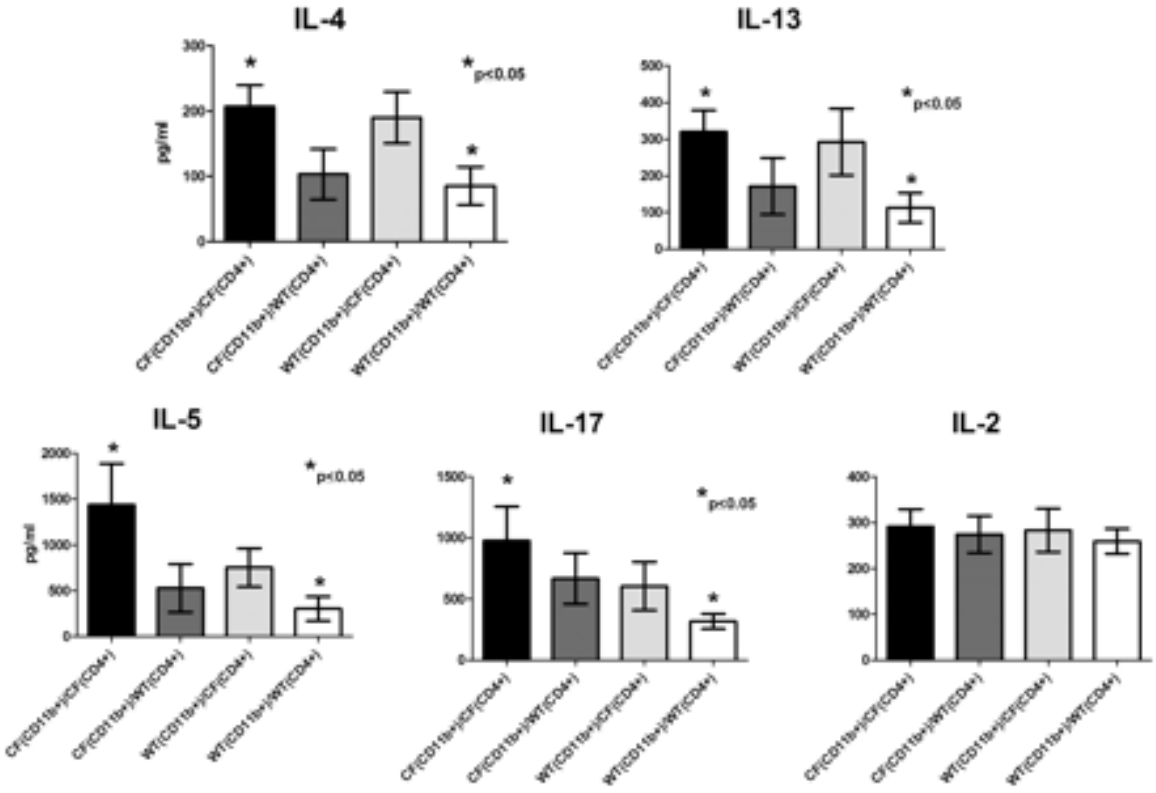

Figure 7.3 *In vitro* antigen recall with mixed cell populations

The floxed *Cftr* gene was maintained as a homozygous allele and mice were crossed to yield both mice that were Lck-Cre+, and thus *Cftr* deficient in the T-cell population and mice that were Cre- and thus maintaining the functional floxed *Cftr* gene in all tissues and cell types. Interestingly, IgE levels in naïve Lck-*Cftr*-/- mice showed a significant upregulation of serum IgE even at basal levels when compared to their littermate controls (Figure 7.4). This suggests an inherently Th2-biased commitment of *Cftr* deficient T-cells even in the absence of stimulation. Next we sensitized and airway challenged these mice along with their littermate controls with Af-cpe. The results further confirmed a role for *Cftr* expression in T cells as evidenced by the divergence in serum IgE levels developing at day 21 (1 week after the 2^{nd} i.p injection) and through day 32 (48 hrs after the final aerosol challenge) (Figure 7-5).

To elucidate possible mechanisms for the CFTR channel altering lymphocyte activation, we tested a recently described model suggesting a link between CFTR and intracellular calcium (iCa^{2+}). While, iCa^{2+} concentration can be controlled by multiple mechanisms including: calcium channels, plasma membrane Ca^{2+} ATPase pumps, and potassium channels among others, the model suggests that the *Cftr* mutation can cause altered iCa^{2+} and its eventual signaling and inflammation. Suggesting that CFTR's effect on cell membrane potentials alters the electrical driving force for Ca^{2+} to enter the cells. In *Cftr*+/+ T84 intestinal epithelial cells it has been demonstrated that changes in membrane potentials caused expected changes in iCa^{2+} during agonist activation

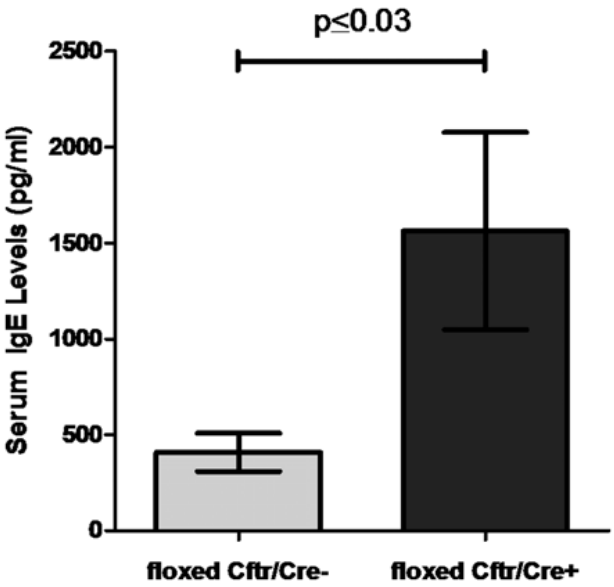

Figure 7.4 Total serum IgE levels in naive conditional CFTR-/- mice

T cell conditional knockout mice created by crossing the floxed Cftr mouse with mice expressing the Cre recombinase expressed from the leukocyte-specific protein tyrosine kinase (Lck) promoter were compared with control animals that were Cftr floxed, but Cre recombinase negative. Basal serum IgE levels were analyzed by ELISA. Data are shown as group averages (±SEM).

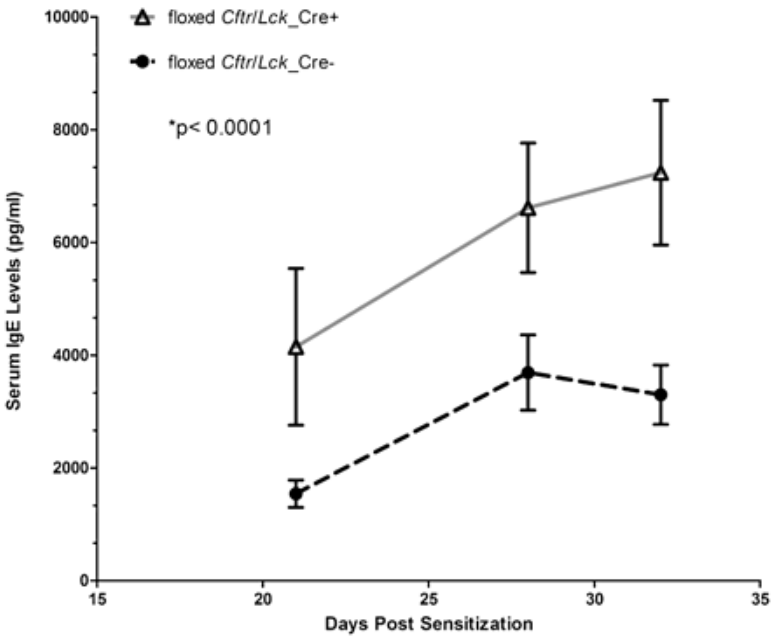

Figure 7.5 Total serum IgE levels in Af-cpe–sensitized conditional CFTR-/- mice

T-cell Cftr knockout mice (Cftr floxed and Lck Cre+) along with WT controls (Cftr floxed and Cre−) were sensitized with 200 µg of Af crude extract dissolved in 100 µl of PBS on Days 1 and 14. Blood samples were collected on Days 21, 28, and 32. Total serum IgE in the Af-sensitized mice was measured by ELISA. Data are shown as group averages (±SEM).

of calcium entry pathways (190, 191). Thus, with a reduction in Cl- permeability in *Cftr*-/- cells their membranes can hyperpolarize and it is predicted that Ca^{2+} entry across the cell membrane would be increased. Alterations in this pathway are important because in lymphocytes, iCa^{2+} initiates a signal transduction pathway through calmodulin and calceneurin eventually leading to the activation of nuclear factor of activated T-cells (NFAT). NFAT has been shown to enhance gene expression of IL-4, IL-13, IL-5, TNF-alpha cytokines among others (192).

To test the above hypothesis and whether the CFTR deficient T cells would have an effect on iCa^{2+} signaling through the T cell receptor (TCR), we measured intracellular calcium fluxes in CD4+ T-cells in response to CD3/CD28 stimulation of the TCR. Measurements of intracellular calcium in CD4+ T cells using the calcium sensitive Indo-1 dye revealed a significantly greater and enhanced calcium flux response in *Cftr* deficient T cells (Figure 7.6).

To show that the increased intracellular calcium fluxes detected in TCR activation in response to CD3/CD28 results in nuclear accumulation of NFAT, we performed a time course where T cells from splenocyte preparations were stimulated with same CD3/CD28 antibody cocktail. Nuclear extracts from the stimulated cells were prepared and used to measure NFAT levels. The results confirm that NFAT is translocated to the nucleus in a time sensitive manner after TCR activation, by CD3/CD28, and that this nuclear localization is significantly increased in *Cftr* deficient T cells (Figure 7.7).

Figure 7.6 Intracellular calcium (iCa2+) flux

Changes in the concentration of intracellular free Ca2+ ions are measured by monitoring the change in its emission spectrum of Indo-1 dye from blue to violet upon binding to Ca2+. The blue emission is measured through a 530/30 band pass filter, and the violet through a 405/20 band pass and 405 low pass filter; thus, a shift in the violet: blue ratio over time is a reflection of the increase in iCa2+ concentration. CD4+ cells were enriched (see inset, top left) from Cftr-ΔF508 and Cftr+/+ mice and stimulated with anti–CD3/CD28 antibodies (Abs), followed by 500 ng/ml of ionomycin (as a positive control; see inset on bottom right). (A) Representative iCa2+ flux for Cftr-ΔF508 and Cftr+/+ CD4+ T cells. (B) The area under the curve for the traces from Cftr-ΔF508 (n = 6) and Cftr+/+ (n = 6) in response to CD3/CD28 Abs. (C) Slopes for the traces from Cftr-ΔF508 (n = 6) and Cftr+/+ (n = 6) in response to CD3/CD28 Abs.

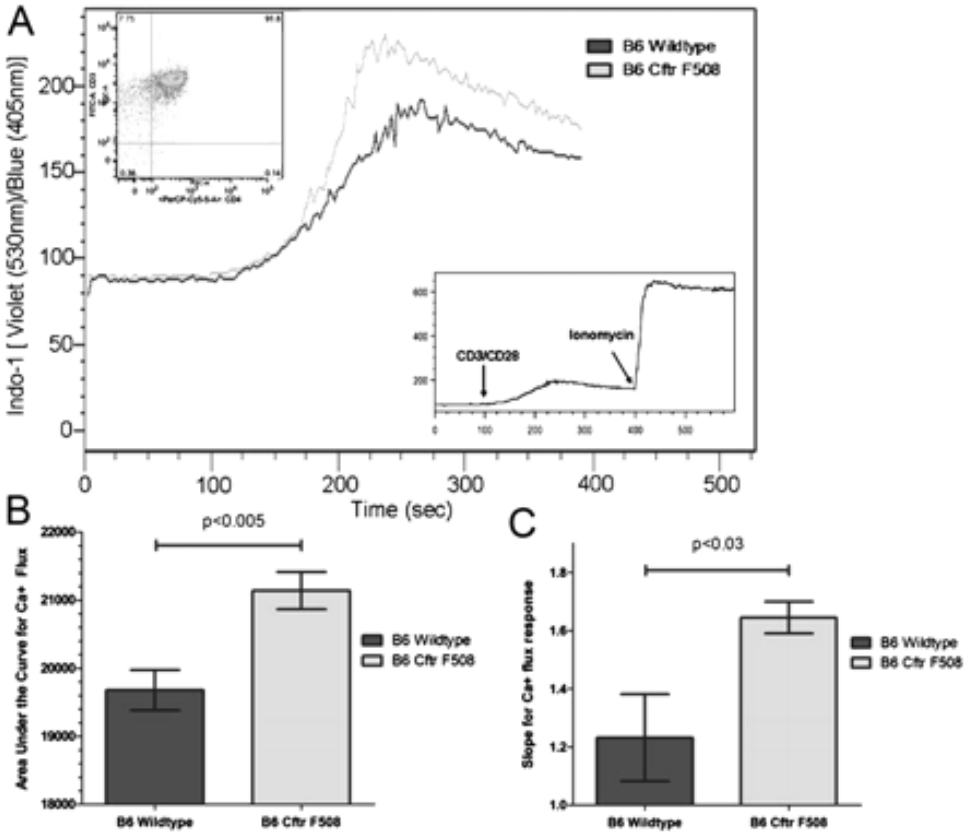

Figure 7.6 Intracellular calcium (iCa2+) flux

Figure 7.7 NFAT nuclear translocation and cytokine secretion in Cftr−/− and Cftr+/+ mice after T cell receptor stimulation.

(A) Nuclear translocation of NFATc1 was measured using a modified ELISA from nuclear splenocyte extracts after CD3/CD28 stimulation at 10, 30, and 90 minutes after stimulation. Parallel plated cells were assessed for cytokine expression after CD3/CD28 stimulation at 1.5, 3, 6, and 24 hours. (B) Time course expression for TNF-α. (C) Expression of IL-13 at 24 hours after stimulation. Data are shown as group averages (±SEM) for a total of n = 5.

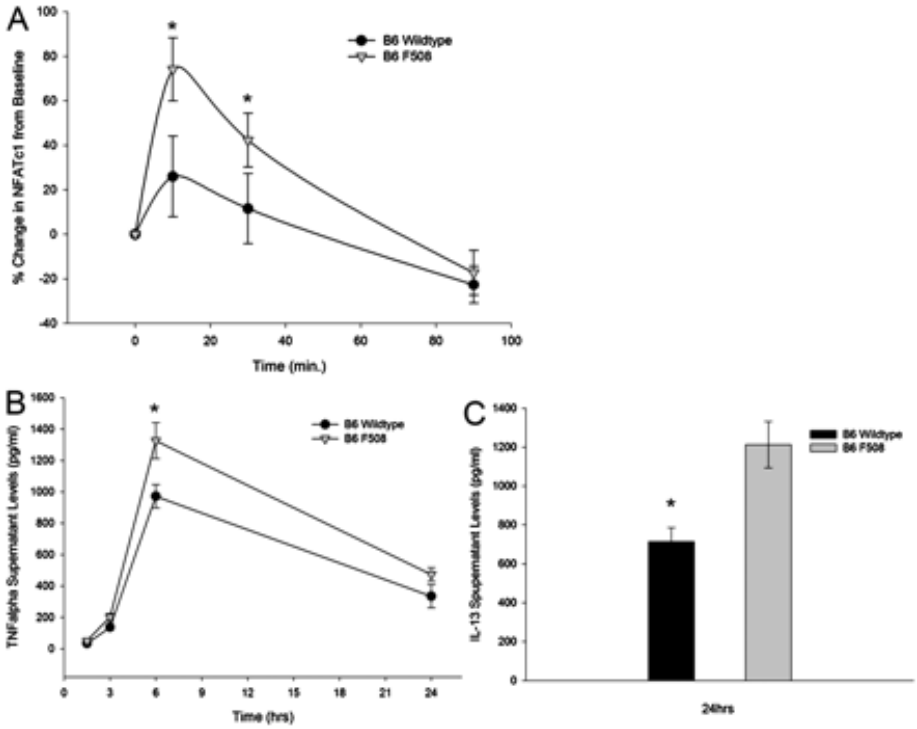

Figure 7.7 NFAT nuclear translocation and cytokine secretion in Cftr−/− and Cftr+/+ mice after T cell receptor stimulation.

To directly show if this nuclear translocation of NFAT would also translate to an upregulation and increased secretion of IL-13 in *Cftr*-/- T-cells, we measured the cytokine levels in the supernatants of CD3/CD28 stimulated cells. The data showed that the secretion pattern of TNF-alpha, an early activated cytokine known to respond to iCa^{2+} signaling through the T cell receptor (193) mimicked the pattern of NFAT and was secreted at significantly higher levels from *Cftr*-/- T cells (Figure 7.7B). While IL-13 was below detection in the earlier time points it was found to be expressed at significantly higher levels from *Cftr*-/- T-cells in supernatants collected 24hrs after stimulation (Figure 7.7C).

Discussion

In the present study, we demonstrate for the first time that CFTR deficient lymphocytes leads to an inherent divergence in the adaptive immune response *in vivo*. Specifically, in this case it is characterized by an aberrant Th2-biased immune response to *Aspergillus fumigatus* that is dependent on CFTR function in lymphocytes alone. We demonstrated that sensitization and aerosol challenge of *Cftr*-/- mice and their wildtype controls leads to an enhanced-IgE response in *Cftr*-/- mice that is reminiscent of CF related allergic asthmatic condition known as allergic broncho-pulmonary aspergillosis (ABPA). While ABPA remains rare outside of the CF population it is common among CF patients, affecting approximately 15% of them(169, 170). Interestingly, we demonstrated that the transfer of naive *Cftr*-deficient splenocytes into congenic Rag-/- mice was enough to confer the high IgE response to the Rag-/- mice. These experiments revealed that a CFTR dependent phenotype could be transferred from CF mice into CFTR sufficient hosts purely through splenocytes.

The expression of CFTR in lymphocytes has been well characterized throughout the years, (182, 185, 194) however the physiological relevance of CFTR expression in lymphocytes is less clear, with some studies implicating it with volume regulation and cytolysis regulation of CD8+ T-cells(195-198). Other models suggest that activation of Cl^- currents by CFTR in response to nitric oxide via a cyclic GMP-dependent mechanism are defective in T cells from CF patients(199). Importantly, electrophysiological studies document a functional

role for CFTR in lymphocytes by recording a defect in cAMP-dependent Cl^- currents in CF- derived lymphocytes using whole cell patch clamp techniques(182, 200). These studies demonstrate the presence and function of CFTR within lymphocytes and lend some credence to the longstanding yet controversial view that a primary immune abnormality is associated with cystic fibrosis. To date it has been difficult to separate aberrant immune response observed in CF from the disease phenotype imparted by epithelial cell dysfunction. Our adoptive cell transfer experiments indicate that a primary immune abnormality is indeed a possibility. Namely, the transfer of naïve splenocytes was able to recapitulate the 2-fold higher IgE response observed in *Cftr*-/- mice. We further investigated what specific cell type from the splenocyte pool was responsible for this phenotype with *in vitro* assays. Since the IgE response is known to be driven by Th2 cytokines and we have previously demonstrated that IL-13 is upregulated in *Cftr*-/- mice challenged with Af-cpe, we designed a series of experiments to analyze the secretion of Th2 cytokines by activated T cells in response to antigen. According to our data, a marked difference in the secretion of IL-4, IL-13, IL-5 and IL-17 was observed from CD4+ and CD11b+ cells that were *Cftr* deficient. Interestingly, antigen specific responses characterized by increased secretion of IL-4 and IL-13 were only observed in the presence of *Cftr*-/- CD4+ T cells, whereas the increased secretion of IL-5 and IL-17 seemed to be dependent on a synergistic interaction between both *Cftr*-/- Cd11b+ and CD4+ cells. Taken together with the adoptive

transfer experiments these data suggested that *Cftr* deficient T-cells imparted a Th2-skewed response, characterized by increased secretion of IL-4 and IL-13 ultimately leading to the high IgE response directed against *Aspergillus fumigatus* crude protein extract. However, based on the secretion of IL-5 and IL-17 in the antigen recall experiments, it is conceivable that skewed responses may be due to the interaction of various *Cftr* deficient immune cells, such as macrophages, dendritic cells and T-cells.

In order to directly determine whether this phenotype can be attributed to *Cftr* deficient T-cells we created T-cell specific *Cftr* knockout mice by using a floxed *Cftr* mouse expressing Cre recombinase under the control of the LCK promoter. These mice presented with an increase in basal IgE levels in the absence of any exogenous antigenic stimulus. These elevated basal IgE circulating antibody levels are consistent with a previous observation in which we recorded higher IgE levels in *Cftr*-/- mice, as compared to controls which had been mocked-PBS sensitized and challenged with Af-cpe(179). Furthermore, these T-cell *Cftr* conditional knockout mice went on to develop dramatically different IgE responses to Af-cpe as was characteristic of *Cftr*-/- mice. With these experiments we were able to finally demonstrate without any confounding variables a primary immune abnormality associated with cystic fibrosis *in vivo*, which, to our knowledge has never been shown before.

A consequence of *Cftr* deficiency in lymphocytes is the reduction in Cl- permeability, which in turn may hyperpolarize their membranes. It is

hypothesized that the altered membrane potential could then alter the electrical driving force for Ca^{2+} to enter the cells. Here we also show that intracellular calcium fluxes in *Cftr*-/- CD4+ T cells are increased in response to CD3/CD28 stimulation as determined by the area under the curve and the slopes of the Ca^{2+} flux response when compared to wildtype CD4+ T cells (Figure 7.6). The relevance of this altered calcium flux in *Cftr*-/- T-cells is that it may lead to increased transcription activity of Ca^{2+} regulated transcription factors. Nuclear factor of activated T-cells (NFAT) activity is modulated by cytoplasmic Ca^{2+} concentration through various Ca^{2+} associated signaling pathways. Ultimately, any increase in cytoplasmic Ca^{2+} concentration induce NFAT dephosphorylation and NFAT translocation to the nucleus where it binds to cis regulatory elements of target genes as a monomer(201). This signaling cascade proceeds through calmodulin and calcineurin, a cytoplasmic serine/threonine phosphatase. Calcineurin upregulates NFAT by dephosphorylating serines in the SP-repeats and in the serine rich N terminus region of NFAT exposing the nuclear localization signal, allowing NFAT to translocate to the nucleus(201). In T cells, TCR stimulation causes an increase in intracellular Ca^{2+} concentration depleting Ca^{2+} sequestered ions in the ER, followed by an influx of extra-cellular calcium ions from Ca^{2+} release activated Ca^{2+} channels (CRAC)(201). While NFAT activation regulates a variety of immune processes, NFAT has been found to regulate a number of other promoters for cytokine genes, including those involved in the regulation of Th2 immune responses as IL-4, IL-13, IL-5 and TNF-

alpha(202). In agreement with the results for the intracellular Ca^{2+} flux experiments we observed a significantly greater increase in the nuclear translocation of NFAT after TCR activation with CD3/CD28 in *Cftr*-/- cells (Figure 7.7). Parallel cell experiments demonstrated that following NFAT nuclear translocation *Cftr*-/- cells had significantly higher expression of TNF-alpha and the key Th2 effector cytokine IL-13. These data suggests that a possible mechanism responsible for the *in vivo* immune aberration observed in the conditional *Cftr* T cell knockout mice may be directly related to the more vigorous TCR mediated calcium flux responses leading to an increase translocation of NFAT and higher induction of IL-13 in *Cftr*-/- T-cells. Exactly how CFTR dysfunction affects Ca2+ signaling in lymphocytes warrants further investigation and the convergence or overlap of other dysregulated pathways related to *Cftr* deficiency can not be ruled out. There is some evidence of CFTR dysfunction imparting elevated antibody secretion in B cell hybridomas; while these data do not explicitly assess CFTR function in B cells they do suggest that regardless of aberrant or normal B cell function in CF, the upstream events of T cell activation and helper function alone are enough to impart a polarized antibody response even in the presence of B cell with intact CFTR function.

The main pathological features associated with cystic fibrosis are pancreatic cysts that lead to a reduction in the secretion of digestive enzymes as well as chronic airway infections most notably by *pseudomonas*. While it has been well established and recognized that impaired CFTR function adversely

affects the secretory epithelium, the role of CFTR in non-epithelial cells has received less attention or has largely eluded investigators. Certainly, if the CFTR alters the function of immune cells it should be expected to result in an aberrant immune response, which could further compromise patients. In summary our data identifies that CFTR dysfunction in T cells can in of itself lead to aberrant immune responses. Specifically we show how it skews responses to *Aspergillus fumigatus,* leading to a higher than normal IgE response. This observation itself is reminiscent ABPA, an otherwise rare but prevalent condition in the CF population. These findings represent a new and important cell population to investigate in order to try to prevent or ameliorate aberrant immune responses in people with cystic fibrosis. Thus, current and future drugs targeting cystic fibrosis should determine if their benefits extend to this cell population, alternatively this also opens a new avenue to test small molecule modulators of immune response as a potential therapy for cystic fibrosis.

CHAPTER VIII: Additional Projects- IL-13 and IL-17e Receptor Therapy

Introduction

Asthma, a chronic disease involving inflammation of the airways, affects ~5% of the population in the United States. This includes ~10%-12% of children under age 18, according to 2003 data from the Centers for Disease Control. Asthma accounts for 12.7 million doctor visits, 1.2 million hospital outpatient visits, 1.9 million visits to the emergency room, 484,000 hospitalizations, and 4,261 deaths per year. Although two general types of asthma medications are available, anti-inflammatory and bronchodilators, they only help control asthma as a life-long affliction; and long-term, daily medications are required over extended periods to achieve and maintain control of persistent asthma. Thus, alternative therapeutic approaches are clearly warranted. Delivery of therapeutic proteins to the systemic circulation using gene therapy has the ability to provide durable expression after a single administration. Gene therapy offers the convenience of replacing frequent injections of recombinant proteins by intra-venous treatment. Asthma and allergic rhinitis are almost invariably accompanied by elevated levels of IgE, and more importantly a genetic link between IgE levels and airway hyper-responsiveness has been established(203). It is known that the interaction of mast cell bound IgE with antigen leads to the release of vasoactive mediators, increased synthesis of Th2 cytokines and the production of leukotrienes and prostaglandins. This acute response leads to immediate-

hypersensitivity in the lungs followed by mucous production, smooth muscle constriction and the eventual inflammatory infiltration. Thus, here we evaluate the possibility of using rAAV to express soluble cytokine receptors as a sequestration- treatment to allergic IgE driven responses in a previously characterized mouse model of exaggerated-IgE driven allergy. Current dogma suggests that asthma is driven by a dysregulated, Th2 biased immune responses to antigen. Our laboratory has previously characterized an allergic exaggerated-IgE phenotype in CF mice where the CFTR defect causes an increased expression of IL-4 and IL-13. This immune aberration may lead to the increased sensitivity of CF patients to develop allergic disease, since approximately 50% of all CF patients have elevated levels of serum IgE (204). Allergic reactions in CF patients complicate diagnosis and more importantly accelerate pulmonary deterioration. Interestingly 10-12% CF patients develop a unique allergic induced asthmatic response to common house mold *Aspergillus fumigatus*, known as allergic broncho-pulmonary aspergillosis (ABPA), which is characterized by an unusually high IgE response. Moreover, a recent study by Hartl et al. revealed the prevalence of a pulmonary Th2 immune response in P. aeruginosa-infected lungs of CF (176). Thus, the modulation of the pulmonary Th2 response may not only be beneficial for treating P. aeruginosa infections but may also lead to a decrease in the prevalence of allergic diseases associated with CF. Clinical asthma and ABPA are accompanied by elevated levels of Th2 cytokines such as IL-4 and IL-13 (205). Interleukin-13 is a pleiotropic cytokine that is secreted from

a wide array of cells including T cells (206), B cells (207), mast cells (208), basophils, natural killer and dendritic cells (209-211) with activities that partially overlap those of IL-4. This is partly explained by the fact that they share receptor components. Over expression of IL-13 in the mouse lung results in an intricate phenotype that recapitulates the classical symptoms of asthma. This includes goblet cell hyperplasia, mononuclear and eosinophil inflammation, subepithelial fibrosis, and airway hyper responsiveness.(212). In addition it has been shown that IL-13 is able to initiate B cell isotype switching for the production of IgE (213-215).

These features of IL-13, along with its major role in the CFTR-/- dependent ABPA model make it an interesting target for immune deviation for exaggerated IgE responses. As an alternative to targeting IL-13 we have also designed a soluble receptor antagonist for the recently discovered IL-17e (IL-25) cytokine. IL-17e is a member of the newly described IL-17 family, which is comprised of 5 members that share between 20-50% homology. Within this family, IL-17e is the only member to date that has been shown to promote the development of Th2 responses (216). In fact IL-17e treatment of mice resulted in the production of the cytokines IL-4, IL-13 and IL-5, extensive eosinophilia, increased serum IgE and striking histologic changes in the lung and gastro-intestinal tract(216). In addition IL-17e was shown to activate NFkB and induce the production of IL-8 human cell lines(217). For these reasons this cytokine was also chosen as an attractive target for deviating the allergic response to

Aspergillus fumigatus. Targeting IL-17e with a soluble receptor is possible due to the recent identification of the IL-17 receptor homologue 1 (IL-17Rh1) which has shown to preferentially bind with IL-17e and somewhat with a lower affinity to IL-17B (217).

Materials and Methods

CB-mIL-13Rα2-Fc:

This construct consists of the extracellular domain (a.a 1-332) of the mouse IL-13Rα2 receptor fused with the CH2and CH3 including the hinge region (Fc) domains of a mouse IgG1 kappa antibody. The IL-13Rα2 receptor was synthesized by RT-PCR from RNA of mouse thymus. The RT-PCR was performed with the one step RT-PCR kit (Qiagen) using the following primers: IL-13_sense 5'AGAATAAATGGCCTCGTG3' and IL-13_antisense 5'AATAACAGAAACACGGAAG3'. The resulting 1Kb fragment was the gel purified (Qiagen gel extraction kit). Subsequently, the CH2 and CH3 domains of a mouse IgG1kappa antibody were amplified by RT-PCR from RNA extracted from a mouse hybridoma cell line. A small Gly-Ser-Gly linker was added to the 5' end of the PCR product. This product was also gel purified. The two fragments were then subjected to a blunt end ligation (T4 DNA ligase) at an equi-molar ratio this ligation was then subjected to 30 rounds of PCR using the forward IL-13 primer and the reverse Fc primer to yield a 1770bp fragment. The fragment was then cloned into a TA vector backbone (Stratagene PCR 2.0), which was used to

transform Top10 cell for subsequent screening. Once the sequence of the fusion gene was verified by sequencing it was cloned into a CBA vector backbone for packaging. This was done by digesting the TA plasmid with the IL-13Rα2Fc fusion with Not1. The linearized plasmid was then treated with Klenow to fill in the 3' overhang. The plasmid was then cut with Spe1 and the resulting 1777bp fragment was gel purified. To create a CBA backbone to clone the insert into, the pTR2-CBA-rIL-10 plasmid was cut with HindIII to linearize it and also treated with Klenow to fill in the 3' overhang. Then it was cut with Nhe1 and the large ~5300bp fragment was gel purified to serve as the pTR2-CBA-backbone for the IL-13Rα2Fc fusion insert. This two fragment were then ligated (T4 DNA ligase) at 5:1 molar ratio (insert: backbone) to yield the final plasmid of 7061bp.

CB-mIL-17Rh1-Fc:

This vector is composed of the extra-cellular domain of the IL-17Rh1 (IL-17BR) fused with the CH2and CH3 including the hinge region (Fc) domains of a mouse IgG1 kappa antibody. The methods used for the cloning of this fusion protein were the same as the ones describe above for the pTR-CBA- mIL-13Rα2Fc vector with the exception of the primer used for the RT-PCR. The following primers were use to amplify the extra-cellular domain of the IL-17Rh1 gene; IL-17Rh1-for 5'GGGCCATGTTGCTAGTGTTG3' and IL-17Rh1-REV 5'TCCCAAATGTAGGTCCCACTC3'.

In Vitro Expression and Analysis of IL-17Rh1Fc:

Expression of IL-17Rh1Fc was first investigated in cell cultures of 293 human kidney epithelial cells. The cells were cultured in T-75 plates with 10mL of Dulbecco Modified Earls Media (DMEM) with 10% fetal bovine serum, FBS, 1% penicillin/streptavidin (Cellgro) in a 37°C humidified CO_2 incubator until cells were 90% confluent Expression of IL-17Rh1Fc was first investigated in cell cultures of 293 human kidney epithelial cells. Cells were transfected at 90% confluency with Lipofectamine 2000. Forty-eight hours post transfection GFP cells were evaluated for expression and supernatants were collected for further western blot analysis.

Serum IL-17Rh1Fc ELISA:

Blood was collected upon sacrificing the mice, centrifuged in a serum separator and stored at –80C until analysis. Total IL-17Rh1Fc levels were measured with the BD IL-17Rh1 (IL-17BR) antibody pairs. They antibodies were used at the suggested concentration for coating and detection (BD Biosciences). Triplicate sera samples were used for each mouse. Tetramethyl-benzidine (TMB) substrate was used to develop the assay and was read at 450 nm with correction at 570nm on the VersaMax Micro Plate Reader (Molecular Devices).

Mouse strains:

The primary CFTR knock-out strain used for these studies was the CFTR S489X -/- neo insertion in C57BL/6 mice developed initially at the University of North Carolina (186) and then modified with the transgenic overexpression of gut-specific expression of human CFTR from the fatty acid binding protein (FABP)- promoter in order to prevent intestinal obstruction and improve viability (187). These mice have then been backcrossed 10 generations onto a C57BL/6 mouse.

Muscle Injection:

For muscle administration of the rAAV1 vectors were injected into five to six week mice anesthetized with 3.5% isofluorane inhalation. 50μLs of viral vector suspension was administered percutaneously by intramuscular injection into the right or left gastrocnemius muscle two weeks prior (day -14) to Af-cpe sensitization.

Aspergillus sensitization and challenge:

Six to eight week old CFTR S489X -/-; FABP-hCFTR (+/+), and wildtype littermate mice were housed in the SPF mouse colony of the University of Massachusetts Medical School according to NIH guidelines and were allowed food and water ad libitum. All experimental procedures were approved by the IACUC of the University of Massachusetts Medical School. Animals were

sensitized to Aspergillus fumigatus crude protein extract (Af-cpe) (Greer Laboratories). Briefly, animals were administered with intraperitoneal (i.p.) injections of 200ug of Af-cpe extract dissolved in 100ul of PBS on days 0 and 14. Aerosol challenge was performed with 0.25 % Af-cpe for 20 min in a 30x30x20 cm acrylic chamber using a jet nebulizer Pari model LC-D with an air flow of 6 liters/min on days 28, 29 and 30.

Serum IgE ELISA:

Blood was collected on day 32 after sacrificing the mice, centrifuged in a serum separator and stored at –80°C until analysis. Total IgE levels were measured with the BD OptEIA ELISA (BD biosciences) triplicate sera samples were used for each mouse. Tetramethyl-benzidine (TMB) substrate was used to develop the assay and was read at 450 nm with correction at 570nm on the VersaMax Micro Plate Reader (Molecular Devices).

Af specific ELISA was performed by coating a 96 well plates with 10ug of Af crude protein extract (Greer Laboratories) and detected using BD OptEIA IgE ELISA (BD biosciences) detection antibody.

Cytokine Determination for Bronchoalveolar Lavage:

Assessments of cytokine profiles from the Bronchoalveolar lavage (BAL) were performed using a commercially available multiplexed kit (Biorad Mouse Multi-Cytokine Detection System; Biorad Laboratories) and the Bioplex

Suspension Array System. Simultaneous measurement of 5 cytokines was performed: specifically, IL-2, IL-5, INF-G, IL-4 and IL-13. All assays were performed according to the manufacturer's protocols. Cytokine concentrations were determined utilizing Bioplex software with four-parameter data analysis. The sensitivity of the assay is less than 10pg/ml and has a range from 0.2-32,000 pg/ml with an inter and intra-assay coefficient of variance of less than 10%.

Intracellular Staining of Cytokines for Flow Cytometry:

Splenocytes were incubated for 3 hours with GolgiStop (BD Biosciences) in RPMI plus 10% Fetal Calf Serum at 37°C to block intracellular transport of cytokines. The cells were then Fc blocked by CD16/CD32 antibodies for 5 minutes at 4°C. Cells were then stained for surface antigens (including CD4, CD44, CD11b, CD14, NK1.1) for 20 minutes at 4°C. Cells were fixed and permeabilized for 20 minutes at 4°C with CytoFix/CytoPerm Buffer (BD Biosciences). Anti-cytokine antibodies (IL-17a, IL-17e, IL-13 and IL-4) were stained for 25 minutes at 4C. Cells were washed and then analyzed on BD LSR II using FACSDIVA software. Analysis was done using FlowJo (Treestar)

Statistical Analysis:

All data were compared using an unequal variance two-tail student t test, unless stated otherwise. Data was considered statistically significant when $p \leq 0.05$.

Results

As previously described, we have recapitulated a peculiar exaggerated-IgE phenotype in Cftr-/- mice in response to *Aspergillus fumigatus* crude protein extract (AF-cpe) sensitization and challenge. Although this model results in an increase in lung eosinophil recruitment and goblet cell hyperplasia in both wildtype and CF mice, it uniquely leads to a more vigorous IgE response in Cftr-/- mice. In the original studies, we show that IL-13 mRNA levels in the lung of sensitized mice were more than 2-fold higher when compared to the control mice (179). Here we extend that finding and show that both wildtype and Cftr -/- mice have substantial increase in the production of IL-13 in NK1.1+ (NK-cell marker) and CD14+ (macrophage marker) cells. Figure 8.1 depicts the change in number and type of cells expressing IL-13 intracellularly; where unsensitized Cftr-/- or wildtype mice served as baseline controls for IL-13 expression. Curiously, while IL-13 levels are detected in CD4+ cells in wildtype mice after Af-cpe sensitization and challenge, we only observed an increase in this cell population after Af-cpe challenge in Cftr-/- mice. The prominent increase of IL-13+ cells in this model along with the newly described role for IL-17e in regulating IL-13 prompted us to attempt immuno-modulating the exaggerated-IgE phenotype targeting IL-13 and IL-17e with soluble receptors.

To create the soluble receptor fusion proteins, the extracellular domains for the IL-13Rα2 (a.a. 1-332) and for 17Rh1 (a.a. 1-489) were cloned in frame using a linker with the mouse IgG1 Fc gene containing the CH2, CH3 domains as

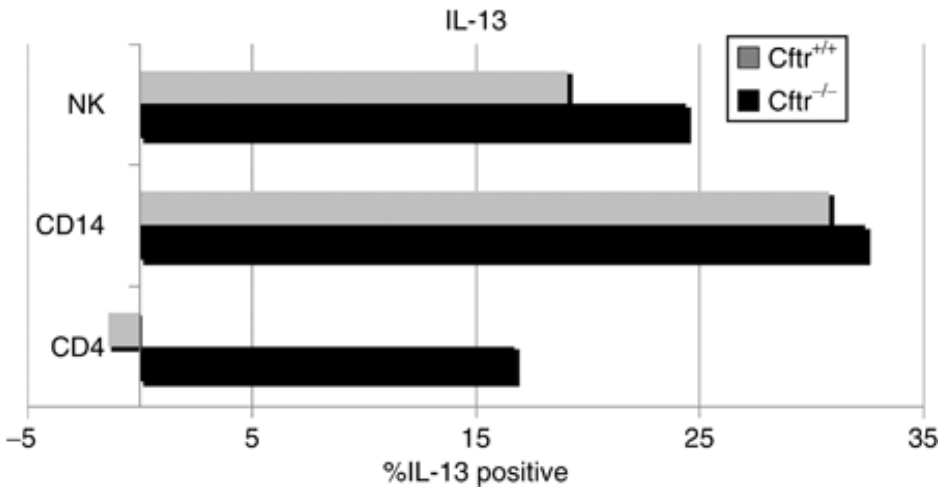

Figure 8.1 Overexpression of IL-13 in Cftr-deficient mice after ABPA

Intracellular staining for the number of cells expressing IL-13 intracellularly after ABPA, graphed as a percent change over unsensitized animals. Gray bars depict wild-type animals whereas black bars are $Cftr^{-/-}$ mice -deficient animals. The number of positively gated cells from NK1.1, CD14, and CD4 divided by the lymphocyte gate determined by FSC and SSC and multiplied by the percent IL-13+ of that population. *N* = 5 except CFTR wild-type ABPA which has an *N* = 6.

well as the hinge region to facilitate the formation of dimers (Figure 8.2A). Although there has not been a published delivery of the IL-13Rα2Fc soluble receptor with rAAV vectors, the characterization and function of the protein have been previously reported by Willis-Karp et al in a mouse model of ovalbumin induced asthma(218). To our knowledge the use of a soluble receptor for IL-17e has never before been tested, thus it was imperative that its function be evaluated *in vitro* before administration *in vivo*. To determine if the fusion construct was expressed and secreted, HEK-293 cells were transfected with CB-IL-17RH1Fc, CB-IL-13Rα2Fc or CB-GFP; the latter two constructs being controls. Forty eight hours after the transfection, the supernatants were collected and run on a western blot assay.

As shown in lane 1 of Figure 8.2B, detectable protein was secreted into the media of the transfected HEK-293 cells. There are two prominent bands that were observed when probed with the antibody against IL-17Rh1 receptor. One of the bands is in line with the expected size of the fusion protein (~58kD) and the second band is above 100kD. This second band may be representative of two fusion protein monomers dimerizing through the hinge region in the Fc portion of the soluble receptor (Figure 8.2A). Supernatants from cells transfected with CB-IL-13Rα2Fc do not contain a soluble receptor detected by antibody raised against the mouse IL-17Rh1 (lane 2 on Figure 8.2B).

Figure 8.2 IL-17Rh1Fc fusion protein is stable and efficiently secreted

(A) Illustration of soluble receptor fusion protein. The extracellular domains of IL-17e or IL-13 are fused to the CHCH3 domains of a mouse IgG1κ antibody. (B) Western blot of IL-17RH1fc protein. Supernatants from transfected HEK-293 cells were blotted with an anti-IL-17Rh1 antibody. Lane 1: IL-17Rh1Fc supernatants; lane 2: IL-13Rα2Fc supernatants; and lane 3: protein ladder. (C) Total serum IL-17RhFc levels after rAAV1 administration. Total serum IL-17RhFc levels in $CFTR^{-/-}$ mice analyzed by ELISA from mice receiving either AAV1-GFP or AAV1-IL-17Rh1Fc (low and high dose). Results are reported as group mean + SEM ($N = 5$) $^{**}P < 0.05$

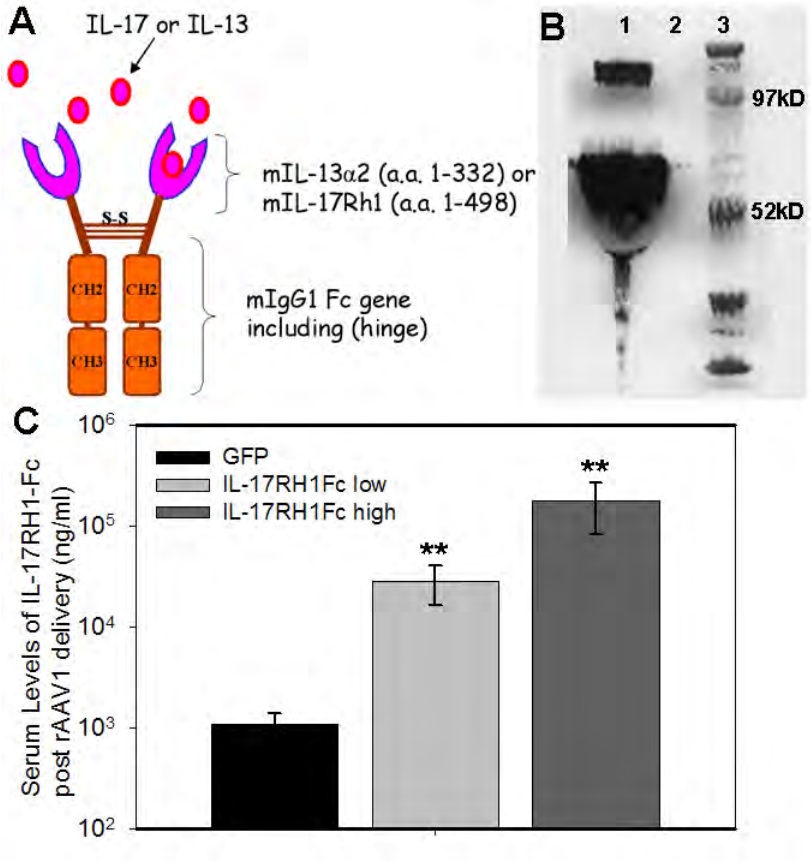

Figure 2

Figure 8.2 IL-17Rh1Fc fusion protein is stable and efficiently secreted

To further determine if the IL-17Rh1 receptor Fc fusion protein would be secreted *in vivo,* we packaged rAAV1 vectors expressing IL-17RH1Fc and injected mice at two different doses. The first cohort of mice received either rAAV1CB-IL-17Rh1Fc or rAAV1CB-GFP at a dose of $1.0x10^{11}$ rAAV vector genomes (vg) per mouse and the second cohort at a dose of $3.0x10^{11}$ vg. A dose dependent detection of IL-17Rh1Fc was observed in the serum of these mice three weeks post injection, with the lowest levels receiving rAAV1-GFP and over a 200-fold increase in the mice injected with $3.0x10^{11}$ vg of rAAV1CB-IL-17Rh1Fc (Figure 8.2C). The serum from mice injected with CB-GFP also showed basal levels of soluble IL-17Rh1, which can be interpreted as the endogenous level of IL-17Rh1 protein. Endogenous protein present in the serum is supported by the evidence of an alternative splice variant of the protein that is secreted as a decoy receptor.

A modified indirect ELISA was used to determine that the secreted IL-17Rh1Fc soluble receptor would be effective at binding IL-17e. A flat bottom 96 well plate was coated with different concentrations of IL-17e protein and subsequently the supernatants from the HEK-293 cell transfections of either the IL-17Rh1Fc or IL-13Rα2Fc plasmids were incubated on the plate with IL-17e protein coated wells. An HRP conjugated secondary antibody directed against Fc portion of the soluble receptors was used to detect if the soluble receptors bound to the wells. Thus, the secondary antibody would detect only supernatants that contained FC fusion proteins able to bind IL-17e. As shown in Figure 8.3 there was a

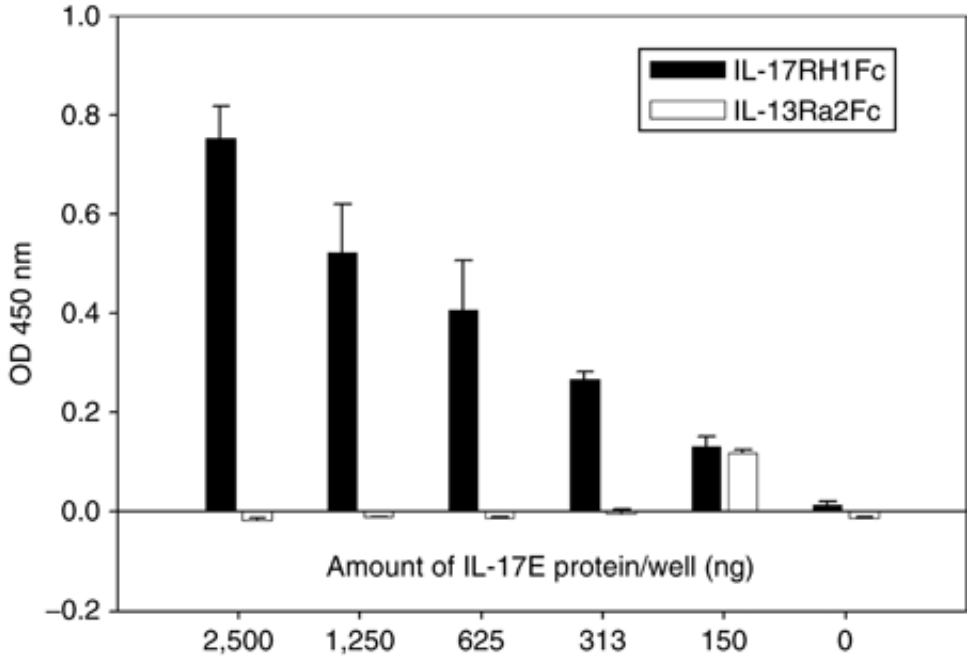

Figure 8.3 Binding capacity of IL-17RhFc

Ninety-six well plated were coated with different amount of IL-17e protein. Cell supernatants from IL-17Rh1Fc and IL-13Rα2Fc cell transfections were incubated in the IL-17e coated wells, after washing an HRP-conjugated mouse anti-IgG (able to bind the Fc portion of the fusion proteins) was used as to analyze the binding capacity of the supernatants to IL-17e.

correlation between the amounts of IL-17e coated on the plate and the signal absorbance from supernatant of the IL-17RH1Fc transfection only, whereas supernatants containing the IL-13Rα2Fc protein did produce an appreciable signal.

Subsequent to the *in vitro* analysis, the IL-17Rh1Fc and the previously characterized IL-13Rα2Fc constructs were packaged into rAAV1 vectors for intramuscular administration in CFTR-/- mice. The mice received IL-13Rα2Fc, IL-17Rh1Fc or CB-mSCAD expressing vectors at a dose of $1.0x10^{11}$ rAAV particles per mouse. Mouse SCAD, short chain acetyl CoA dehydrogenase (mSCAD), was used as a control instead of GFP because the foreign protein could potentially skew the Th2 response in favor of a Th1, CTL response in order to clear cells expressing GFP, thus inadvertently lowering IgE levels. Recombinant AAV was administered two weeks prior to *Aspergillus fumigatus* sensitization and challenge, to allow for vector uncoating, second strand synthesis and gene expression. Two weeks post i.m. delivery of the therapeutic soluble receptors the mice were subjected to the previously described exaggerated-IgE allergy model, which consists of a series of i.p. injections with *Aspergillus fumigatus* crude protein extract (Af-cpe) followed by airway challenges with nebulized Af-cpe (179, 180).

To determine whether the therapies offered protection from the B cell isotype switching into an IgE mediated allergic response; the serum samples were evaluated for total IgE levels. As identified in Figure 8.4A the total

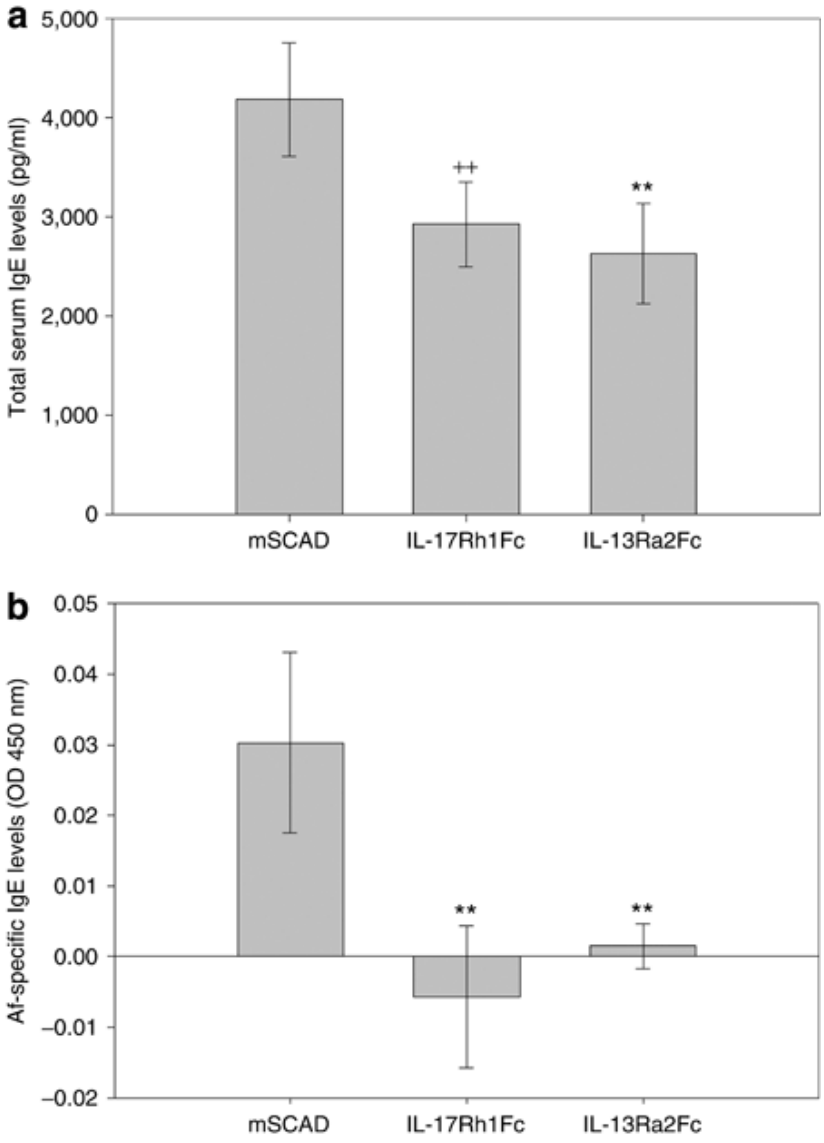

Figure 8.4 Reduction in circulating IgE levels after soluble receptor therapy

(a) Total serum IgE levels after intramuscular rAAV delivery and Af-cpe sensitization and challenge. (b) $Cftr^{-/-}$ mice were injected with rAAV1-IL-17Rh1Fc, rAAV1-IL-13Rα2Fc, rAAV1mSCAD, and rAAV1-GFP. Total Serum IgE in the Af-sensitized mice was measured by ELISA. Serum IgE levels specific for Af-cpe. $N = 5$ Results expressed as a mean + SEM $^{**}P < 0.05$, ++ $P < 0.1$

circulating serum IgE levels were about 30-40% lower in mice receiving either of the two soluble receptors, this is comparable to the decrease we have observed in other studies using IL-10 as means to reduce IgE responses by immunomodulation (219). Further analysis of Af-specific IgE responses revealed that both soluble receptors were able to completely abrogate this response as detected by our assay (Figure 8.4B). This is in contrast to the Af-specific IgE levels observed in the mSCAD control injected mice.

In order to determine if the systemically circulating soluble receptors were having an effect locally in the lung, bronchoalveolar lavages (BALs) from the three vector treated groups were analyzed for various cytokines. As shown in Figure 8.5, the BALs of mice receiving the IL-13 soluble receptor had very high levels of IL-13 in the lungs while there was a slight but not significant decrease in the IL-13 levels between the mSCAD group and the IL-17Rh1Fc treated group. Furthermore the BAL analysis revealed that both of the soluble receptor treatments were significantly effective at lowering the KC response to *Af-cpe* in the lung (Figure 8.5). Also shown in Figure 8-5, IL-17Rh1Fc therapy resulted in downregulation of IL-5 whereas IL-13Rα2Fc therapy was not as statistically significant (Figure 8.5). IL-5 is an important cytokine involved in the maturation and recruitment of eosinophils. Consistent with this role, there was a decrease in the eosinophil infiltration found in the BALs from the lungs of the IL-17Rh1Fc treated mice (Table 8.1).

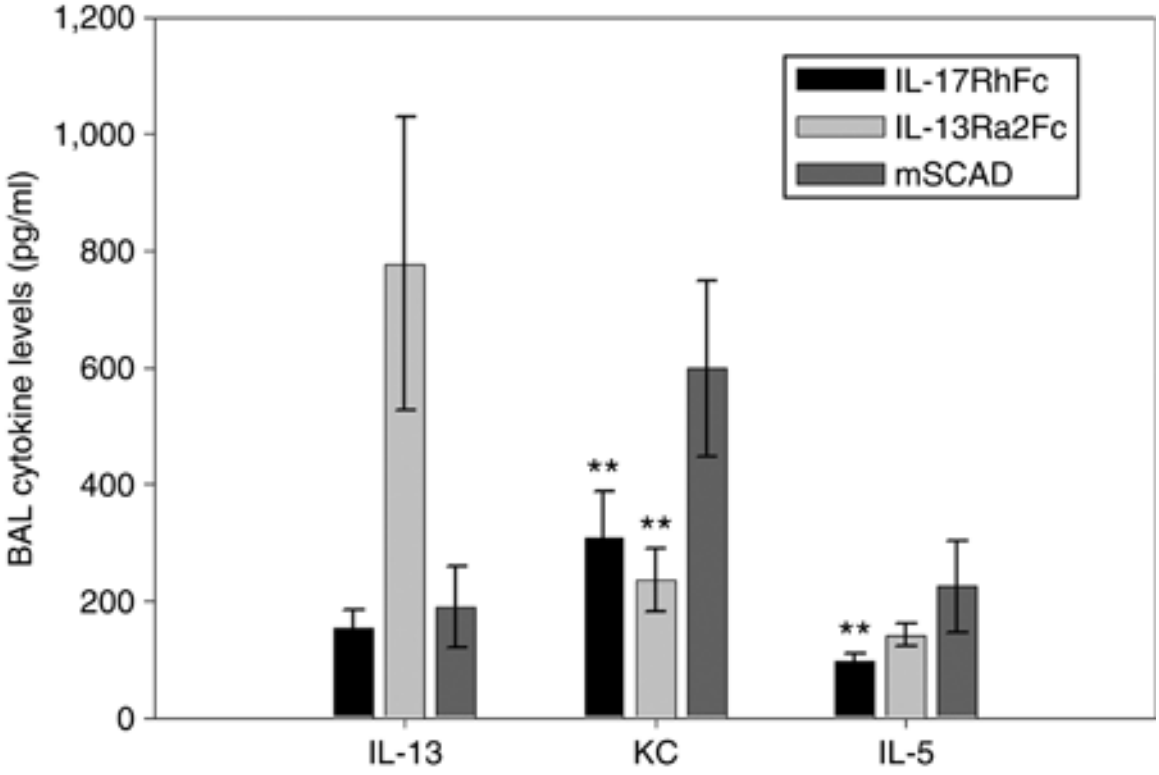

Figure 8.5 Cytokine levels in the BAL of mice treated with rAAV1 expressing; IL-13Rα2Fc, IL-17Rh1Fc, or mSCAD.

N = 5. Results expressed as a mean + SEM ***P* < 0.05.

	Macrophages	Lymphocytes	Neutrophils	Eosinophils
IL-17Rh1Fc	42.9 ± 4.7	10.7 ± 0.6	5.2 ± 1.2	41.3 ± 4.2**
IL-13Rα2Fc	32.2 ± 5.2	9.8 ± 2.1	7.2 ± 1.3	50.8 ± 3.8
mSCAD	33.9 ± 2.0	9.2 ± 1.4	2.7 ± 0.7	54.2 ± 3.1**

Abbreviations: BAL, bronchoalveolar lavages; IL, interleukin; mSCAD, mouse short-chain acetyl CoA dehydrogenase.
Mean ± SEM.
**$P \leq 0.03$.

Table 8.1 Proportions of inflammatory cells in the BAL

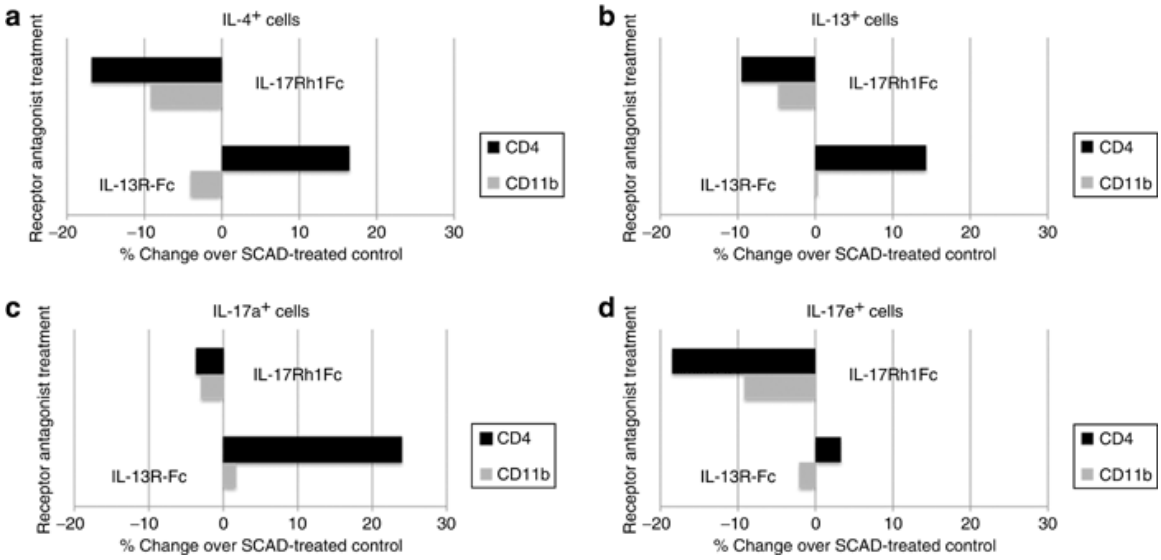

Figure 8.6 Intracellular cytokines produced after receptor agonist treatment

Cells were stained for surface markers and intracellular cytokines using fluorescently conjugated antibodies that were detected by FACS analysis. CD4+ staining cells were gated and are depicted by the black bars; CD11b+ staining cells were gated and are depicted by the gray bars. IL-17Rh1Fc and IL-13Rh1Fc receptor agonist-treated mice cytokine expression after ABPA treatment are graphed as a percent change over the SCAD-treated control. (a) IL-4 staining, (b) IL-13 (c) IL-17a, and (d) IL-17e. *n* = 6 per group.

The broader effect on cytokine responses from mice receiving IL-17Rh1Fc was also observed from studying the splenocytes by flow cytometry after intracellular cytokine staining (Figure 8.6). The Th-2 cytokines, IL-4 and IL-13 and IL-17 family members, IL-17a, IL-17e intracellular cytokines were measured from soluble receptor treated mice and compared to mSCAD treated controls. Th-2 cytokines and IL-17 cytokines were reduced in both CD4 positive cells and CD11b positive cells treated with the IL-17e antagonist (Fig. 8.6). The IL-13 antagonist had minimal effect on the levels of the Th-2 cytokines as well as the IL-17 cytokines in the CD11b positive population of cells. Curiously, the CD4+ population of mice treated with the IL-13 antagonist showed an increase of IL-4, IL-13 and IL-17a, with little to no change in IL-17e (Fig.8.6). In contrast to IL-13Rα2Fc treatment the IL-17Rh1Fc soluble receptor seems to be inhibiting IL-17e signaling which may be acting upstream of both CD4+ and CD11b+ cells as observed by the decrease in cytokines in these cells (Fig 8.6). To determine what cell types could be the source of IL-17e in this ABPA model we compared splenocytes from Cftr-/- and Cftr+/+ mice before and after Af-cpe sensitization and challenge. As identified in Figure 8.7, we detected only slight differences in the levels of IL-17e between Cftr-/- and Cftr+/+ mice with a modest reduction in the percent of IL-17e positive cells Cftr-/- mice after Af-cpe challenge. More importantly we identified that CD14+ macrophages are a significantly more abundant source of IL-17e than CD4+ T cells (Figure 8.7).

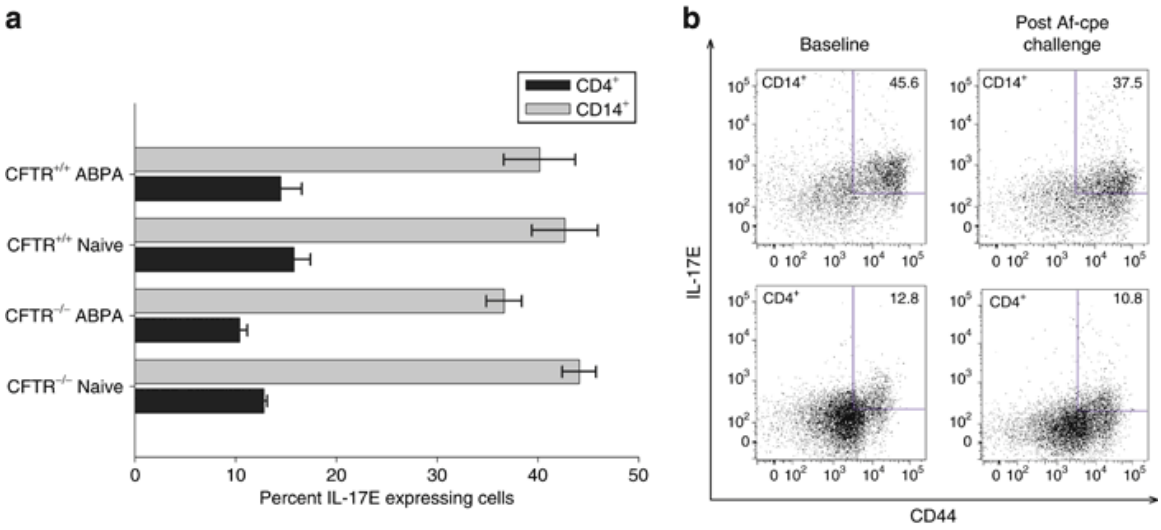

Figure 8.7 Expression of IL-17e in CD14+ and CD4+ cells

Intracellular staining for IL-17e with and without ABPA. (a) Graph of the mean percent IL-17e+ cells. *n* = 5 except Cftr+$^{/}$+ ABPA which has a *n* = 6. Gray bars are CD4+ cells expressing IL-17e; black bars are CD14+ cells expressing IL-17e. Error bars are SE. (b) Representative dot blot of data depicted in a. Activation marker CD44 staining is on the x axis, IL-17e is on the y axis. CD14+ gated cells are on the top; CD4+ cells are on the bottom. Cells without ABPA are on the left and ABPA cells are on the right.

Discussion

These studies extend the potential utility of rAAV vectors for gene therapy targeting allergic disease and offer another example of the use of these vectors for the expression of therapeutic proteins designed to deviate allergic immune responses. The experiments described here compared the efficacy of the neutralization of IL-17e and IL-13 with a single intramuscular injection of rAAV vectors expressing soluble receptors targeting these cytokines. Intra-muscular injection of the vectors led to a significant production of protein as determined by the ELISA for serum levels of IL-17Rh1Fc. While the IL-13 soluble receptor was previously shown to bind IL-13 with high affinity, the IL-17Rh1 receptor has not been as well characterized. We demonstrated that fusing the extracellular domain of the IL-17e receptor to the Fc portion of a mouse IgG1 antibody resulted in stable secreted soluble receptors able to bind IL-17e protein. Intramuscular delivery of rAAV vectors resulted in the reduction of total IgE levels by both IL-13Rα2Fc and IL-17Rh1Fc soluble receptor therapy. When total IgE levels were analyzed, the 13Rα2Fc treated mice had a more significant reduction; however, when Af-specific IgE was analyzed it was evident that both soluble receptors were equally effective at completely abrogating the antigen specific IgE response.

Further characterization of the effects of the soluble receptors was performed by looking at the cytokine levels in the lung compartment. Analysis of the BALs unexpectedly revealed that neutralization of IL-13 with IL-13Rα2Fc led

to higher levels of IL-13 in the lung. It is possible that IL-13 may act as a negative regulator of its own production, so interrupting this negative feedback loop may be causing cells in the lungs to secrete more IL-13. It is also possible, that the soluble receptor may be acting as depot or reservoir for IL-13, which would likely extend the half-life of IL-13 and thus artificially increase its concentration. In this scenario, although there is a higher concentration of IL-13, the cytokine would be mostly bound to the decoy receptor and thus would have little biologic activity. This scenario is far more likely taking into account that there was no increase in goblet cell hyperplasia accompanying the increase the IL-13 levels in the lung (data not shown). In fact the increase in the IL-13 has also been documented before in a model of helminth infection that employed IL-13Rα2 protein as a therapy (220). While IL-17Rh1Fc treatment did not seem to reduce the levels of IL-13 in the lung compartment, both treatments reduced levels of KC, a chemokine that has been previously shown to be upregulated in CF and has been implicated in pulmonary neutrophil mediated inflammation. However more importantly for allergy and asthma associated inflammation, IL-5 was significantly reduced in mice treated with rAAV-CB-IL-17Rh1Fc. Since IL-5 is responsible for the recruitment and maturation of eosinophils, the reduction of this response is also important for control of allergy driven inflammation. As shown in Table 8.1, this reduction in IL-5 was accompanied by a reduction in BAL infiltration of eosinophils in the IL-17Rh1Fc treated group. The reduction in eosinophil recruitment by dampening IL-5 and the prevention of Af-specific IgE responses

with IL-17Rh1Fc hint that a broader effect is achieved by targeting IL-17e rather than IL-13. In fact when comparing intra-cellular cytokine staining of CD11b+ monocytes and CD4+ T cells from these mice in comparison to control treated mice, it was determined that IL-17Rh1Fc treated mice had a significant reduction in IL-4, IL-13 and IL-17e in both cell populations. In contrast, macrophages in mice treated with IL-13Rα2Fc did not show any significant changes in the production of IL-13, IL-17a or IL-17e and only a slight decrease in production of IL-4. Even more compelling are differences detected in CD4+ T cells, where IL-13Rα2Fc treated mice have increased production of IL-13 and IL-4, again hinting at a feedback inhibition loop, which surprisingly led to an increase in the production of IL-17a.

This phenomenon may partially be explained by the recent discovery that a functional IL-13 receptor is present on CD4+ Th-17 cells and that in the presence of IL-13 signaling IL-17 production is attenuated (221). In case the absence of IL-13 signaling may be causing an increase production of IL-17 lending further proof that IL-13 may also be involved in the regulation of TH-17 response. On the one hand the broader effect of IL-17Rh1Fc therapy achieved in this allergy model suggests that IL-17e is acting upstream of CD4+ T and B cells, and interferes with the signaling mediated by IL-17e dampening the cytokine production of Th2 CD4+ T cells thereby curbing downstream B cell isotype switching to IgE and Th2 cytokine mediated eosinophil mediated inflammation

(Figure 8.8). On the other hand this data seems to suggest that targeting IL-13 signaling, which is mainly an effector cytokine, may be useful at inhibiting downstream processes such as B cell isotype switching but may not be helpful at curbing responses at the CD4+ T cell level (Figure 8.8). In fact it seems that reduced bioavailability of IL-13 seems to make CD4+Tcells increase the production of both IL-4 and IL-13. Having established that interfering with IL-17e signaling with a soluble IL-17Rh1Fc receptor may offer broader benefits for allergic driven pulmonary inflammation we tried to determine what cell type may be the primary source of this cytokine. To begin to elucidate what cells may be possible sources of the IL-17e in the ABPA model, we stained splenocytes for the production of IL-17e in both Cftr-/- and Cftr+/+ mice before and after *Aspergillus* challenge. As shown in the figure 7 it seems that the more abundant source of this cytokine is present in CD14+ monocytes as opposed to CD4+ T cells.

In conclusion these studies demonstrate a marked therapeutic effect of IL-13 and IL-17e immuno-neutralization with the use of soluble receptors fusion proteins delivered with rAAV. The striking abrogation of Af-specific IgE response from the two different therapies has important implications for the treatment of ABPA and other allergic diseases. This data in combination with the IL-17e staining data in the ABPA model suggests that IL-17e is an innate cytokine that may help bridge and regulate the production of Th-2 cytokines. IL-17e is substantially produced by CD14+ macrophage cells, and the receptor antagonist

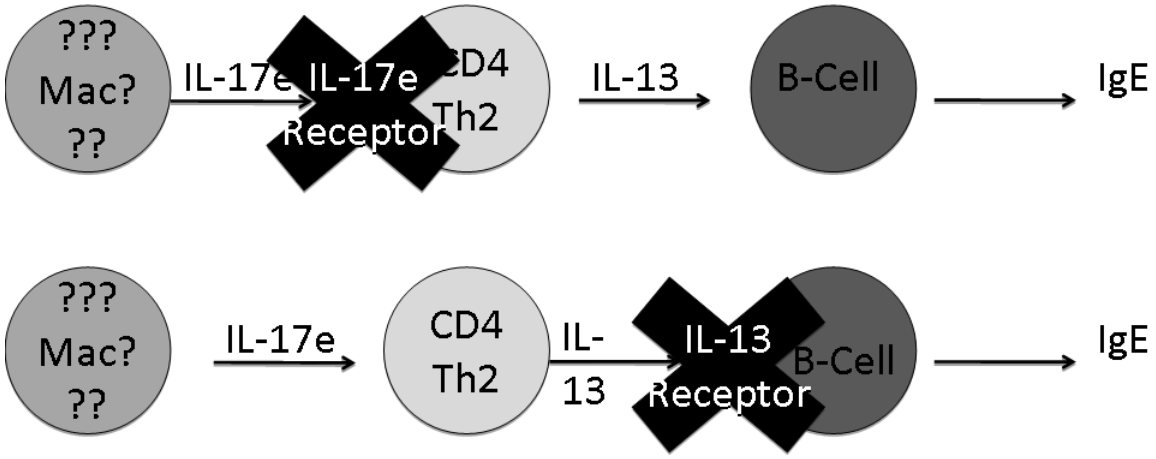

Figure 8.8 Model of IL-17e and IL-13 Receptor Therapy

reduced production of IL-17a, IL-17e, IL-13 and IL-4 when compared to the SCAD control both in CD4+ T cells and macrophages. As discussed above, the IL-13 antagonist appears to have more downstream affects as illustrated by the BAL cytokine data and flow cytometry. Although, IL-13 antagonists did not reduce Th-2 or IL-17 cytokines, it did greatly reduce total and Af-specific IgE responses. Presumably the IL-13 antagonist blocks the IL-13 from signaling the B-cells to isotype switch to make IgE, whereas the IL-17e antagonist acts further upstream in preventing Th-2 and IL-17 signaling to T cells as well as B-cells. Future experiments should look at the possibility that interfering with the signaling of both cytokines in combination may produce a synergistic effect in decreasing allergic response to Aspergillus fumigatus as well as to other antigens. Finally, while these experiments are proof-of-concept animal studies, in light of recent data from intra-muscular delivery of rAAV1 vectors in humans it is conceivable that a single administration with rAAV1 could provide sustained serum levels of the recombinant soluble receptors for up to one year (222).

Final Remarks

Altogether this work describes two different gene therapy strategies, (1) as gene replacement and (2) receptor mediated correction of aberrant signaling after antigen exposure, for two different diseases (Chapter 5, Chapter 8). It also describes methods of potentially new therapeutic options through novel transductions efficiencies (Chapter 3, 4) as well as a disease phenotype which had not been previously described for which therapy could be directed (Chapter 7).

Clearly in order to develop a therapy, the mechanisms of disease must be fairly well understood. Chapter 8 investigates the role T-cells play in CF, which allow for better therapeutic options like those described in Chapter 7. Using the knowledge gained from earlier work on acyl-CoA dehydrogenase therapies and disorders of long chain FAO, our hypothesis was designed to target the liver, cardiac and skeletal muscle. In vector selection for those specific targets, we also discovered efficient transduction and expression of both the brown fat and the brain. Finally, clinically relevant disease specific phenotypes were corrected by gene transfer to the liver, cardiac and skeletal muscle resulting in correction of VLCAD-/- mice.

Bibliography

1. Neely JR, M.H. 1974. Relationship between carbohydrate and lipid metabolism and the energy balance of heart muscle. *Annu Rev Physiol* 36:413-459.
2. Bing RJ, S.A., Ungar I, Gilbert M. 1954. Metabolism of the human heart: Studies on fat, ketone and amino acid metabolism. *The American Journal of Medicine* 16:504-515.
3. Spiekerkoetter U, B.J., Gillingham M, Morris A, Wijburg F, Wilcken B. 2010. Current issues regarding treatment of mitochondrial fatty acid oxidation disorders. *J Inherit Metab Dis* 33.
4. Goetzman, E. 2011. Modeling disorders of fatty acid metablism in the mouse. *Prog Mol Biol Transl Sci* 100:389-417.
5. Chohan KK, J.M., Grossmann JG, Frerman FE, Scrutton NS, Sutcliffe MJ. 2001. Protein dynamics enhance electronic coupling in electron transfer complexes. *J Biol Chem*:276.
6. Leys D, B.J., Talfournier F, Sutcliffe MJ, Scrutton NS. 2003. Extensive conformational sampling in a ternary electron transfer complex. *Nat Struct Biol* 10:219-225.
7. Toogood HS, v.T.A., Basran J, Sutcliffe MJ, Scrutton NS, Leys D. 2004. Extensive domain motion and electron transfer in the human electron transferring flavoprotein medium chain Acyl-CoA dehydrogenase complex. *J Biol Chem* 279.
8. Izai K, U.Y., Orii T, Yamamoto T, . 1992. Novel fatty acid Beta-oxidation enzymes in rat liver mitochondria. I. Purifcation and properties of very-long-chain acyl-coenzyme A dehydrogenase. *J Biol Chem* 267:1027-1033.
9. Lindner M, H.G., Matern D. 2010. Newborn screening for disorders of fatty acid oxidation: experience and recommondations from an expert meeting. *J Inherit Metab Dis* 33:521-526.

10. Fatty Acid Disorders. In *Expanded Newborn Screening Using Tandem Mass Spectrometry Financial, Ethical, Legal and Social Issues*.
11. Brage S Andresen, S.O., Ben J. H. M. Poorthuis, Hans R. Scholte, Christine Vianey-Saban, Ronald Wanders, Lodewijk Ijlst, Andrew Morris, Morteza Pourfarzam, Kim Bartlett, E. Regula Baumgartner, Johannis B.C. deKlerk, Lisbeth Dahl Schroeder, Thomas J. Corydon, Hans Lund, Vibeke Winter, Peter Bross, Lars Bolund and Niels Gregersen. 1999. Clear Correlation of Genotype with Disease Phenotype in Very-Long-Chain Acyl-CoA Dehydrogenase Deficiency. *Am J Hum Genet* 64:479-494.
12. Lars Hoffmann, U.H., Martina Mueller, Ute Spiekerkoetter. 2012. VLCAD enzyme activitiy determinations in newborns identified by screening: a valuable tool for risk assesment. *J Inherit Metab Dis* 35:269-277.
13. Curtis R. Coughlin II, C.F. Genotype-phenotype correlations: sudden death in an infant with very-long-chain acyl-CoA dehydrogenase deficiency. *J Inherit Metab Dis*.
14. Boles RG, B.E., Blitzer MG, Platt MS, Cowan TM, Martin SK, Yoon H, Madsen JA, Reyes-Mugica M, Rinaldo P. 1998. Retrospective biochemical screening of fatty acid oxidation disorders in postmortem livers of 418 cases of sudden death in the first year of life. *J Pediatr* 132:924-933.
15. Vellekoop P, D.E., van Tuijl I, de Vries MM, van Hasselt PM, Visser G. 2011. Perioperative measures in very long chain acyl-CoA dehydrogenase deficiency. *Mol Genet Metab* 103:96-97.
16. Pervaiz MA, K.F., Hegde M, Singh RH. 2011. MCT oil-based diet reverses hypertrophic cardiomyopathy in a patient with very long chain acyl-CoA dehydrogenase deficiency. *Indian J Hum Genet* 17:29-32.
17. Brown-Harrison MC, N.M., Sprecher H, Vianey-Saban C, Farguhar J Jr, Gilladoga AC, Roe CR. 1996. Very long chain acyl-CoA dehydrogenase deficiency: successful treatment of acute cardiomyopathy. *Biochem Mol Med* 58:59-65.

18. Tucci, S., Flogel, U., Sturm, M., Borsch, E., and Spiekerkoetter, U. 2011. Disrupted fat distribution and composition due to medium-chain triglycerides in mice with a beta-oxidation defect. *The American journal of clinical nutrition* 94:439-449.
19. Tucci S, P.S., Ter Veld F, Spiekerkoeter U. 2010. Medium-chain triglycerides impari lipid metabolism and induce hepatic steatosis in very long-chain acyl-CoA dehydrogenase (VLCAD)-deficent mice. *Mol Genet Metab* 101:40-47.
20. Primassin, S., Tucci, S., Herebian, D., Seibt, A., Hoffmann, L., ter Veld, F., and Spiekerkoetter, U. 2010. Pre-exercise medium-chain triglyceride application prevents acylcarnitine accumulation in skeletal muscle from very-long-chain acyl-CoA-dehydrogenase-deficient mice. *Journal of inherited metabolic disease* 33:237-246.
21. Behrend, A.M., Harding, C.O., Shoemaker, J.D., Matern, D., Sahn, D.J., Elliot, D.L., and Gillingham, M.B. 2011. Substrate oxidation and cardiac performance during exercise in disorders of long chain fatty acid oxidation. *Molecular genetics and metabolism*.
22. Orngreen MC, N.M., van Engelen BG, Vistisen B, Vissing J. 2007. Effects of IV glucose and orgal medium-chain triglycerides in patients with VLCAD deficiency. *Neurology* 69:313-315.
23. Vockley J, S.R., Whiteman DA. 2002. Diagnosis and management of defects of mitochondrial beta-oxidation. *Curr Opin Clin Nutr Metab Care* 5:601-609.
24. Liebig M, G.M., Brauers G, Ruiter JP, Wendel U, Mayatepek E, Strauss AW, Wanders RJ, Spiekerkoetter U. 2006. Carnitine supplementation induces long-chain acylcarnitine production–studies in the VLCAD-deficient mouse. *J Inherit Metab Dis* 29:343-344.
25. Primassin S, T.V.F., Mayatepek E, Spiekerkoetter U. 2008. Carnitine supplementation induces acylcarnitine production in tissues of very long-

chain acyl-CoA dehydrogenase-deficient mice, withough replenishing low free carnitine. *Pediatr Res* 63:632-637.

26. Roe CR, S.L., Roe DS, David F, Brunengraber H. 2002. Treatment of cardiomyopathy and rhabdomyolysis in long-chain fat oxidation disorders using and anaplerotic odd-chain triglyceride. *J Clin Invest* 110:259-269.
27. Djouadi F, A.F., Schlemmer D, Ruiter JPN, Wanders RJA, Strauss AW, Jean Bastin. 2005. Bezefibrate increase very-long-chain acyl-CoA dehydrogenase protein and mRNA expression in deficient fibroblasts and is a potential therapy for fatty acid oxidation disorders. *Hum Mol Genet* 14:2695-2703.
28. Gobin-Limballe S, D.F., Aubey F, Olpin S, Andresen BS, Yamaguchi S, Mandel H, Fukao T, Ruiter JPN, Wanders RJA, McAndrew F, Kim JJ and Bastin J. 2007. Genetic Basis for Correction of Very-long-chain Acyl-coenzyme A dehydrogenase deficiency by Bezafibrate in Patient Fibroblasts: Toward a Genotype-Based Therapy. *Am J Hum Genet* 81:1133-1143.
29. Bonnefont JP, B.J., Laforet P, Aubey F, Mogenet A, Romano S, Ricquier D, Gobin-Limballe S, Vassault A, Behin A, Eymard B, Bresson JL, Djouadi F. 2010. Long-Term Follow-up of Bezafibrate Treatment in Patients with the Myopathic Form of Carnitine Palmitoyltransferase 2 Deficiency. *Clin Pharmacol Ther* 88:101-108.
30. Voermans NC, P.P., Kluijtmans LA, van Engelen BG. 2005. The effect of dentrolene sodium in Very Long Chain Acyl-CoA Dehydrogenase Deficiency. *Neuromuscular Disord* 15:844-846.
31. Bastin J, L.-C.A., Djouadi F. 2011. Exposure to resveratrol triggers pharmacological correction of fatty acid utilization in human fatty acid oxidation-deficient fibroblasts. *Hum Mol Genet* 20:2048-2057.
32. Zhang J, Z.W., Zou D, Chen G, Wan T, Zhang M, Cao X. 2002. Cloning and functional characterization of ACAD-9, a novel member of human

acyl-CoA dehydrogenase family. *Biochem Biophys Res Commun* 297:1033-1042.

33. He M, R.S., Kelly DR, Palmer CA, Murdoch G, Majumder N, Nicholls RD, Pei Z, Watkins PA, Vockley J. 2007. A New Genetic Disorder in Mitochondrial Fatty Acid Biochem B-Oxidation: ACAD9 Deficiency. *Am J Hum Genet*:87-103.
34. Ensenauer R, H.M., Willard JM, Goetzman ES, Corydon TJ, Vandahl BB, Mohsen AW, Isaya G, Vockley J. 2005. Human acyl-CoA dehydrogenase-9 plays a novel role in the mitochondrial beta-oxidation of unsaturated fatty acids. *J Biol Chem* 280:32309-32316.
35. Nouws J, N.L., Houten SM, van den Brand M, Huynen M, Venselaar H, Hoefs S, Gloerich J, Kronick J, Hutchin T, Willems P, Rodenburg R, Wanders R, van den Heuvel L, Smeitink J, Vogel RO. 2010. Acyl-CoA dehydrogenase 9 is required for the biogenesis of oxidative phosphorylation complex I. *Cell Metab* 12:283-294.
36. Gerards M, v.d.B.B., Danhauser K, Serre V, van Weeghel M, Wanders RJA, Nicolaes GAF, Sluiter W, Schoonderwoerd K, Scholte HR, Prokisch H, Rotig A, de Coo IFM, Smeets HJM. 2010. Riboflavin-responsive oxidative phosphorylation complex I deficiency cause by defective ACAD9: new function for an old gene. *Brain* 134.
37. Chegary M, B.H., Ruiter JP, Wijburg FA, Stoll MS, Minkler PE, van Weeghel M, Schulz H, Hoppel CL, Wanders RJ, Houten SM. 2009. Mitochondrial long chain fatty acid beta-oxidation in man and mouse. *Biochim Biophys Acta* 1791.
38. Maher, A.C., Mohsen, A.W., Vockley, J., and Tarnopolsky, M.A. 2010. Low expression of long-chain acyl-CoA dehydrogenase in human skeletal muscle. *Molecular genetics and metabolism* 100:163-167.

39. S.D. Grosse, M.J.K., C.L. Greene, K.S. Crider, R.J. Pollit. 2006. The epidemiology of medium chain acyl-CoA dehydrogenase deficiency: an update. *Genet Med* 8:205-212.
40. Smith EH, T.C., McHugh D, Gavrilov D, Raymond K, Rinaldo P, Tortorelli S, Matern D, Highsmith WE, Oglesbee D. 2010. Allelic diveristy in MCAD deficiency: the biochemical classifcation of 54 variants identififed during 5 years of ACADM sequencing. *Mol Genet Metab* 100:241-250.
41. Heptinstall LE, T.J., Wraith JE, Besley GT. 1995. Common MCAD mutation in a healthy parent of two affected siblings. *J Inherit Metab Dis* 18:638-639.
42. Dessein AF, F.M., Andresen BS, Gregersen N, Brivet M, Rabier D, Napuri-Gouel S, Dobbelaere D, Mention-Mulliez K, Marin-Ponthieu A, Briand G, Millington DS, Vianey-Saban C, Wanders RJ, Vamecq. 2010. A novel mutation of the ACADM gene (c.145C>G) assiocaited with the common c985A>G mutation on the other ACADM allele causes mild MCAD deficieny: a case report. *Orphanet J Rare Dis* 5:26.
43. Zschocke J, S.A., Linder M, Fiesel S, Olgermoller K, Hoffmann GF, Penzien J, Ruiter JP, Wanders RJ, Mayatepek E. 2001. Molecular and functional chactherization of mild MCAD deficiency. Hum Genet:404-408.
44. Rinaldo P, M.D., Bennett MJ. 2002. Fatty Acid oxidation disorders. *Annu Rev Physiol* 64:477-502.
45. Grosse, S.D., Khoury, M.J., Greene, C.L., Crider, K.S., and Pollitt, R.J. 2006. The epidemiology of medium chain acyl-CoA dehydrogenase deficiency: an update. *Genetics in medicine : official journal of the American College of Medical Genetics* 8:205-212.
46. Yusupov, R., Finegold, D.N., Naylor, E.W., Sahai, I., Waisbren, S., and Levy, H.L. 2010. Sudden death in medium chain acyl-coenzyme a dehydrogenase deficiency (MCADD) despite newborn screening. *Molecular genetics and metabolism* 101:33-39.

47. Raymond K, B.A., Barnes CA, Rinaldo P. 1999. Medium-chain acyl-CoA dehydrogenase deficiency: Sudden and unexpected death of a 45 year old woman. *Genet Med* 1:293-294.
48. TF, L. 2009. Adult presentation of medium-chain acyl-CoA dehydrogenase deficiency MCADD. *J Inherit Metab Dis* 32:675-683.
49. Boles RG, B.E., Blitzer MG, Platt MS, Cowan TM, Martin SK, Yoon H, Madsen JA, Reyes-Mugica M, Rinaldo P. 1998. Retrospective biochemcial screening of fatty acid oxidation disorders in postmortem livers of 418 cases of sudden death in the first year of life. *J Pediatr* 132.
50. Derks TG, R.D., Waterham HR, Gerver WJ, Van Den Berg MP, Sauer PJ, Smit GP. 2006. The natural history of medium-chain acyl CoA dehydogenase deficiency in the Netherlands: clinical presentation and outcome. *J Pediatr* 148.
51. van Maldegem BT, D.M., Wanders RJ, Niezen-Koning KE, Hogeveen M, Ijlst L, Waterham HR, Wijburg FA. 2006. Clinical, biochemical, and genetic heterogeneity in short chain acyl-coenzyme A dehydrogenase deficiency. *JAMA* 286:943-952.
52. Schmidt SP, C.T., Pedersen CB, Bross P, Gregersen N. 2010. Misfolding of short-chain acyl-CoA dehydrogenase leads to mitochondrial fission and oxidative stress. *Mol Genet Metab* 100:156-162.
53. van Maldegem BT, D.M., Wanders RJ, Waterham HR, de Koning TJ, Rubio E, Wijburg FA. 2010. Fasting and fat-loading tests provide pathophysiological insight into short-chain acyl-coenzyme a dehydrogenase deficiency. *J Pediatr* 156:121-127.
54. Bennett, M. 2010. Pathophysiology of fatty acid oxidation disorders. *J Inherit Metab Dis* 333:533-537.
55. Wolfe L, J.R., Oglesbee D, Vockley J. 2011. Short-Chain Acyl-CoA Dehydogenase Deficiency.

56. Pedersen CB, K.S., Kolvraa A, Stenbroen V, Kjeldsen M, Ensenauer R, Tein I, Matern D, Rinaldo P, Vianey-Saban C, Ribes A, Lehnert W, Christensen E, Corydon TJ, Andresen BS, Vang S, Bolund L, Vockley J, Bross P, Gregersen N. 2008. The ACADS gene variation spectrum in 114 patients with short-chain acyl-CoA dehydrogenase (SCAD) deficency is dominated by missense variations leading to protein misfolding at the cellular level. *Hum Genet* 124:43-56.

57. Young SP, M.D., Gregersen N, Stevens RD, Bali D, Liu HM, Koeberl DD, Millington DS. 2003. A comparison of in vitro acylcarnitine profiling methods for the diagnosis of classical and varient short chain acyl-CoA dehydrogenase deficiency. *Clin Chim Acta* 337:103-113.

58. van Maldegem BT, D.M., Wanders RJ, Waterham HR, Wijburg FA. 2010. Flavin adenine dinucleotide status and the effects of high-dose riboflavin treatment in short-chain acyl-CoA dehydrogenase deficiency. *Pediatr Res* 67:304-308.

59. Wolfgang MJ, C.S., Millington DS, Cline G, Shulman GI, Suwa A, Asaumi M, Kurama T, Shimokawa T, Lane MD. 2008. Brain-specific carnitine palmitoyl-transferase-1c: role in CNS fatty acid metabolism, food intakem and body weight. *J Neurochem* 105:1550-1559.

60. den Boer ME, W.R., Morris AA, IJIst L, Heymans HS, Wijburg FA. 2002. Long-chain 3-hydroxyacyl-CoA dehydrogenase deficency: clinical presentation and follow-up of 50 patients. *Pediatrics* 109:99-104.

61. den Boer ME, D.-V.C., Chakrapani A, van Thuijl AO, Wanders RJ, Wijburg FA. 2003. Mitochondrial trifunctional protein deficiency: a severe fatty acid oxidation disorder with cardiac and neurologyic involvement. *J Pediatr* 142:684-689.

62. Tyni T, K.T., Lappi M, Summanen P, Nikoskelainen E, Pihko H. 1998. Opthalmologic findings in long-chain 3-hydroxyacyl-CoA dehydrogenase

deficiency caused by the G1528C mutation: a new type of hereditary metabolic chorioretinopathy. *Opthalmology* 105:810-824.

63. U, S. 2010. Mitochondrial fatty acid oxidation disorders: clinical presentation of long-cahin fatty acid oxidation defects before and after newborn screening. *J Inherit Metab Dis* 33:527-532.
64. Blackwell NR, H.M., Kapikian AZ, Austin JB, Rowe WP. 1968. Epidemiology of adenovirus-associated virus infection in a nursery population. *Am J Epidemiol* 88:368-378.
65. Blackwell NR, H.M., Rowe WP. 1968. Serlogic evidence for human infection with adenovirus-associated viruses. *J Natl Cancer Inst.* 40:319-327.
66. Afione SA, C.C., Flotte TR. 1995. Gene therapy vectors as drug delivery systems. *Clin Pharmacokinet* 28:181-189.
67. Carter BJ, K.G., Denhardy DT. 1975. Physical map and strand polarity of specific fragments of adenovirus-associated virus DNA produced by endonuclease R-EcoRI. *J Virol* 16:559-568.
68. Hermonant PL, L.M., Wright R, Berns KI, Muzyczka N. 1984. Genetics of adeno-assoicated virus: isolation and preliminary charactherization of adeno-associated virus type 2 mutatnts. *J Virol* 51:329-339.
69. Sonntag F, S.K., Kleinschmidt JA. 2010. A viral assemby factor promotes AAV2 capis formation in the nucleolus. *Proc Natl Acad Sci USA* 107:10220-10225.
70. Gao G, V.L., Alvira MR, Lu Y, Calcedo R, Zhou X, Wilson JM. 2004. Clades of adeno-associated viruses are widely disseminated in human tissues. *J Virol* 78:6381-6388.
71. Gao G, V.L., Wilson JM. 2005. New recombinant serotypes of AAV vectos. *Curr Gene Ther* 5:285-297.
72. Vandenberghe LH, B.E., Nam HJ, Gao G, Xiao R, Sandhu A, Johnston J, Debyser Z, Agbandje-McKenna M, Wilson. 2009. Naturally occurring

singleton residues in AAV capsid impact vector performance and illustrate structural constraints. *Gene Ther* 16:1416-1428.

73. Chen S, K.M., Loiler SA, Zolotukihin S, Glushakova OY, Madesen KM, Samulski RJ, Hauswirth WW, Campbell-Thompson M, Berns KI, Flotte TR, Atkinson MA, Tisher CC, Agarwal A. 2005. Efficient transduction of vascular endothelial cells with recombinant adeno-associated virus serotype 1 and 5 vectors. *Hum Gene Ther* 16:235-247.
74. Rabinowitz JE, R.F., Li C, Conrath H, Xiao W, Xiao X, Samulski RJ. 2002. Cross-packaging of a simple adeno-associated virus (AAV) type 2 vector genome into multiple AAV serotypes enables transduction with broad specificity *J Virol* 76:791-801.
75. Wu Z, M.E., Agbandje-McKenna M, Samulski RJ. 2006. Alpha2,3 and alpha2,6 N-linked sialic acids facilitate efficent binding and transduction by adeno-associated virus types 1 and 6. *J Virol* 80:9093-9103.
76. Berns KI, L.R. 1995. The cryptic life style of adeno-associated virus. *Bioessays* 17:237-245.
77. Summerford C, S.R. 1998. Membrane-associated heparan sulfate proteoglycan is a receptor for adeno-assoicated virus type 2 virions. *J Virol* 72:1438-1445.
78. Summerford C, S.R. 1999. Viral receptors and vector purification: new apporaches for generating clinical-grade reagents. *Nat Med* 5:587-588.
79. Qing K, M.C., Hansen J, Zhou S, Dwarki V, Srivastava A. 1999. Human fibroblast growth factor receptor 1 is a co-receptor for infection by adeno-associated virus 2. *Nat Med* 5:71-77.
80. Kaludov N, B.K., Walters RW, Zabner J, Chiorini JA. 2001. Adeno-associated virus serotype 4 (AAV4) and AAV5 both require sialic acid binding for hemagglutination and efficient transduction but differ in sialic acid linkage specificity. *J Virol* 75:6884-6893.

81. Walters RW, Y.S., Keshavjee S, Brown KE, Welsh MJ, Chiorini JA, Zabner J. 2001. Binding of adeno-assoicated virus type 5 to 2,3-linked sialic acid is required for gene transfer. *J Biol Chem* 276:20610-20616.
82. Wu Z, A.A., Grieger JC, Govindasamy L, Agbandje-McKenna M, Samulski RJ. 2006. Single amino acid changes can influence titer, heparin binding, and tissue tropism in different adeno-assoicated virus serotypes. *J Virol* 80:11393-11397.
83. Akache B, G.D., Pandey K, Yant SR, Xu H, Kay MA. 2006. The 37/67-kilodalton laminin receptor is a receptor for adeno-assicated virus serotypes 8,2,3, and 9. *J Virol* 80:9831-9836.
84. Shen S, B.K., Brwon SM, Randell SH, Asokan A. 2011. Terminal N-linked galactose is the primary receptor for adeno-associated virus 9. *J Biol Chem* 286:13532-13540.
85. Hirata RK, R.D. 2000. Design and packaging of adeno-associated virus gene targeting vectors. *J Virol* 74:4612-4620.
86. McCarty DM, M.P., Samulski RJ. 2001. Self-complementary recombinant adeno-associated (scAAV) vectors promotoe efficient transduction independently of DNA synthesis. *Gene Ther* 8:1248-1254.
87. Wang Z, M.H., Li J, Sun L, Zhang J, Xiao X. 2003. Rapid and highly efficient transduction by double-stranded adeno-associated virus vectors in vitro and in vivo. *Gene Ther* 10:2105-2111.
88. Bish LT, M.K., Sleeper MM, Sanmiguel J, Wu D, Gao G, Wilson JM, Sweeney HL. 2008. Adeno-associated virus (AAV) serotype 9 provides global cardiac gene transfer superior to AAV1, AAV6, AAV7 and AAV8 in the mouse and rat. *Hum Gene Ther* 19:1359-1368.
89. Zincarelli, C., Soltys, S., Rengo, G., and Rabinowitz, J.E. 2008. Analysis of AAV serotypes 1-9 mediated gene expression and tropism in mice after systemic injection. *Molecular therapy : the journal of the American Society of Gene Therapy* 16:1073-1080.

90. Lei B, Z.K., Yue Y, Ghosh A, Duan D. 2010. Adeno-associated virus serotype-9 mediated retinal outer plexiform layer transduction is mainly through the photoreceptors. *Adv Exp Med Biol* 664:671-678.
91. Cearley CN, V.L., Parente MK, Carnish ER, Wilson JM, Wolfe JH. 2008. Expanded repetoire of AAV vector serotypes mediate unique patterns of transduction in mouse brain. *Mol Ther* 16:1710-1718.
92. Zhong L, L.B., Mah CS, Govindasamy L, Agbandje-McKenna M, Cooper M, Herzong RW, Zolotukhin I, Warrington KH Jr, Weigel-Van Aken KA, Hobbs JA, Zolotukhin S, Muzyczka N, Srivastava A. 2008. Next generation of adeno-associated virus 2 vectors: point mutations in tyrosines lead to high-efficiency transduction at lower doses. *Proc Natl Acad Sci USA* 105:7827-7832.
93. Michelfelder S, V.K., Raupp C, Hunger A, Korbelin J, Pahrmann C, Schrepfer S, Muller OJ, Kleinschmidt JA, Trepel M. 2011. Peptide ligands incorporated into the the threefold spike capsid domain re-direct gene trandsuction of AAV8 and AAV9 in vivo. *PLoS One* 6:8.
94. Girod A, R.M., Wobus C, Lahm H, Leike K, Kleinschmidt J, Deleage G, Hallek M. 1999. Genetic capsid modifications allow efficient re-targeting of adeno-associated virus type 2. *Nat Med* 5:1052-1056.
95. Grimm D, L.J., Wang L, Desi T, Akache B, Storm TA, Kay MA. 2008. In vitro and in vivo gene therapy vector evolution via multispecifes interbreeding and re-targing of adeno-associated viruses. *J Virol* 82:5887-5911.
96. Koerber JR, J.J., Schaffer DV. 2008. DNA shuffling of adeno-associated virus yields functionally diverse viral progeny. *Mol Ther* 16:1703-1709.
97. Li W, A.A., Wu Z, Van Dyke T, DiPrimio N, Johnson JS, Govindaswamy L, Agbandje-McKenna M, Leichtle S, Redmond DE Jr, McCown TJ, Petermann KB, Sharpless NE, Samulski RJ. 2008. Engineering and

selection of shuffled AAV genomes: a new strategy for producing targeted biological nanoparticles. *Mol Ther* 16:1252-1260.

98. Lochrie MA, T.G., Christie B, McDonnell JW, Zhou S, Surosky R, Pierce GF, Colosi P. 2006. Mutations on the external surfaces of adeno-associated virus type 2 capsids that affect transduction and neutralization. *J Virol* 80:821-834.
99. Xie J, X.Q., Zhang H, Ameres SL, Hung JH, Su Q, He R, Mu X, Seher Ahmed S, Park S, Kato H, Li C, Mueeler C, Mello CC, Weng Z, Flotte TR, Zamore PD, Gao G. 2011. MicroRNA-regulated, systemically deliverd rAAV9: a step closer to CNS-restricted transgene expression. *Mol Ther* 19:526-535.
100. Flotte T, C.B., Conrad C, Guggino W, Reynods T, Rosenstein B, Taylor G, Walden S, Wetzel R. 1996. A phase I study of an adeno-assocaited virus-CFTR gene vector in adult CF patients with mild lung disease. *Hum Gene Ther* 7:1145-1159.
101. Manno CS, P.G., Arruda VR, Glader B, Ragni M, Rasko JJ, Ozelo MC, Hoots K, Blatt P, Konkle B, Dake M, Kaye R, Razavi M, Zajko A, Zehnder J, Rustagi PK, Nakai H, Chew A, Leonard D, Wright JF, Lessard RR, Sommer JM, Tigges M, Sabtino D, Luk A, Jiang H, Mingozzi F, Couto L, Ertl HC, High KA, Kay MA. 2006. Successful transduction of liver in hemphilia by AAV-Factor IX and limitations imposed by host immune response. *Nat Med* 12:342-347.
102. Brantly ML, C.J., Wang L, Mueller C, Humphries M, Spencer LT, Rouhani F, Conlon TJ, Calcedo R, Betts MR, Spencer C, Byrne BJ, Wilson JM, Flotte TR. 2009. Sustained transgene expression despite T lymophcyte response in a clinical trail of rAAV1-AAT gene therapy. *Proc Natl Acad Sci USA* 106:16363-16368.
103. Flotte TR, T.B., Humphries M, Carey B, Calcedo R, Rouhani F, Campbell-Thompson M, Yachnis AT, Sandhaus RA, McElvaney NG, Mueller C,

Messina LM, Wilson JM, Brantly M, Knop DR, Ye GJ, Chulay JD. 2011. Phase 2 clinical trial of a recombinant adeno-associated viral vector expressing α1-antitrypsin: interim results. *Hum Gene Ther* 22:1239-1247.

104. Kelly CL, R.W., Kutschke WK, Brix AE, Hamm DA, Pinkert CA, Lindsey JR, Wood PA. 1997. Functional Correction of Short-Chain Acyl-CoA Dehydrogenase Deficency in Transgenic Mice: Implications for Gene Therapy of Human Mitochondrial Enzyme Deficiences. *Hum Mol Genet* 6:1451-1455.
105. Holm DA, D.-H.F., Simonsen H, Gregersen N, Bolund L, Jensen TG, Corydon TJ. 2003. Expression of short-chain acyl-CoA dehydrogenase (SCAD) protiens in the liver of SCAD deficient mice after hydrodynamic gene transfer. *Molecular genetics and metabolism* 78:250-258.
106. Conlon, T.W.G., Owen R, Cossette T, Erger K, Gutierrez G, Goetzman E, Matern D, Vockley J, Flotte TR. 2006

. Systemic correction of fatty acid oxidation defect by intramuscular injection of a recombinant adeno-associated virus vector. *Human gene therapy* 17:71-80.
107. Beattie, S.G., Goetzman, E., Conlon, T., Germain, S., Walter, G., Campbell-Thompson, M., Matern, D., Vockley, J., and Flotte, T.R. 2008. Biochemical correction of short-chain acyl-coenzyme A dehydrogenase deficiency after portal vein injection of rAAV8-SCAD. *Human gene therapy* 19:579-588.
108. Schowalter DB, M.D., Vockley J. 2005. In vitro correction of medium chain acyl CoA dehydorgenase deficiency with a recombinant adenoviral vector. *Mol Genet Metab* 85:88-95.
109. Cox KB, H.D., Milington DS, Matern D, Vockley J, Rinaldo P, Pinkert CA, Rhead WJ, Lindsey JR, Wood PA. 2001. Gestational, pathologic and biochemical differences between very long-chain acyl-CoA dehyrogenase

deficency and long-chain acyl-CoA dehydrogenase deficiecny in the mouse. *Hum Mol Genet* 10:2069-2077.

110. Beattie, S.G., Goetzman, E., Tang, Q., Conlon, T., Campbell-Thompson, M., Matern, D., Vockley, J., and Flotte, T.R. 2008. Recombinant adeno-associated virus-mediated gene delivery of long chain acyl coenzyme A dehydrogenase (LCAD) into LCAD-deficient mice. *The journal of gene medicine* 10:1113-1123.
111. Merritt JL 2nd, M.D., Vockley J, Daniels H, Nguyen TV, Schowalter DB. 2006. In vitro charachterization and in vivo expression of human very-long chain acyl-CoA dehydrogenase. *Mol Genet Metab* 88:351-358.
112. Merritt, J.L., 2nd, Nguyen, T., Daniels, J., Matern, D., and Schowalter, D.B. 2009. Biochemical correction of very long-chain acyl-CoA dehydrogenase deficiency following adeno-associated virus gene therapy. *Molecular therapy : the journal of the American Society of Gene Therapy* 17:425-429.
113. Keeler AM, C.T., Walter G, Zeng H, Shaffer SA, Dungtao F, Erger K, Cossette T, Tang Q, Mueller C, Flotte TR. 2012. Long-term Correction of Very Long-chain Acyl-CoA Dehydrogenase Deficiency in Mice Using AAV9 Gene Therapy. *Mol Ther*.
114. Spiekerkoetter U, L.M., Santer R, Grotzke M, Baumgartner MR, Boehles H, Das A, Haase C, Hennermann JB, Karall D, de Klerk H, Knerr I, Koch HG, Plecko B, Röschinger W, Schwab KO, Scheible D, Wijburg FA, Zschocke J, Mayatepek E, Wendel U. 2009. Management and outcome in 75 individuals with long-chain fatty acid oxidation defects: results from a workshop. *J Inherit Metab Dis* 32:488-497.
115. Xu L, D.T., Gao C, Flotte TR, Song S, Byrne BJ, Sands MS, Parker Ponder K. 2001. CMV-beta-actin promoter directs higher expression from an adeno-associated viral vector in the liver than the cytomegalovirus or

elongation factor 1 alpha promoter and results in therapeutic levels of human factor X in mice. *Hum Gene Ther* 12:563-573.

116. Inagaki, K., Fuess, S., Storm, T.A., Gibson, G.A., McTiernan, C.F., Kay, M.A., and Nakai, H. 2006. Robust systemic transduction with AAV9 vectors in mice: efficient global cardiac gene transfer superior to that of AAV8. *Molecular therapy : the journal of the American Society of Gene Therapy* 14:45-53.
117. Gao, G., Alvira, M.R., Somanathan, S., Lu, Y., Vandenberghe, L.H., Rux, J.J., Calcedo, R., Sanmiguel, J., Abbas, Z., and Wilson, J.M. 2003. Adeno-associated viruses undergo substantial evolution in primates during natural infections. *Proceedings of the National Academy of Sciences of the United States of America* 100:6081-6086.
118. Cideciyan, A.V., Aleman, T.S., Boye, S.L., Schwartz, S.B., Kaushal, S., Roman, A.J., Pang, J.J., Sumaroka, A., Windsor, E.A., Wilson, J.M., et al. 2008. Human gene therapy for RPE65 isomerase deficiency activates the retinoid cycle of vision but with slow rod kinetics. *Proceedings of the National Academy of Sciences of the United States of America* 105:15112-15117.
119. Davidoff AM, N.C., Zhour J, Spence Y, Nathwani AC. 2003. Sex significantly influences transduction of murine liver by recombinant adeno-associated viral vectors through an androgen-dependent pathway. *Blood* 102:480-488.
120. Hiroaki Mizukami, J.M., Tsuyoshi Ogura, Takashi Okada, Masashi Urabe, Akihiro Kume, Yoichi Sakata and Keiya Ozawa. 2006. Adipose Tissue as a Novel Target for In Vivo Gene Tranfer by Adeno-Associated Viral Vectors. *Human gene therapy* 17:921-926.
121. Zhang, F.L., Jia, S.Q., Zheng, S.P., and Ding, W. 2011. Celastrol enhances AAV1-mediated gene expression in mice adipose tissues. *Gene therapy* 18:128-134.

122. Pañeda A, V.L., Mauleon I, Crettaz JS, Berraondo P, Timmermans EJ, Beattie SG, Twisk J, van Deventer S, Prieto J, Fontanellas A, Rodriguez-Pena MS, Gonzalez-Aseguinolaza G. Effect of adeno-associated virus serotype and genomic structure on liver transduction and biodistribution in mice of both genders. Effect of adeno-associated virus serotype and genomic structure on liver transduction and biodistribution in mice of both genders. *Hum Gene Ther* 20:908-917.
123. Foust, K.N.E., Montgomery CL, Hernandez A, Chan CM, Kaspar BK. 2009. Intravascular AA9 preferentially targets neonatal neurons and adult astrocytes. *Nat Biotechnol* 27:59-65.
124. Saunders NR, J.E.C., Dziegielewka KM. 2009. The neonatal blood-brain barrier is functionally effective, and immaturity does not explain differential targeting of AAV9. *Nat Biotechnol* 27:804-805.
125. Lowenstein, P. 2009. Crossing the rubicon. *Nat Biotechnol* 27:42-44.
126. Gray SJ, M.V., Bachaboina L, Yadav S, Ojeda SR, Samulski RJ. 2011. Preclinical differences in intravascular AA9 delivery to neurons and glia: a comparative study of adult mice and nonhuman primates. *Mol Ther* 19:1058-1069.
127. Miyake N, M.K., Yamamoto M, Hirai Y, Shimada T. 2011. Global gene transfer into the CNS across the BBB after neonatal systemic delivery of single-stranded AAV vectors. *Brain Res* 10:19-26.
128. Fu H, D.J., Killedar S, Zaraspe K, McCarthy. 2011. Correction of neurological disease of mucopolysaccharidosis IIIB in adult mice by rAAV9 trans-blood-brain barrier gene delivery. *Mol Ther* 19:1025-1033.
129. Bevan AK, D.S., Foust KD, Morales PR, Braun L, Schmelzer L, Chan CM, McCrate M, Chicoine LG, Coley BD, Porensky PN, Kolb SJ, Mendell JR, Burghes AH, Kaspar BK. 2011. Systemic gene delivery in large animal species for targeting spinal cord, brain, and peripheral tissues for pediatric disorders. *Mol Ther* 19:1971-1980.

130. Spiekerkoetter, U., Sun, B., Zytkovicz, T., Wanders, R., Strauss, A.W., and Wendel, U. 2003. MS/MS-based newborn and family screening detects asymptomatic patients with very-long-chain acyl-CoA dehydrogenase deficiency☆. *The Journal of Pediatrics* 143:335-342.

131. Arnold, G.L., Van Hove, J., Freedenberg, D., Strauss, A., Longo, N., Burton, B., Garganta, C., Ficicioglu, C., Cederbaum, S., Harding, C., et al. 2009. A Delphi clinical practice protocol for the management of very long chain acyl-CoA dehydrogenase deficiency. *Molecular genetics and metabolism* 96:85-90.

132. Christine Vianey-Saban, P.D., Michele Brivet, Mohamed Nada, Marie-Therese Zabot, Monique Mathieu, Charles Roe. 1998. Mitochondrial very-long-chain acyl-coenzyme A dehydrogenase deficiency: clinical characteristics and diagnostic consideration in 30 patients. *Clinca Chimica Acta* 269:43-62.

133. Smelt AH, P.B., Onkenhout W, Scholte HR, Andresen BS, van Duinen SG, Gregersen N, Wintzen AR. 1998. Very long chain acyl-coenzyme A dehyrdogenase deficiency with adult onset. *Ann Neurol.* 43:540-544.

134. Niels Gregersen, B.S.A., Morten J. Corydon, Thomas J. Corydon, Rikke K.J. Olsen, Lars Bolund, and Peter Bross. 2001. Mutation Anaylsis in Mitochondrial Fatty Acid Oxidation Defects: Exemplified by Acyl-CoA Dehydrogenase Deficiencies, With Special Focus on Genotype-Phenotype Relationship. *Human Mutation* 18:169-189.

135. Online Medelian Inheritance in Man, O.J.H.U., Baltimore, MD. MIM Number: 201475: April 27, 2011.

136. Roser Pons, P.C., Silvia Baratta, Federica Invernizzi, Eleonora Lamantea, Barbara Garavaglia and Franco Taroni. 2000. Clinical and Molecular hetergeneity in very-long chain acyl-coenzyme a dehydrogenase deficiency. *Pediatric Neurology* 22:98-105.

137. Thomas H. Zytkovicz, E.F.F., Deborah Marsden, Cecilia A. Larson, Vivian E. Shih, Donna M. Johnson, Arnold W. Strauss, Anne Marie Comeau, Roger B. Eaton and George F. Grady. 2001. Tandem Mass Spectrometric Analysis for Amino, Organic and Fatty Acid Disorders in Newborn Dried Blood Spots: A Two-Year Summary from the New England Screening Program. *Clinical Chemistry* 47:1945-1955.

138. Spiekerkoetter U, T.C., Wendel U, Mayatepek E, Ijlst L, Vaz FM, van Vlies N, Overmars H, Duran M, Wijburg FA, Wanders RJ, Strauss AW. 2005. Tissue carnitine homeostasis in very-long-chain acyl-CoA dehydrogenase-deficient mice. *Pediatr Res* 57:760-764.

139. Damien Bonnet, D.M., Pascale de Lonlay, Elizabeth Villain, Philippe Jouvet, Daniel Rabier, Michele Brivet and Jean-Marie Saudubray. 1999. Arrhythmias and Conduction Defects as Presenting Symptoms of Fatty Acid Oxidation Disorders in Children. *Circulation* 100:2248-2258.

140. Amit Mathur, H.F.S., Deepika Gopalakrishnan, Beverly Gibson, Piero Rinaldo, Jerry Vockley, George Hug and Arnold W. Strauss. 1999. Molecular Heterogeneity in Very-Long-Chain Acyl-CoA Dehydrogenase Deficiency Causing Pediatirc Cardiomyopathy and Sudeen Death. *Circulation* 99:1337-1343.

141. Pascal Laforêt, C.A.-B., Odile Rigal, Michèle Brivet, Isabelle Penisson-Besniere, Brigitte Chabrol, Denys Chaigne, Odile Boespflug-Tanguy, Cécile Laroche, Anne-Laure Bedat-Millet, Anthony Behin, Isabelle Delevaux, Anne Lombès, Brage S. Andresen, Bruno Eymard, Christine Vianey-Saban. 2009. Diagnostic assessment and long-term follow-up of 13 patients with Very Long-Chain Acyl-Coenzyme A dehydrogenase (VLCAD) deficiency. *Neuromuscular Disorders* 19:324-329.

142. U. Spiekerkoetter, C.T., U. Wendel, E. Mayatepek, V. Exil, M. Duran, F.A.Wijburg, R.J.A. Wanders and A.W. Strauss. 2004. Changes in blood carnitine and acylcarnitine profiles of very long-chain acyl-CoA

dehydrogenase-deficient mice subjected to stress. *Eur J Clin Invest* 34:191-196.

143. Conlon, T.J., Cossette, T., Erger, K., Choi, Y.K., Clarke, T., Scott-Jorgensen, M., Song, S., Campbell-Thompson, M., Crawford, J., and Flotte, T.R. 2005. Efficient hepatic delivery and expression from a recombinant adeno-associated virus 8 pseudotyped alpha1-antitrypsin vector. *Molecular therapy : the journal of the American Society of Gene Therapy* 12:867-875.
144. Barbara Cannon, J.N. 2004. Brown Adipose Tissue: Function and Physiological Significance. *Physiol Rev* 84:277-359

.

145. Skilling, H., Coen, P.M., Fairfull, L., Ferrell, R.E., Goodpaster, B.H., Vockley, J., and Goetzman, E.S. 2010. Brown adipose tissue function in short-chain acyl-CoA dehydrogenase deficient mice. *Biochemical and biophysical research communications* 400:318-322.
146. Exil, V.J., Gardner, C.D., Rottman, J.N., Sims, H., Bartelds, B., Khuchua, Z., Sindhal, R., Ni, G., and Strauss, A.W. 2006. Abnormal mitochondrial bioenergetics and heart rate dysfunction in mice lacking very-long-chain acyl-CoA dehydrogenase. *American journal of physiology. Heart and circulatory physiology* 290:H1289-1297.
147. Wilcken, B. 2010. Fatty acid oxidation disorders: outcome and long-term prognosis. *Journal of inherited metabolic disease* 33:501-506.
148. Primassin, S., Tucci, S., and Spiekerkoetter, U. 2011. Hepatic and muscular effects of different dietary fat content in VLCAD deficient mice. *Molecular genetics and metabolism*.
149. Orellana-Gavaldà JM, H.L., Malandrino MI, Pañeda A, Sol Rodríguez-Peña M, Petry H, Asins G, Van Deventer S, Hegardt FG, Serra D. 2011. Molecular therapy for obesity and diabetes based on a long-term increase in hepatic fatty-acid oxidation. *Hepatology* 53:821-832.

150. Kluge S, K.P., Block A, Merkel M, Gocht A, Lukacs Z, Kohlschütter A, Kreymann G. 2003. A young woman with persistent hypoglycemia, rhabdomyolysis, and coma: recognizing fatty acid oxidation defects in adults. *Crit Care Med* 31:1273-1276.

151. Tucci S, P.S., Ter Veld F, Spiekerkoeter U. 2010. Medium-chain triglycerides impair lipid metabolism and induce hepatic steatosis in very long-chain acyl-CoA dehydrogenase (VLCAD)-deficient mice. *Mol Genet Metab* 101:40-47.

152. Cideciyan AV, A.T., Boye SL, Schwartz SB, Kaushal S, Roman AJ, Pang JJ, Sumaroka A, Windsor EA, Wilson JM, Flotte TR, Fishman GA, Heon E, Stone EM, Byrne BJ, Jacobson SG, Hauswirth WW. 2008. Human gene therapy for RPE65 isomerase deficiency activates the retinoid cycle of vision but with slow rod kinetics. *Proc Natl Acad Sci USA* 105:15112-15117.

153. Durie, P.R., Kent, G., Phillips, M.J. & Ackerley, C.A. . 2004. Characteristic multiorgan pathology of cystic fibrosis in a long-living cystic fibrosis transmembrane regulator knockout murine model. *Am J Pathol* 164:1482-1493

.

154. Jiang, C., Finkbeiner, W.E., Widdicombe, J.H., and Miller, S.S. 1997. Fluid transport across cultures of human tracheal glands is altered in cystic fibrosis. *J Physiol* 501 (Pt 3):637-647.

155. Widdicombe, J.H. 2002. Regulation of the depth and composition of airway surface liquid. *J Anat* 201:313-318.

156. Li, C., and Naren, A.P. 2005. Macromolecular complexes of cystic fibrosis transmembrane conductance regulator and its interacting partners. *Pharmacol Ther* 108:208-223.

157. de Bentzmann, S., Roger, P., Dupuit, F., Bajolet-Laudinat, O., Fuchey, C., Plotkowski, M.C., and Puchelle, E. 1996. Asialo GM1 is a receptor for

Pseudomonas aeruginosa adherence to regenerating respiratory epithelial cells. *Infect Immun* 64:1582-1588.

158. Zar, H., Saiman, L., Quittell, L., and Prince, A. 1995. Binding of Pseudomonas aeruginosa to respiratory epithelial cells from patients with various mutations in the cystic fibrosis transmembrane regulator. *J Pediatr* 126:230-233.
159. Bastonero, S., Gargouri, M., Ortiou, S., Gueant, J.L., and Merten, M.D. 2005. Inhibition by TNF-alpha and IL-4 of cationic lipid mediated gene transfer in cystic fibrosis tracheal gland cells. *J Gene Med* 7:1439-1449.
160. Terheggen-Lagro, S.W., Rijkers, G.T., and van der Ent, C.K. 2005. The role of airway epithelium and blood neutrophils in the inflammatory response in cystic fibrosis. *J Cyst Fibros* 4 Suppl 2:15-23.
161. Conese, M., Copreni, E., Di Gioia, S., De Rinaldis, P., and Fumarulo, R. 2003. Neutrophil recruitment and airway epithelial cell involvement in chronic cystic fibrosis lung disease. *J Cyst Fibros* 2:129-135.
162. Sagel, S.D., and Accurso, F.J. 2002. Monitoring inflammation in CF. Cytokines. *Clin Rev Allergy Immunol* 23:41-57.
163. Venkatakrishnan, A., Stecenko, A.A., King, G., Blackwell, T.R., Brigham, K.L., Christman, J.W., and Blackwell, T.S. 2000. Exaggerated activation of nuclear factor-kappaB and altered IkappaB-beta processing in cystic fibrosis bronchial epithelial cells. *Am J Respir Cell Mol Biol* 23:396-403.
164. Rottner, M., Kunzelmann, C., Mergey, M., Freyssinet, J.M., and Martinez, M.C. 2007. Exaggerated apoptosis and NF-kappaB activation in pancreatic and tracheal cystic fibrosis cells. *Faseb J* 21:2939-2948.
165. van Heeckeren, A., Ferkol, T., and Tosi, M. 1998. Effects of bronchopulmonary inflammation induced by pseudomonas aeruginosa on adenovirus-mediated gene transfer to airway epithelial cells in mice. *Gene Ther* 5:345-351.

166. van Heeckeren, A.M., Schluchter, M.D., Xue, W., and Davis, P.B. 2006. Response to acute lung infection with mucoid Pseudomonas aeruginosa in cystic fibrosis mice. *Am J Respir Crit Care Med* 173:288-296.

167. van Heeckeren, A.M., Schluchter, M.D., Drumm, M.L., and Davis, P.B. 2004. Role of Cftr genotype in the response to chronic Pseudomonas aeruginosa lung infection in mice. *Am J Physiol Lung Cell Mol Physiol* 287:L944-952.

168. van Heeckeren, A.M., Tscheikuna, J., Walenga, R.W., Konstan, M.W., Davis, P.B., Erokwu, B., Haxhiu, M.A., and Ferkol, T.W. 2000. Effect of Pseudomonas infection on weight loss, lung mechanics, and cytokines in mice. *Am J Respir Crit Care Med* 161:271-279.

169. Becker, J.W., Burke, W., McDonald, G., Greenberger, P.A., Henderson, W.R., and Aitken, M.L. 1996. Prevalence of allergic bronchopulmonary aspergillosis and atopy in adult patients with cystic fibrosis. *Chest* 109:1536-1540.

170. Skov, M., McKay, K., Koch, C., and Cooper, P.J. 2005. Prevalence of allergic bronchopulmonary aspergillosis in cystic fibrosis in an area with a high frequency of atopy. *Respir Med* 99:887-893.

171. Eaton, T.E., Weiner Miller, P., Garrett, J.E., and Cutting, G.R. 2002. Cystic fibrosis transmembrane conductance regulator gene mutations: do they play a role in the aetiology of allergic bronchopulmonary aspergillosis? *Clin Exp Allergy* 32:756-761.

172. Marchand, E., Verellen-Dumoulin, C., Mairesse, M., Delaunois, L., Brancaleone, P., Rahier, J.F., and Vandenplas, O. 2001. Frequency of cystic fibrosis transmembrane conductance regulator gene mutations and 5T allele in patients with allergic bronchopulmonary aspergillosis. *Chest* 119:762-767.

173. Laufer, P., Fink, J.N., Bruns, W.T., Unger, G.F., Kalbfleisch, J.H., Greenberger, P.A., and Patterson, R. 1984. Allergic bronchopulmonary aspergillosis in cystic fibrosis. *J Allergy Clin Immunol* 73:44-48.

174. Miller, P.W., Hamosh, A., Macek, M., Jr., Greenberger, P.A., MacLean, J., Walden, S.M., Slavin, R.G., and Cutting, G.R. 1996. Cystic fibrosis transmembrane conductance regulator (CFTR) gene mutations in allergic bronchopulmonary aspergillosis. *Am J Hum Genet* 59:45-51.

175. Skov, M., Poulsen, L.K., and Koch, C. 1999. Increased antigen-specific Th-2 response in allergic bronchopulmonary aspergillosis (ABPA) in patients with cystic fibrosis. *Pediatr Pulmonol* 27:74-79.

176. Hartl, D., Griese, M., Kappler, M., Zissel, G., Reinhardt, D., Rebhan, C., Schendel, D.J., and Krauss-Etschmann, S. 2006. Pulmonary T(H)2 response in Pseudomonas aeruginosa-infected patients with cystic fibrosis. *J Allergy Clin Immunol* 117:204-211.

177. Knutsen, A.P., Hutchinson, P.S., Albers, G.M., Consolino, J., Smick, J., and Kurup, V.P. 2004. Increased sensitivity to IL-4 in cystic fibrosis patients with allergic bronchopulmonary aspergillosis. *Allergy* 59:81-87.

178. Xu, Y., Clark, J.C., Aronow, B.J., Dey, C.R., Liu, C., Wooldridge, J.L., and Whitsett, J.A. 2003. Transcriptional adaptation to cystic fibrosis transmembrane conductance regulator deficiency. *J Biol Chem* 278:7674-7682.

179. Muller, C., Braag, S.A., Herlihy, J.D., Wasserfall, C.H., Chesrown, S.E., Nick, H.S., Atkinson, M.A., and Flotte, T.R. 2006. Enhanced IgE allergic response to Aspergillus fumigatus in CFTR-/- mice. *Lab Invest* 86:130-140.

180. Mueller, C., Torrez, D., Braag, S., Martino, A., Clarke, T., Campbell-Thompson, M., and Flotte, T.R. 2008. Partial correction of the CFTR-dependent ABPA mouse model with recombinant adeno-associated virus gene transfer of truncated CFTR gene. *J Gene Med* 10:51-60.

181. Bubien, J.K. 2001. CFTR may play a role in regulated secretion by lymphocytes: a new hypothesis for the pathophysiology of cystic fibrosis. *Pflugers Arch* 443 Suppl 1:S36-39.

182. McDonald, T.V., Nghiem, P.T., Gardner, P., and Martens, C.L. 1992. Human lymphocytes transcribe the cystic fibrosis transmembrane conductance regulator gene and exhibit CF-defective cAMP-regulated chloride current. *J Biol Chem* 267:3242-3248.

183. Chen, J.H., Schulman, H., and Gardner, P. 1989. A cAMP-regulated chloride channel in lymphocytes that is affected in cystic fibrosis. *Science* 243:657-660.

184. Krauss, R.D., Berta, G., Rado, T.A., and Bubien, J.K. 1992. Antisense oligonucleotides to CFTR confer a cystic fibrosis phenotype on B lymphocytes. *Am J Physiol* 263:C1147-1151.

185. Krauss, R.D., Bubien, J.K., Drumm, M.L., Zheng, T., Peiper, S.C., Collins, F.S., Kirk, K.L., Frizzell, R.A., and Rado, T.A. 1992. Transfection of wild-type CFTR into cystic fibrosis lymphocytes restores chloride conductance at G1 of the cell cycle. *Embo J* 11:875-883.

186. Grubb, B.R., Pickles, R.J., Ye, H., Yankaskas, J.R., Vick, R.N., Engelhardt, J.F., Wilson, J.M., Johnson, L.G., and Boucher, R.C. 1994. Inefficient gene transfer by adenovirus vector to cystic fibrosis airway epithelia of mice and humans. *Nature* 371:802-806.

187. Zhou, L., Dey, C.R., Wert, S.E., DuVall, M.D., Frizzell, R.A., and Whitsett, J.A. 1994. Correction of lethal intestinal defect in a mouse model of cystic fibrosis by human CFTR. *Science* 266:1705-1708.

188. Hodges, C.A., Cotton, C.U., Palmert, M.R., and Drumm, M.L. 2008. Generation of a conditional null allele for Cftr in mice. *Genesis* 46:546-552.

189. June, C.H., Abe, R., and Rabinovitch, P.S. 2001. Measurement of intracellular calcium ions by flow cytometry. *Curr Protoc Cytom* Chapter 9:Unit 9 8.
190. Machen, T.E. 2006. Innate immune response in CF airway epithelia: hyperinflammatory? *Am J Physiol Cell Physiol* 291:C218-230.
191. Fischer, H., Illek, B., Negulescu, P.A., Clauss, W., and Machen, T.E. 1992. Carbachol-activated calcium entry into HT-29 cells is regulated by both membrane potential and cell volume. *Proc Natl Acad Sci U S A* 89:1438-1442.
192. Peng, S.L., Gerth, A.J., Ranger, A.M., and Glimcher, L.H. 2001. NFATc1 and NFATc2 together control both T and B cell activation and differentiation. *Immunity* 14:13-20.
193. Kaminuma, O., Kitamura, F., Kitamura, N., Hiroi, T., Miyoshi, H., Miyawaki, A., and Miyatake, S. 2008. Differential contribution of NFATc2 and NFATc1 to TNF-alpha gene expression in T cells. *J Immunol* 180:319-326.
194. Yoshimura, K., Nakamura, H., Trapnell, B.C., Chu, C.S., Dalemans, W., Pavirani, A., Lecocq, J.P., and Crystal, R.G. 1991. Expression of the cystic fibrosis transmembrane conductance regulator gene in cells of non-epithelial origin. *Nucleic Acids Res* 19:5417-5423.
195. Grinstein, S., Rothstein, A., Sarkadi, B., and Gelfand, E.W. 1984. Responses of lymphocytes to anisotonic media: volume-regulating behavior. *Am J Physiol* 246:C204-215.
196. Lee, S.C., Price, M., Prystowsky, M.B., and Deutsch, C. 1988. Volume response of quiescent and interleukin 2-stimulated T-lymphocytes to hypotonicity. *Am J Physiol* 254:C286-296.
197. Prochazka, G., Landon, C., and Dennert, G. 1988. Transmembrane chloride flux is required for target cell lysis but not for Golgi reorientation in cloned cytolytic effector cells. Golgi reorientation, N alpha-

benzyloxycarbonyl-L-lysine thiobenzyl ester serine esterase release, and delivery of the lethal hit are separable events in target cell lysis. *J Immunol* 141:1288-1294.

198. Gray, L.S., and Russell, J.H. 1986. Cytolytic T lymphocyte effector function requires plasma membrane chloride flux. *J Immunol* 136:3032-3037.
199. Dong, Y.J., Chao, A.C., Kouyama, K., Hsu, Y.P., Bocian, R.C., Moss, R.B., and Gardner, P. 1995. Activation of CFTR chloride current by nitric oxide in human T lymphocytes. *Embo J* 14:2700-2707.
200. Bubien, J.K., Kirk, K.L., Rado, T.A., and Frizzell, R.A. 1990. Cell cycle dependence of chloride permeability in normal and cystic fibrosis lymphocytes. *Science* 248:1416-1419.
201. Crabtree, G.R., and Olson, E.N. 2002. NFAT signaling: choreographing the social lives of cells. *Cell* 109 Suppl:S67-79.
202. Rao, A., Luo, C., and Hogan, P.G. 1997. Transcription factors of the NFAT family: regulation and function. *Annu Rev Immunol* 15:707-747.
203. Postma, D.S., Bleecker, E.R., Amelung, P.J., Holroyd, K.J., Xu, J., Panhuysen, C.I., Meyers, D.A., and Levitt, R.C. 1995. Genetic susceptibility to asthma--bronchial hyperresponsiveness coinherited with a major gene for atopy. *N Engl J Med* 333:894-900.
204. Hauber, H.P., Gholami, D., Koppermann, G., Heuer, H.E., Meyer, A., and Pforte, A. 2003. Increased expression of Interleukin-13 but not Interleukin-4 in cystic fibrosis patients. *J Cyst Fibros* 2:189-194.
205. Kotsimbos, T.C., Ernst, P., and Hamid, Q.A. 1996. Interleukin-13 and interleukin-4 are coexpressed in atopic asthma. *Proc Assoc Am Physicians* 108:368-373.
206. Brown, K.D., Zurawski, S.M., Mosmann, T.R., and Zurawski, G. 1989. A family of small inducible proteins secreted by leukocytes are members of a new superfamily that includes leukocyte and fibroblast-derived

inflammatory agents, growth factors, and indicators of various activation processes. *J Immunol* 142:679-687.

207. Kindler, V., Matthes, T., Jeannin, P., and Zubler, R.H. 1995. Interleukin-2 secretion by human B lymphocytes occurs as a late event and requires additional stimulation after CD40 cross-linking. *Eur J Immunol* 25:1239-1243.
208. Burd, P.R., Thompson, W.C., Max, E.E., and Mills, F.C. 1995. Activated mast cells produce interleukin 13. *J Exp Med* 181:1373-1380.
209. Gibbs, B.F., Haas, H., Falcone, F.H., Albrecht, C., Vollrath, I.B., Noll, T., Wolff, H.H., and Amon, U. 1996. Purified human peripheral blood basophils release interleukin-13 and preformed interleukin-4 following immunological activation. *Eur J Immunol* 26:2493-2498.
210. de Saint-Vis, B., Fugier-Vivier, I., Massacrier, C., Gaillard, C., Vanbervliet, B., Ait-Yahia, S., Banchereau, J., Liu, Y.J., Lebecque, S., and Caux, C. 1998. The cytokine profile expressed by human dendritic cells is dependent on cell subtype and mode of activation. *J Immunol* 160:1666-1676.
211. Hoshino, T., Winkler-Pickett, R.T., Mason, A.T., Ortaldo, J.R., and Young, H.A. 1999. IL-13 production by NK cells: IL-13-producing NK and T cells are present in vivo in the absence of IFN-gamma. *J Immunol* 162:51-59.
212. Zhu, Z., Homer, R.J., Wang, Z., Chen, Q., Geba, G.P., Wang, J., Zhang, Y., and Elias, J.A. 1999. Pulmonary expression of interleukin-13 causes inflammation, mucus hypersecretion, subepithelial fibrosis, physiologic abnormalities, and eotaxin production. *J Clin Invest* 103:779-788.
213. Briere, F., Bridon, J.M., Servet, C., Rousset, F., Zurawski, G., and Banchereau, J. 1993. IL-10 and IL-13 as B cell growth and differentiation factors. *Nouv Rev Fr Hematol* 35:233-235.

214. Cocks, B.G., de Waal Malefyt, R., Galizzi, J.P., de Vries, J.E., and Aversa, G. 1993. IL-13 induces proliferation and differentiation of human B cells activated by the CD40 ligand. *Int Immunol* 5:657-663.

215. Carballido, J.M., Schols, D., Namikawa, R., Zurawski, S., Zurawski, G., Roncarolo, M.G., and de Vries, J.E. 1995. IL-4 induces human B cell maturation and IgE synthesis in SCID-hu mice. Inhibition of ongoing IgE production by in vivo treatment with an IL-4/IL-13 receptor antagonist. *J Immunol* 155:4162-4170.

216. Fort, M.M., Cheung, J., Yen, D., Li, J., Zurawski, S.M., Lo, S., Menon, S., Clifford, T., Hunte, B., Lesley, R., et al. 2001. IL-25 induces IL-4, IL-5, and IL-13 and Th2-associated pathologies in vivo. *Immunity* 15:985-995.

217. Lee, J., Ho, W.H., Maruoka, M., Corpuz, R.T., Baldwin, D.T., Foster, J.S., Goddard, A.D., Yansura, D.G., Vandlen, R.L., Wood, W.I., et al. 2001. IL-17E, a novel proinflammatory ligand for the IL-17 receptor homolog IL-17Rh1. *J Biol Chem* 276:1660-1664.

218. Wills-Karp, M., Luyimbazi, J., Xu, X., Schofield, B., Neben, T.Y., Karp, C.L., and Donaldson, D.D. 1998. Interleukin-13: central mediator of allergic asthma. *Science* 282:2258-2261.

219. Mueller, C., Braag, S.A., Martino, A.T., Tang, Q., Campbell-Thompson, M., and Flotte, T.R. 2008. The pros and cons of immunomodulatory IL-10 gene therapy with recombinant AAV in a Cftr(-/-)-dependent allergy mouse model. *Gene Ther*.

220. Chiaramonte, M.G., Mentink-Kane, M., Jacobson, B.A., Cheever, A.W., Whitters, M.J., Goad, M.E., Wong, A., Collins, M., Donaldson, D.D., Grusby, M.J., et al. 2003. Regulation and function of the interleukin 13 receptor alpha 2 during a T helper cell type 2-dominant immune response. *J Exp Med* 197:687-701.

221. Newcomb, D.C., Zhou, W., Moore, M.L., Goleniewska, K., Hershey, G.K., Kolls, J.K., and Peebles, R.S., Jr. 2009. A functional IL-13 receptor is

expressed on polarized murine CD4+ Th17 cells and IL-13 signaling attenuates Th17 cytokine production. *J Immunol* 182:5317-5321.

222. Brantly, M.L., Chulay, J.D., Wang, L., Mueller, C., Humphries, M., Spencer, L.T., Rouhani, F., Conlon, T.J., Calcedo, R., Betts, M.R., et al. 2009. Sustained transgene expression despite T lymphocyte responses in a clinical trial of rAAV1-AAT gene therapy. *Proc Natl Acad Sci U S A*.